MASTER
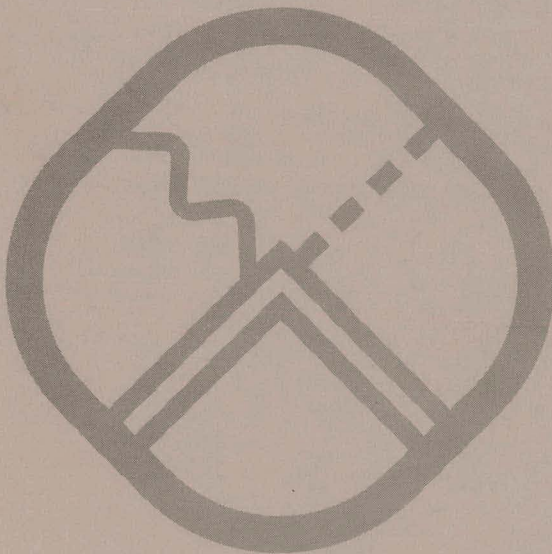
STATUS AND PERSPECTIVES OF PHOTOPRODUCTION EXPERIMENTS

C. A. HEUSCH

SEPTEMBER 1968

SYNCHROTRON LABORATORY

CALIFORNIA INSTITUTE OF TECHNOLOGY

PASADENA

DISCLAIMER

This report was prepared as an account of work sponsored by an agency of the United States Government. Neither the United States Government nor any agency Thereof, nor any of their employees, makes any warranty, express or implied, or assumes any legal liability or responsibility for the accuracy, completeness, or usefulness of any information, apparatus, product, or process disclosed, or represents that its use would not infringe privately owned rights. Reference herein to any specific commercial product, process, or service by trade name, trademark, manufacturer, or otherwise does not necessarily constitute or imply its endorsement, recommendation, or favoring by the United States Government or any agency thereof. The views and opinions of authors expressed herein do not necessarily state or reflect those of the United States Government or any agency thereof.

DISCLAIMER

Portions of this document may be illegible in electronic image products. Images are produced from the best available original document.

Status and Perspectives of Photoproduction Experiments[*]

Lectures Delivered at

The International School of Physics, "Ettore Majorana", Erice, Sicily

July 13-27, 1968

Clemens A. Heusch

California Institute of Technology

Status and Perspectives of Photoproduction Experiments

In the three lectures presented this year at the Erice Summer School, I shall attempt to give an up-to-date picture of what is new and, to some, exciting in the photoproduction field. There are a few severe limitations forced on us by the width of the field and the finite time available. I will therefore assume that the student is acquainted with the general trend of modern particle physics; that he has some knowledge of techniques such as used in partial wave analysis of scattering amplitudes, of the simplest consequences of the invariance of strong interaction parameters under SU(2) and SU(3) transformation, of the basics of the non-relativistic quark model, and the concept of Regge poles. But even for strictly data-oriented people, I hope to give a fairly full picture of what has recently been happening in the field of photon-initiated hadronic interactions leading to a nucleon-plus-boson final state. No attempt was made to avoid personal bias for particular aspects of the field. We will deal primarily with the photoproduction of single non-strange pseudoscalar and vector mesons - data, problems they pose, and current ideas toward their interpretation.
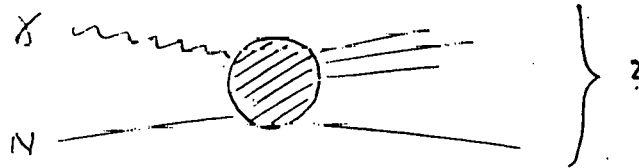
Contents

Lecture 1 Photoproduction of Pseudoscalar Mesons in the Isobar Region.

1.1 Introduction: Features of Photoproduction Experiments.

We will investigate processes of the type

with, to start with, an arbitrary final state. The coupling of the

photons to the strong vertex is the distinctive feature. We will,

in this context, completely disregard purely electromagnetic inter-

actions. We'll just keep in mind that, as of this time, theorists

and experimentalists alike are confident that quantum electrodynamics

describes them adequately. We therefore focus our interest on the

more problematic field of the strong interactions as coupled to the

photon-nucleon initial state.

    To fully define the incoming channel, let us recall the quantum

numbers of the photon:

$$J^P = 1^-; \ C = -1$$

helicity for real photons: $\lambda_k = \pm 1$
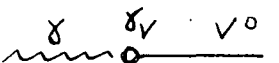
helicity for virtual photons: $\lambda_k = 0, \pm 1$

We further know that the Gell-Mann-Nishijima formula, $Q = \frac{Y}{2} + I_3$,

suggests that the photon behaves partly like an isovector, partly

like an isoscalar (the hypercharge Y is invariant under transform-

ations in isospin space). The electromagnetic interactions are

further known to be invariant under rotations in U spin space, so
that we have the SU(2) content of the photon as that of an
$a(I = 1) + b(I = 0)$, and $(U = 0)$ object. In SU(3) space, we
conventionally view the photon as the $U = 0$ member of an octet
(an assignment which is yet waiting for unambiguous experimental
verification · cf. lecture 3).

We notice immediately that, since we have focused on hadronic
interactions, we find several hadrons with quantum numbers similar
to those of the photon. These are the vector mesons, ρ^0, ω, Φ.
This similarity of space-time properties stimulated the idea of
describing the hadronic electromagnetic field in terms of the vector
meson fields. We will therefore attempt to tie up the vertices
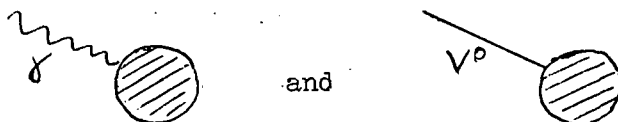
with a possible direct coupling of the type .
If such a direct coupling exists, then we may have a chance to
describe γ-hadronic interactions in terms of purely hadronic inter-
actions; we will just have to combine properly the corresponding
isospin states of V-mesonic interactions; the coefficients will be
related to the photon-vector meson coupling constants γ_ρ, γ_ω, γ_Φ.
This aspect will be explicitly dealt with in the second lecture; its
fundamental importance appears obvious.

Let us turn, for a minute, to experimental aspects; how can
we perform γ-hadronic experiments such that they are of the type
of V-hadronic reaction studies?

There are experimental limitations: the photons are available only as secondary beams. Like all neutral secondary beams, they have the disadvantage of being non-focusable, and, in general, their momentum is not defined. Worse than neutral kaon or neutron beams, their masslessness forbids the identification of spectral components by time-of-flight techniques. This means then that

1. Spatial definition is possible only through collimation (meaning intensity loss and some unavoidable production of secondaries);

2) Momentum definition, short of kinematical reconstruction from the final state, is effected only through fairly tricky techniques. They yield low intensities (as in "photon tagging", because of thin radiator requirements), and mostly degrade the obtainable maximum photon energy (as in positron annihilation, bremsstrahlung production from crystals, and backward Compton scattering of laser photons). Unavoidable backgrounds and collimation problems add to the difficulty.

3) For the definition of polarization components, the absence of a photon magnetic moment excludes direct methods. Crystal bremsstrahlung and scattered laser photons can be used, but there is always a price to pay, as above. For virtual photons, definite polarization states are available in electron- or muon-initiated reactions.

Worst of all, non-hadronic processes see to it that the experiment, if not carefully and ingeniously defined, may be swamped by backgrounds which stem from the abundance of final-state particles due to purely electromagnetic processes (pair production, Compton effect) in the target and along the beam line.

1.2 The Isobar Region in π Photoproduction.

If we take a look at the total cross section data for the photo-
production of single pions below a total energy of ~ 2 GeV,
(Fig. 1.2-1), a pronounced resonance structure suggests that the
production may proceed dominantly through resonant intermediate
states. We might therefore try to interpret the experimentally
observed phenomena in terms of diagrams of this type:
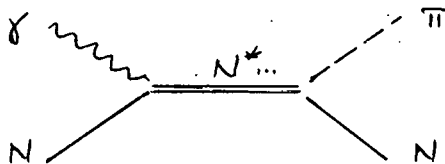
(where the photon, at the left vertex, couples either to the charge
or to the magnetic moment of the nucleon). Fig. 1.2-2 shows that
the differential cross-sections at 0° and 180° do not exhibit the
same structure as the total cross-section: We will therefore look
into terms which will be present in addition to these s-channel poles.
The Born diagrams
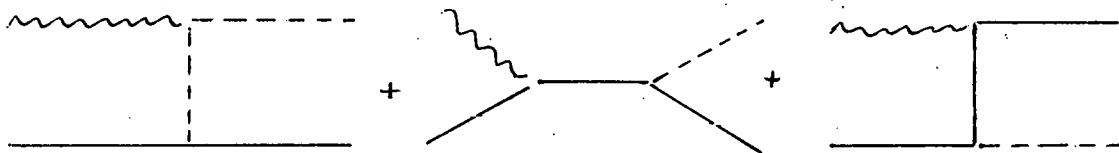
associated with the lowest-mass poles in the s, t, and u-channels,
are obvious candidates. The first diagram (the π pole) will exist
for charged π production only (C conservation forbids the vertex

K_LAB, INCIDENT PHOTON ENERGY IN LAB., IN GEV

π^+, σ_T

×2
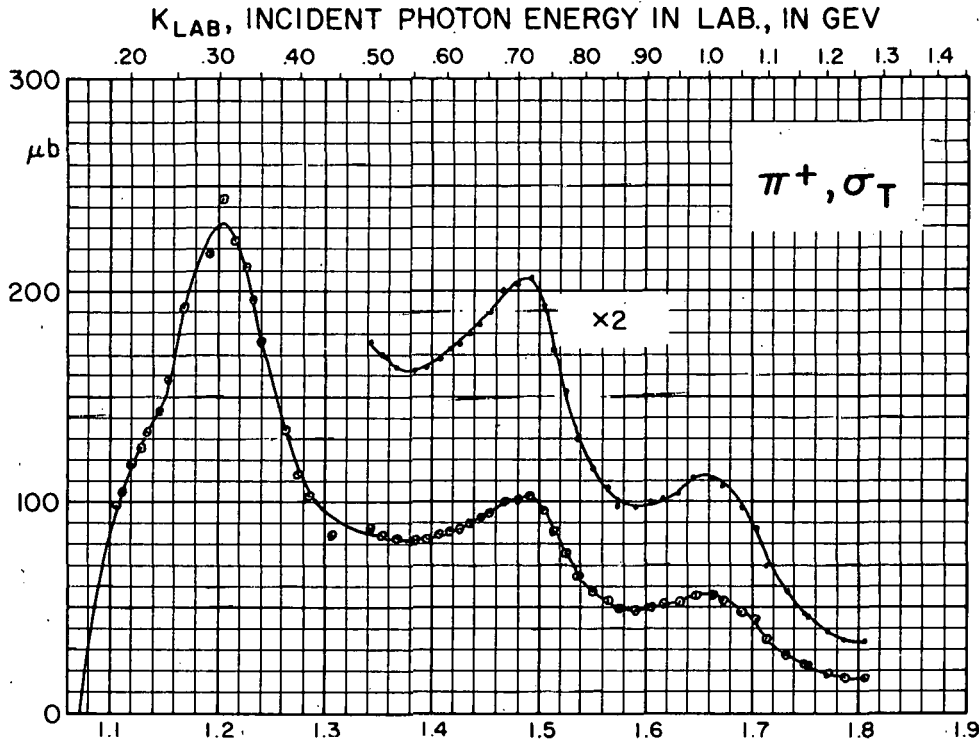
<u>Fig. 1.2-1</u> Total cross-section for $\gamma p \rightarrow \pi^+ n$ from threshold
to $E_\gamma = 1.4$ GeV. (From Ref. No. 7)

K_LAB, INCIDENT PHOTON ENERGY IN LAB., IN GEV

$\mu b/Ster$ π^+

$\sigma(0°)$

$\sigma(180°)$

W, TOTAL ENERGY IN CM SYSTEM, IN GEV
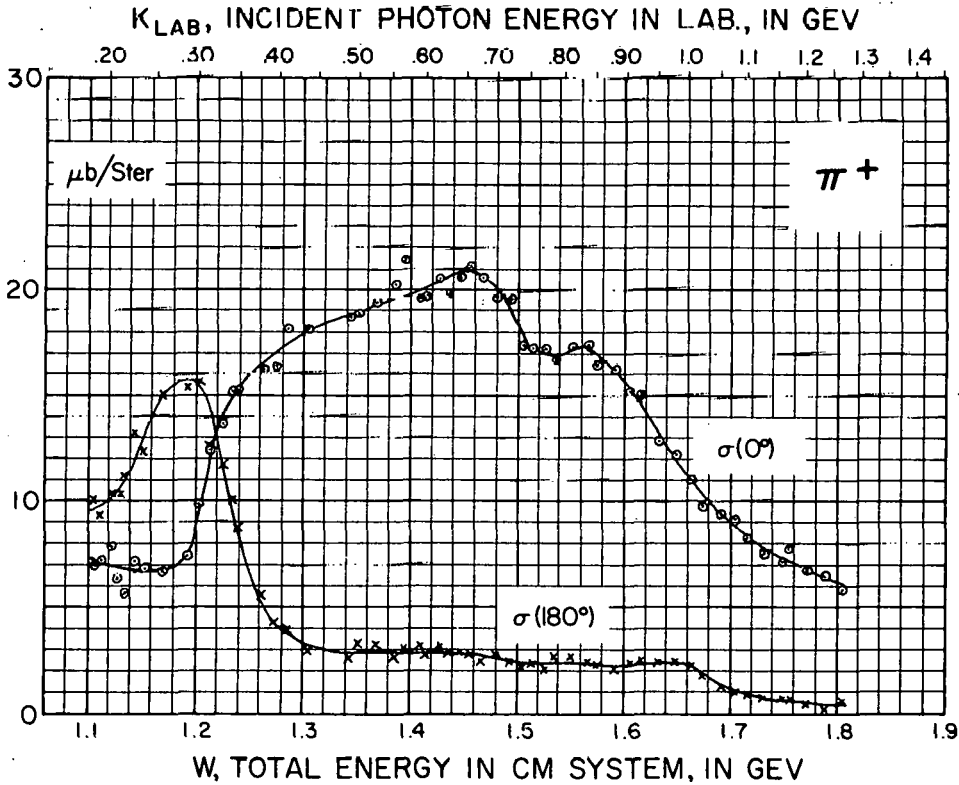
<u>Fig. 1.2-2</u> Differential cross-section for $\gamma p \rightarrow \pi^+ n$ at $0°, 180°$.
(From Ref. No. 7)

$\gamma \pi^{o}\pi^{o}$). The photon coupling to the meson current will give a contribution of the form $\vec{\epsilon}\cdot\vec{q}$ ($\vec{\epsilon}$ = photon polarization, $\vec{q}$ = π momentum). When averaged over photon polarizations, it will give a contribution to the cross-section of the form

$$\frac{d\sigma}{d\Omega} \sim e^2 \sin^2\Theta \, \vec{q}^{\,2} \qquad (1.2\text{-}1)$$

i.e., it will not influence the 0° or 180° cross-sections. Since we need a forward and backward contribution to the cross-section, we add the second diagram (direct channel nucleon pole, whose addition is necessary to make the "Born approximation" gauge invariant) and, possibly, the third (crossed or u-channel nucleon pole).

s channel poles are characterized by quantum numbers J^{P}, I; m, Γ. They show up as resonance-like behavior in one particular partial wave and may therefore lead to a typical angular structure in the cross-section. t- and u-channel poles, on the other hand, when projected into the s channel,will lead to <u>many</u> multipoles contributing to the angular distribution.

For the π exchange diagram, where the small-t behavior is close to the pole at $\cos \Theta = \frac{1}{\beta_{\pi}}$ (β_{π} = π velocity), i.e., close to the exchange of a physical particle, a large number of multipoles are expected to contribute to the amplitude A.

$$A_{\pi\text{exch}} \sim \frac{1}{1 - \beta_{\pi} \cos \Theta} \sim \frac{1}{t - m_{\pi}^2} \qquad (1.2\text{-}2)$$

For $\cos \Theta \approx 1$, $\beta_{\pi} \approx 1$, many ℓ waves will be involved; the forces are long-range. To still find the effect of isobars in the presence of this pole term, the recipe of Moravcsik[1] is to divide out the π pole,

then expand in terms of powers of cos Θ

$$(1 - \beta_\pi \cos \Theta)^2 \frac{d\sigma}{d\Omega} = \sum_n c_n \cos^n \Theta \qquad (1.2\text{-}3)$$

in order to find angular characteristics, which may then be correlated with individual resonant s-channel contributions.

1.3 Helicity Formulation of Partial Wave Analysis.

"Isobar models", consisting of the analysis of photoproduction data in terms of the diagrams mentioned above in the framework of some pragmatic fitting procedure, have been increasingly successful in the phenomenological interpretation of experimental material below ~ 2 GeV in recent years. Gourdin and Salin[2], Salin[3], Beder[4], and, most recently, Walker[5] have been able to reproduce experimentally observed features well with such models. (See also Chau et. al.[16])

Let us stop briefly and give the relevant formulation in terms of the helicity language as spelled out by Jacob and Wick[6], which has proven to be particularly suited to the problem.

We quantize the spins in the initial and final states of the interaction along the directions of photon and pion momenta k and q, respectively, for the process $\gamma N \rightarrow \pi N$, in the center-of-mass system. We can then define the helicity amplitudes

$$A_{\mu,\lambda} (\Theta, \Phi), \text{ with } \mu = \lambda_q - \lambda_2 = -\lambda_2, \text{and } \lambda = \lambda_k - \lambda_1$$

the final and initial-state helicities (λ_1, λ_2 refer to the corresponding nucleon helicities). For real, transverse photons, $\lambda_k = \pm 1$. λ then has four possible values, $\pm 1/2$, $\pm 3/2$; with $-\lambda_2 = \mu$

being $\pm$ 1/2, we have a choice of 8 helicity amplitudes. However, parity conservation provides a link between the $\lambda_k = +1$ and -1 amplitudes.

$$A_{-\mu, -\lambda} (\theta, \Phi) = e^{i(\lambda - \mu)(\pi - 2\Phi)} A_{\mu, \lambda} (\theta, \Phi) \qquad (1.3-1)$$

so that we are left with four independent amplitudes; we choose $\lambda = + 1$, and restrict ourselves to the plane $\Phi = 0$; we then obtain the "helicity amplitudes"

$$H_1 \cdots H_4 (\theta) = A_{\mu\lambda} (\theta, \Phi = o) \; ; \; \lambda_k = + 1 \; . \qquad (1.3-2)$$

In terms of these amplitudes, we write down the experimentally observable quantities. The differential cross-section is

$$\frac{d\sigma}{d\Omega} (\theta) = \frac{1}{2} \frac{q}{k} \sum_{i=1}^{4} |H_i|^2 \qquad (1.3-3)$$

The polarization of the final-state nucleon in the direction $\vec{q} \times \vec{k}$ is then (we denote the differential cross-section briefly by $\sigma(\theta)$)

$$P(\theta) = \frac{q}{k} \frac{1}{\sigma(\theta)} \text{Im} (H_1 H_3^* + H_2 H_4^*) \qquad (1.3-4)$$

If we have a polarized nucleon target, we can define the asymmetry parameter $T(\theta) = \dfrac{\sigma_+ - \sigma_-}{\sigma_+ + \sigma_-}$, with σ_+, σ_- the differential cross-sections for target polarization up or down with respect to $\vec{k} \times \vec{q}$. Then, we can express

$$T(\theta) = \frac{q}{k} \frac{1}{\sigma(\theta)} \text{Im} (H_1 H_2^* + H_3 H_4^*) \qquad (1.3-5)$$

Last, we define an asymmetry parameter $\Sigma(\theta) = \dfrac{\sigma_\perp - \sigma_{||}}{\sigma_\perp + \sigma_{||}}$ for

processes initiated by polarized photons, where the $\sigma_\perp$, $\sigma_{||}$
are the cross-sections for photon polarization perpendicular and
parallel to the production plane. We find

$$\Sigma(\Theta) = \frac{q}{k} \frac{1}{\sigma(\Theta)} \text{Re} \ (H_1 H_4^* - H_2 H_3^*) \qquad (1.3\text{-}6)$$

Determination of all these observable parameters would lead to a more
complete picture; however, final-state nucleon polarization P and
polarized photon asymmetry Σ have been measured only at a few angles
and energies,[7] and polarized nucleon targets suited to photopro-
duction work are only now starting to be practically considered[8].
The polarized proton targets used in πp scattering experiments up to
now, contained heavy elements which will not allow for a recon-
struction of the full kinematics in the presence of a continuous
incoming photon spectrum. Even the existing cross-section data are
by no means as complete and consistent as one would wish; particu-
larly the photoproduction processes

$$\gamma n \to n\pi^o$$
$$\gamma n \to p\pi^- \qquad (1.3\text{-}7)$$

have been investigated only sparsely.[7]

To decompose the observables into partial-wave contributions,
we now write down the partial-wave expansion for the helicity
amplitudes

$$A_{\mu\lambda} \ (\Theta,\Phi) = \sum_j A_{\mu\lambda}^j \ (2j + 1) \ d_{\lambda\mu}^j \ (\Theta) e^{\ i(\lambda - \mu)\Phi} \qquad (1.3\text{-}8)$$

For our specific case, with $\Phi = 0$, we have

$$H_i(\theta) = \sum_j H_i^{\ j} (2j + 1) d_{\lambda\mu}^{\ j}(\theta) \qquad (1.3-9)$$

The $A_{\mu\lambda}^{\ j}$ and $H_i^{\ j}$ are the helicity coefficients, for given helicity and angular momentum; the angular functions are mutually orthogonal and appropriately normalized when integrated over the solid angle. In order to have helicity coefficients corresponding to states of definite parity, we have to take sums and differences of final states having opposite helicity, $+ \mu$ and $- \mu$, in order to define

$$A_{n+} = -\frac{1}{\sqrt{2}} (A_{\frac{1}{2} \frac{1}{2}}^{\ j} + A_{-\frac{1}{2},\frac{1}{2}}^{\ j})$$

$$A_{(n + 1)-} = \frac{1}{\sqrt{2}} (A_{\frac{1}{2} \frac{1}{2}}^{\ j} - A_{-\frac{1}{2},\frac{1}{2}}^{\ j})$$

$$B_{n+} = \sqrt{\frac{2}{n(n + 2)}} (A_{\frac{1}{2} \frac{3}{2}}^{\ j} + A_{-\frac{1}{2} \frac{3}{2}}^{\ j}) \qquad (1.3-10)$$

$$B_{(n + 1)-} = -\sqrt{\frac{2}{n(n + 2)}} (A_{\frac{1}{2} \frac{3}{2}}^{\ j} - A_{-\frac{1}{2} \frac{3}{2}}^{\ j})$$

The A and B are seen to refer to initial helicities $\frac{1}{2}$ and $\frac{3}{2}$, respectively. The subscript notation, with $n = j - 1/2$, is that used in the CGLN formalism[9]. The brackets are the same as $(H_2^j \pm H_4^j)$, $(H_1^j \pm H_3^j)$. It is then straight-forward to express the four independent helicity amplitudes in terms of these coefficients A, B and the angular functions introduced in (1.3-8).

It is interesting to look at the angular structure of a few of the helicity amplitudes, as they are influenced by the "helicity elements" A, B from eq. (1.3-10). Fig. 1.3-1 shows the dependence
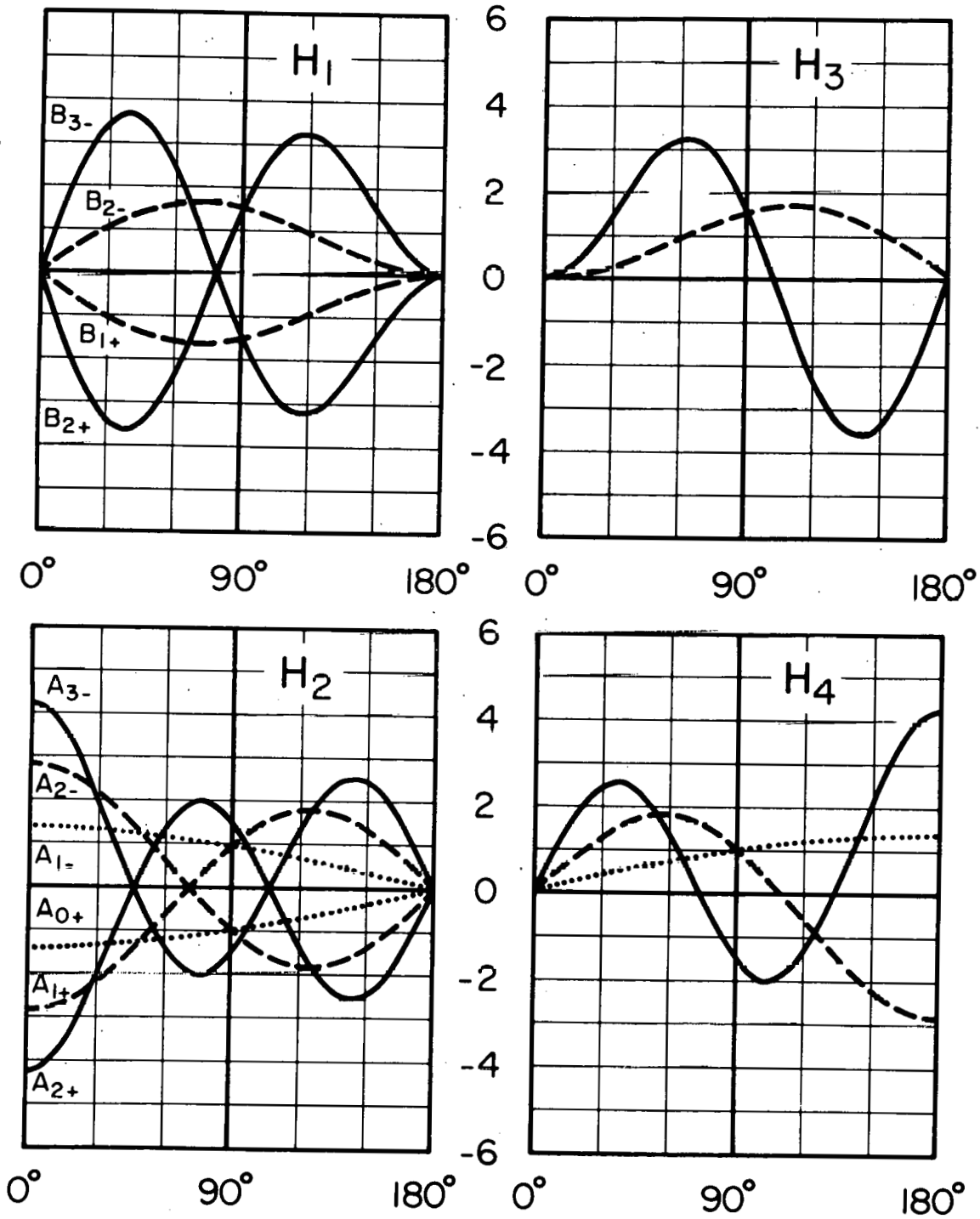
Fig. 1.3-1 Influence of the helicity elements A, B on the helicity amplitudes $H_1 \ldots H_4$, for $j \leq \frac{5}{2}$ (From Ref. No. 5).

of H_1 . . . H_4 on the individual A's and B's for $j \leq \frac{5}{2}$. Two features stand out: with increasing j, the angular behavior gets more complicated (as we expect); and the forward and backward amplitudes each show contributions from one helicity amplitude only (H_2, and H_4, respectively). This points up a particularly useful feature of the formalism employed.

Using the helicity language, R. Walker[5] at CalTech has recently finished an extensive phenomenological study of single π photoproduction data from many laboratories. He fits the data for all isospin amplitudes as far as they are experimentally accessible, in terms of a model incorporating Born terms (electric coupling only), s-channel resonances as known from πN phase shift analysis, and a non-resonant background in the low partial waves which is required to vary smoothly with energy. Resonances are inserted in a Breit-Wigner form with an appropriate phase-space factor.

Notwithstanding the incompleteness of the data and the obvious limitations of the model, the method is fairly powerful. Resonances show up when the real or imaginary parts of a particular partial wave amplitude demonstrate a typical behavior with energy like the one in Fig. 1.3-2. Since the π^+ data are the most accurately known, we show a few examples of Walker's fits in Fig. 1.3-3.

We now revert to the general picture of section 1.2, and ask which features of photoproduction in the isobar region have emerged from such analysis.
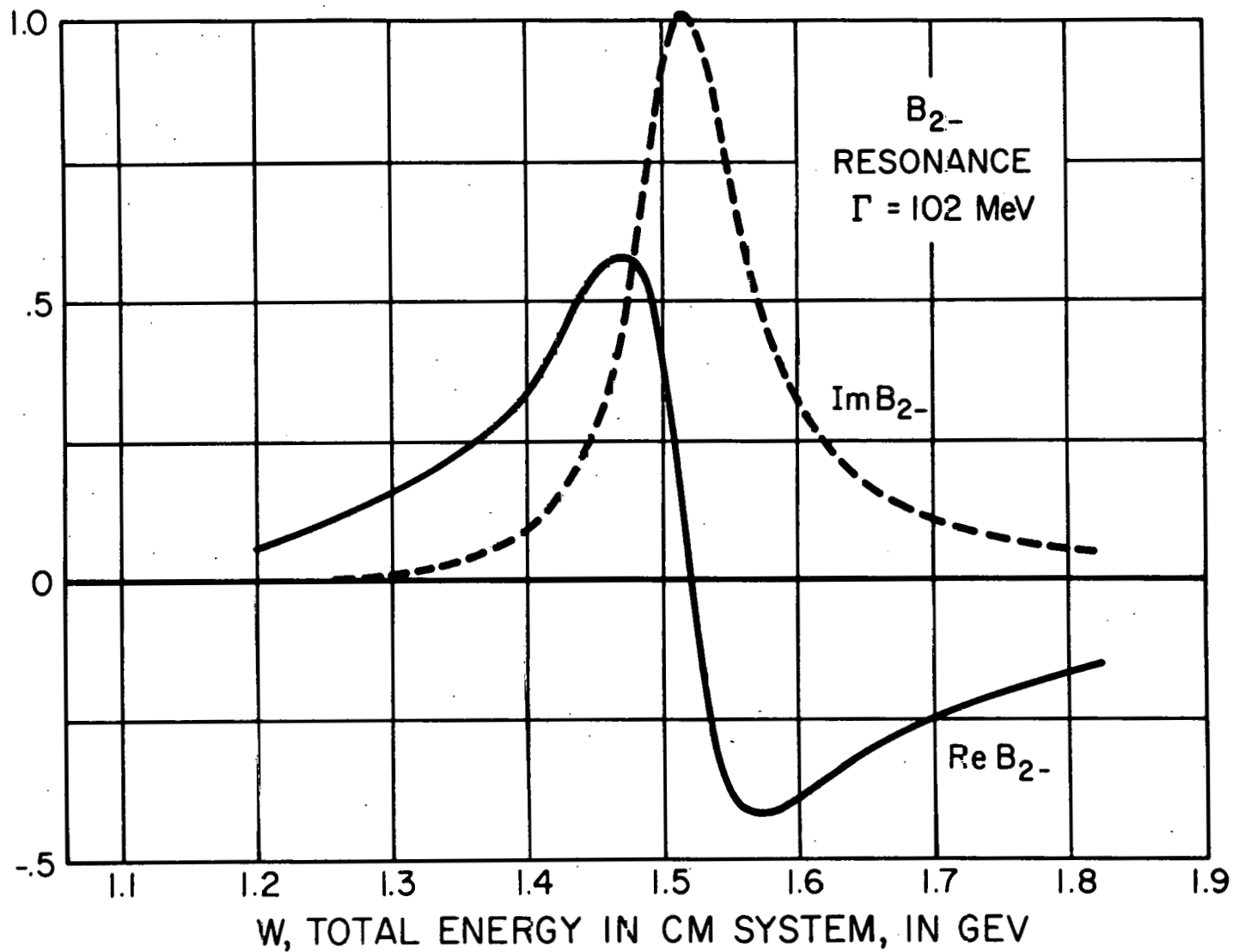
Fig. 1.3-2 Typical resonant form of partial wave: Re and Im parts of B2-amplitude at resonance peak of D_{13} (1520). (From Ref. No. 5)
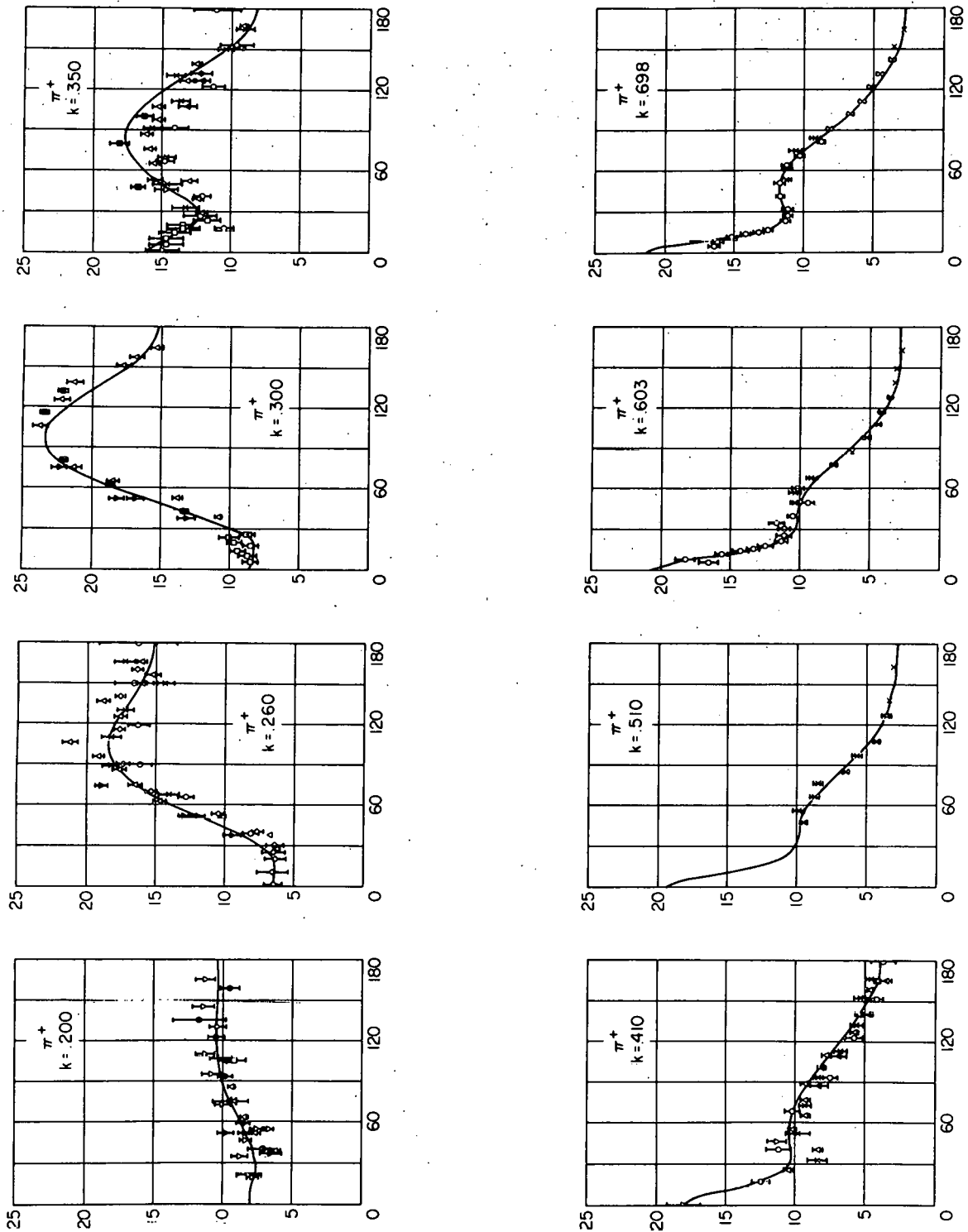
Fig. 1.3-3 Examples of Isobar Model Fits to π⁺ Production Data.
From Ref. No. 5)

1) It is confirmed that the "first resonance" (Δ 1238) is predominantly excited by the magnetic dipole (Fig. 1.3-4 shows, for π^o photoproduction, the relevant H_i's; the dominant 90° contribution comes from the imaginary part of B_{1+}). The resulting strength for this photo-excitation is close to that given by the quark model or by SU(6) (cf. section 1.8). There is a small admixture ($\sim 6\%$) of electric quadrupole excitation, found from a comparison of 0° and 180° data with the 90° cross-section.

2) The D_{13} (1527), the old "second resonance", is produced mainly in the B_{2-} amplitude; the F_{15} (1688), the old "third resonance", predominantly in B_{3-}. This implies they are both produced from initial helicity 3/2. The absence of A amplitudes (initial helicity 1/2) is reflected in the small effect made by these states on the 0° and 180° cross sections (cf. Fig. 1.2-2). (Remember that angular momentum conservation demands that at these angles, only helicity 1/2 can determine the s-channel behavior.

3) The S_{11} (1570) isobar, which is likely to produce the ηN enhancement close to the threshold for this final state, is indicated in the A_{o+} amplitude (cf. section 1.7).

4) There is little if any evidence for the production of the D_{15} (1670). Improvement of polynomial fits in this energy region by the addition of a small amount of D_{15} was reported earlier by Ecklund and Walker[10] for π^+ photoproduction, but the corresponding amplitude B_{2+} is very small (cf. section 1.8).
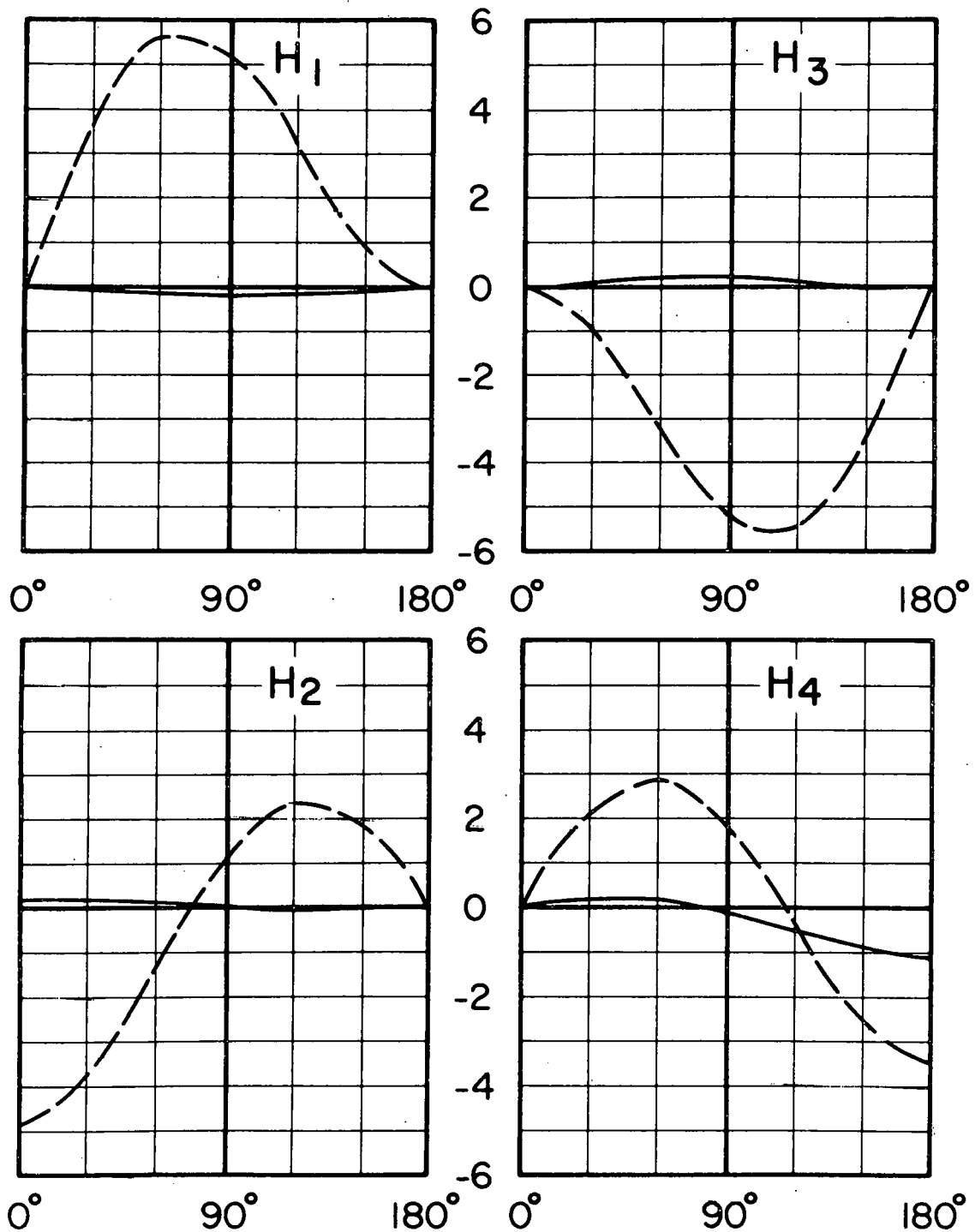
Fig. 1.3-4 Best fits for helicity amplitudes at position of $\Delta(1238)$.
Comparison with Fig. 1.3-1 shows that, for the positive-
parity state, B_{1+} is the dominant mode. A_{1+} admixture
shows up at 0°, 180°.   (Solid curves: real part;
dashed curves: imaginary part). (From Ref. No. 5).

5) The S_{11} (1709) does not emerge in the photoproduction of π's. This may be due to the nature of the fitting procedure employed, and to the fact that the state lies close in energy to other resonant states. We will see (cf. 1.7) that in the photoproduction of η mesons we may have a better chance to investigate this question quantitatively.

6) Similarly, the P_{11} (1400), the "Roper resonance", has not been uniquely identified in the photoproduction of single π's.

7) Most isobars appear to be produced predominantly by isovector photons. Clearly, to make this statement firm, we will need more data (especially from π^- production); and we will need new ideas to understand their implications. Many of the features emerging here have interesting implications in terms of symmetry considerations and the quark model. We will deal with them in sections 1.7 and 1.8.

Extension to Higher Energies

Phenomenological models of the type discussed have been successful for total energies up to $\sim$ 1.7 GeV. Beyond that range, too many partial waves will have to be considered, and interpretation becomes less stringent. Also, exchange graphs of the type
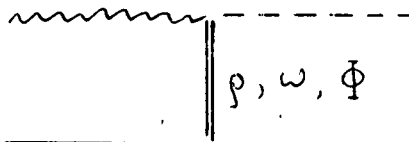
can probably no longer be disregarded. One attempt to include such exchanges was made by Bloom et. al.[11], who found that a reggeized vector meson exchange (one can safely assume ω exchange only)

considerably improves their fit to cross-section and polarization
data in the intermediate energy region. Elementary vector exchange
does <u>not</u> fit. In their fit, isobars up to the F_{17} (1920) were included,
and the trajectory exchange was slowly "turned on" in an empirical
way (with the residues assumed to be constant along the trajectory
in the t range covered).

We will treat the Regge picture in lecture 3 and remark here
only that we will need more, and more precise experimental informa-
tion before we will be able to link up intelligently the isobar
region and the region which is more successfully described in terms
of t channel singularities.

1.4 Sum Rules for Photoproduction Amplitudes

Various sum rules have been proposed in recent years to test
physical assumptions, particularly the ideas of current algebra and
super-convergence relations. It is often hard to check these
against experiment due to a lack of precise information about ampli-
tudes which are hard to extract from the data (like small amplitudes
in processes dominated by a resonant term).

Nevertheless, analyses like the above-mentioned isobar models
go a long way toward making such evaluations feasible.

I am going to mention two of these sum rules explicitly here;
both are currently being reported[12] to be in good numerical
agreement with experiment.

The Cabibbo-Radicati sum rule[13] ties up the mean-square
isovector proton charge radius, $\langle r^2 \rangle^V_{GE}$, and the total isovector

nucleon magnetic moment, μ^V_{tot}, with an integral over the total

absorption cross-section for isovector photons into $I = 1/2$ and

$I = 3/2$ states, σ^V_{tot} (1/2) and σ^V_{tot} (3/2):

$$\frac{1}{6} \langle r^2 \rangle^V_{GE} = \frac{1}{2} \left(\frac{\mu^V_{tot}}{2m_N} \right)^2 + \frac{1}{4\pi^2 \alpha} \int_0^\infty \frac{dk}{k} [2 \sigma^V_{tot}(\tfrac{1}{2}) - \sigma^V_{tot} (\tfrac{3}{2})]$$

$$(1.4-1)$$

According to Gilman and Schnitzer[14], the contributions of the

various resonances, plus a large non-resonant S-wave term resulting

from the fits, largely cancel each other under the integral, and the

terms other than the integral dominate.

Agreement up to $k = 800$ MeV is good to a few percent. The

Drell-Hearn sum rule[15] relates the proton anomalous magnetic

moment, μ'_p , to an integral over total photo-absorption cross-sections

for photons with spins parallel or anti-parallel to the proton spin,

σ_p and σ_A:

$$\frac{2\pi^2 \alpha}{m_N^2} \mu'_p{}^2 = \int_0^\infty \frac{dk}{k} [\sigma_p - \sigma_A]$$

$$(1.4-2)$$

An evaluation by Chau et. al.[16] reports the relation to hold within

the errors inherent in the evaluation of the integral.

1.5 Other Mesons: K and η Photoproduction in the Isobar Region

A: η Photoproduction

Our interest in the study of the process $\gamma p \to p\eta$ is due mainly

to two features:

1) The isoscalarity of the η makes this process a selective

probe for the I = 1/2 channel in $\gamma p \to p + (0^-)$ reactions, whereas the πN final state allows for both I = 1/2, 3/2.

2)   The assignment, together with the π^0, of the η to the weight - 2 position of the 0^- octet of SU(3), makes comparisons with the relatively well-studied $\pi^0 N$ final state fruitful for tests of symmetry predictions.

Experimentally, the short life-time ($\approx 10^{-20}$ sec.) and the many decay modes make η production comparatively hard to study. Most photoproduction studies with counter techniques use the partial mode $\eta \to 2\gamma$ for definition of the final state[17], although some work has been done using precise momentum analysis of the recoil proton alone. Experiments at CalTech have obtained η samples good to $\leq 96\%$[18]; thereby, not only cross-section data but also information on recoil proton polarization becomes available, and we can hope to look for an analysis of these data in a spirit similar to that outlined for the πN final state in section 1.3.

The experimental data available at present can be summarized briefly as follows: the Bubble Chamber data [19] on the total cross section, shown in Fig. 1.5-1, show a sharp rise above threshold, and a fairly dramatic decrease within ~ 150 MeV. Counter experiments measuring differential cross-sections show this feature with somewhat smaller errors. Recent data from Frascati[99] confirm approximate isotropy of the cross-section up to photon energies of ~ 350 MeV (Fig. 1.5-2). New data from CalTech show up features of the 50°, 70°, and 90° cross sections as shown in Fig. 1.5-3, again confirming the
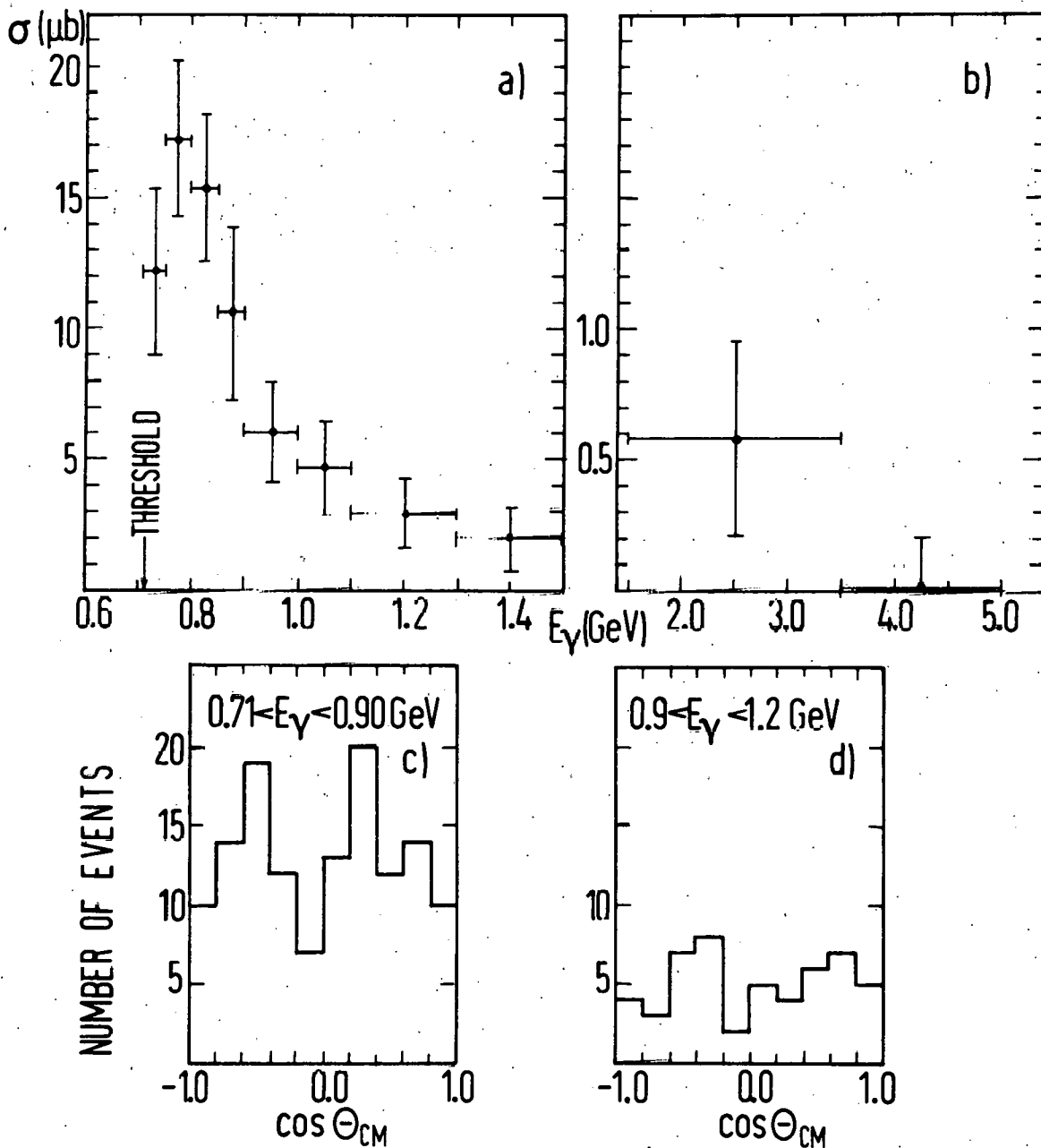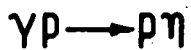
Fig. 1.5-1 Total cross-sections and angular distributions for
$\gamma p \rightarrow p\eta$, from bubble chamber analysis. (From Ref. No. 19)
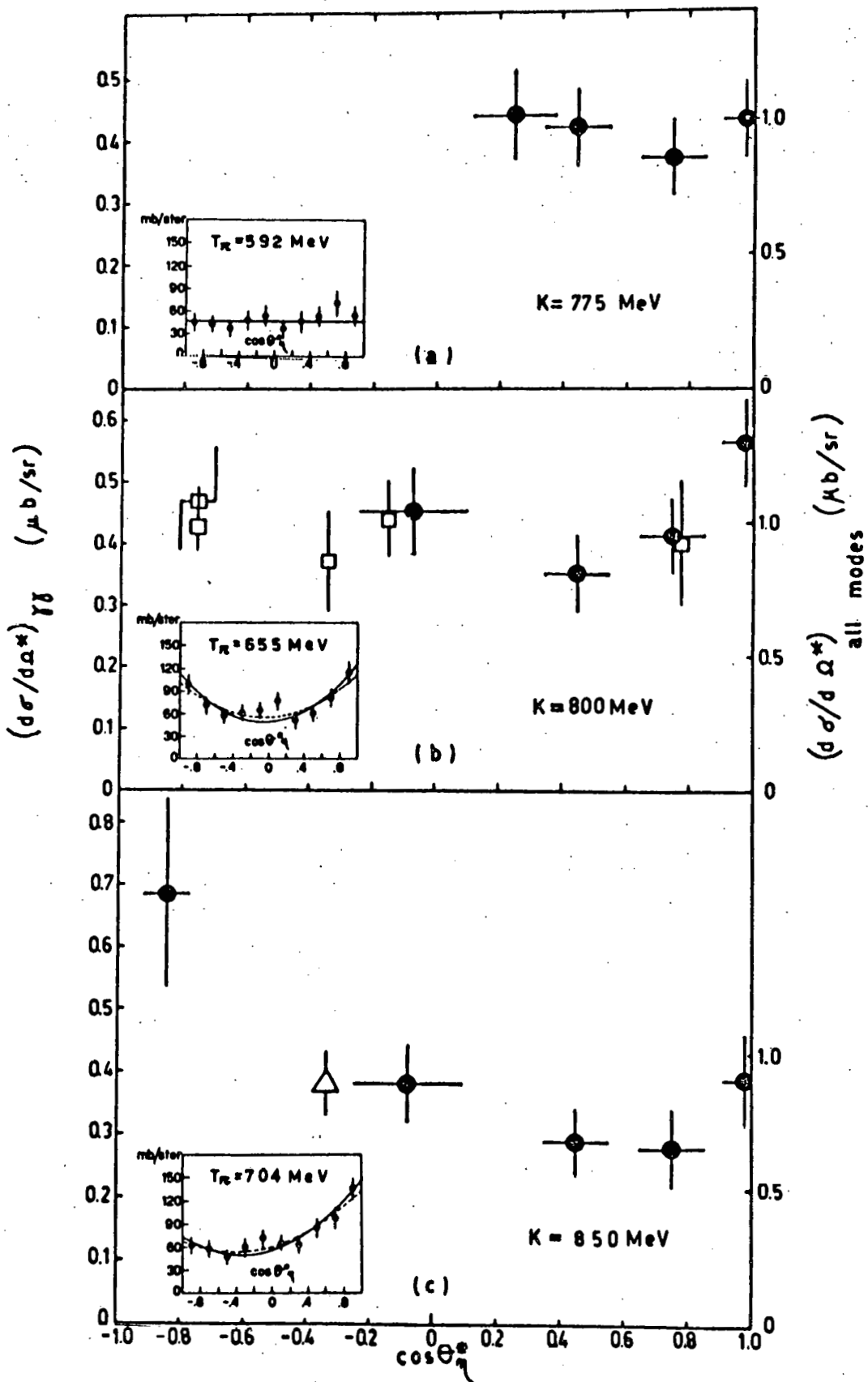
Fig. 1.5-2 Angular distributions for the differential cross section $\frac{d\sigma}{d\Omega}(\gamma p \rightarrow p\eta)$, from counter experiments at Frascati. Insets show πp data at same energies. (From Ref. No. 99)
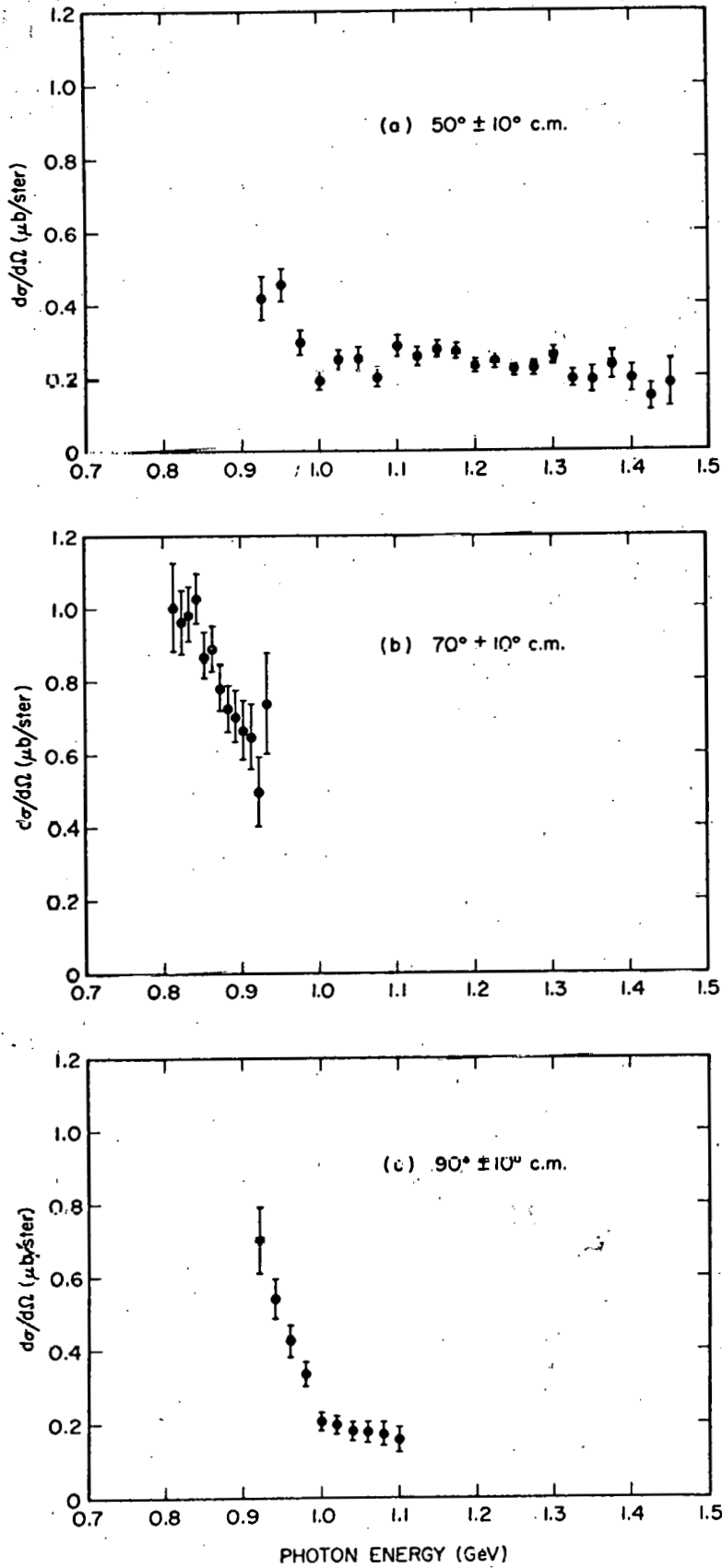
Fig. 1.5-3   η photoproduction cross sections at
50°, 70°, 90°. Caltech counter data.
(From Ref. No. 18)

quick decay of the ηN threshold enhancement, a probable small dip of the 50° cross-section in the region of k = 1000 - 1100 MeV, a long shoulder at energies k = 1100 - 1300, and a consistently lower value for the 90° cross-section for $1000 \leq k \leq 1100$ MeV. Polarization data are not available yet, but have been taken at CalTech, where some 300,000 spark-chamber frames are presently being analyzed.

To try to interpret the cross-section data in terms of some isobar model along the lines discussed in 1.2, let us look at the possible diagrams. As in section 1.2, we have the Born terms. For s-channel resonances we have the I = 1/2 isobars only. We may add vector meson exchange and higher mass poles in the t and u channels.

Fits to the data have been made in this way, involving the s-channel nucleon pole and the S_{11}(1570) isobar, plus some possible admixtures of D_{13}(1527), F_{15} (1688), and vector exchange[20]. With the new data from CalTech extending up to 1450 MeV, further work is under way trying to clarify these questions:

1. Can the S_{11} (1570) alone account for the large enhancement above threshold, or is there some contribution from the P_{11} (~1400) below threshold, or from the D_{13} (1527)? The latter appears to be ruled out by angular momentum barrier effects ($\sim q^{2\ell + 1} = q^5$ near threshold); a contribution of the P_{11}, whose mass is not precisely known, can be isolated only by a 90° polarization measurement on the recoil proton; it would interfere with the opposite-parity S_{11} and give a large polarization close to threshold. Its presence in photoproduction would pose a serious problem to the non-rela-

tivistic quark model (cf. sections 1.7, 1.8).

2. Since the photoproduction of η's through the F_{15} (1688) appears to be strongly suppressed[21], as can be understood in terms of the proper SU(3) Clebsch-Gordan coefficients[22], we may be able to see whether the shoulder apparent in <u>Fig. 1.5-3</u> for the 50° cross-section at 1.1-1.2 GeV is due to decay of the S_{11} (1709) isobar, whose presence is hard to detect in π photoproduction (cf. section 1.3). Its presence again poses problems for a quark model interpretation of the photoexcitation of nucleon isobars.

1.5 B. K Photoproduction

The photoproduction cross-sections of K mesons are relatively poorly known when compared with π or even η. K^{+} production, for which the most data exist, shows no suggestive bump structure as we would expect from the previously mentioned data; specifically, there is no convincing evidence for the decay of the $F_{15}(1688)$ into $K^{+}\Lambda$ or $K^{+}\Sigma$, which we would expect to see (the kinematic threshold excludes the lowest isobar).

In principle we expect the phenomenology of K production to run along similar lines to that of π and η production, with proper regard for the isospin and strangeness quantum numbers.

For charged K production, we expect the diagrams
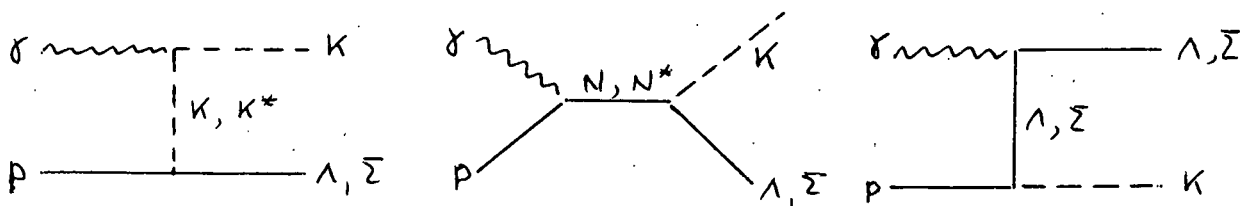
to describe the experimental situation, but the data are too incomplete to allow for a detailed analysis. An additional difficulty is the possibility to produce either a $K^+\Lambda$ or a $K^+\Sigma^0$ final state. For charged K's, we can resolve this by looking at the K yield curve as an excitation function.
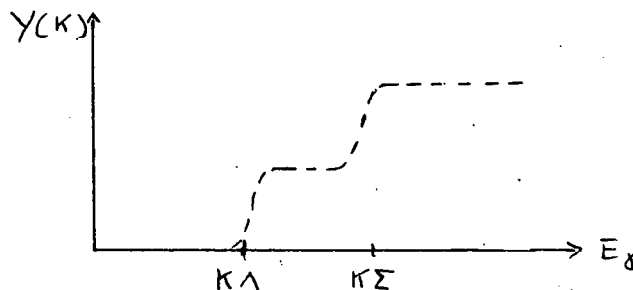
In practice, it is often difficult to separate these final states.

A recent experiment by the Yale group at the CEA[23] has used this excitation function (or "missing mass") technique to investigate the final-state production of strange resonances. Fig. 1.5-4 shows their results as suggestive of the production of various Y_o^*'s according to

$$\gamma p \rightarrow Y^{o*} + K^+ \qquad (1.5-1)$$
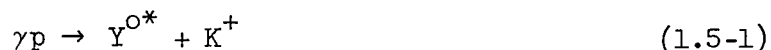
Their results for Y^*'s up to masses of ~2600 MeV coincide largely with recent measurements of the K^--p total cross-section. (The proper subtraction of multiparticle backgrounds is always a difficult problem in such experiments).

A similar experiment by the same group switched the polarity of the spectrometer magnets and looked for K^- in search of processes like

$$\gamma p \rightarrow B^{++} (S = +1) + K^- \qquad (1.5-2)$$
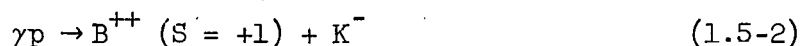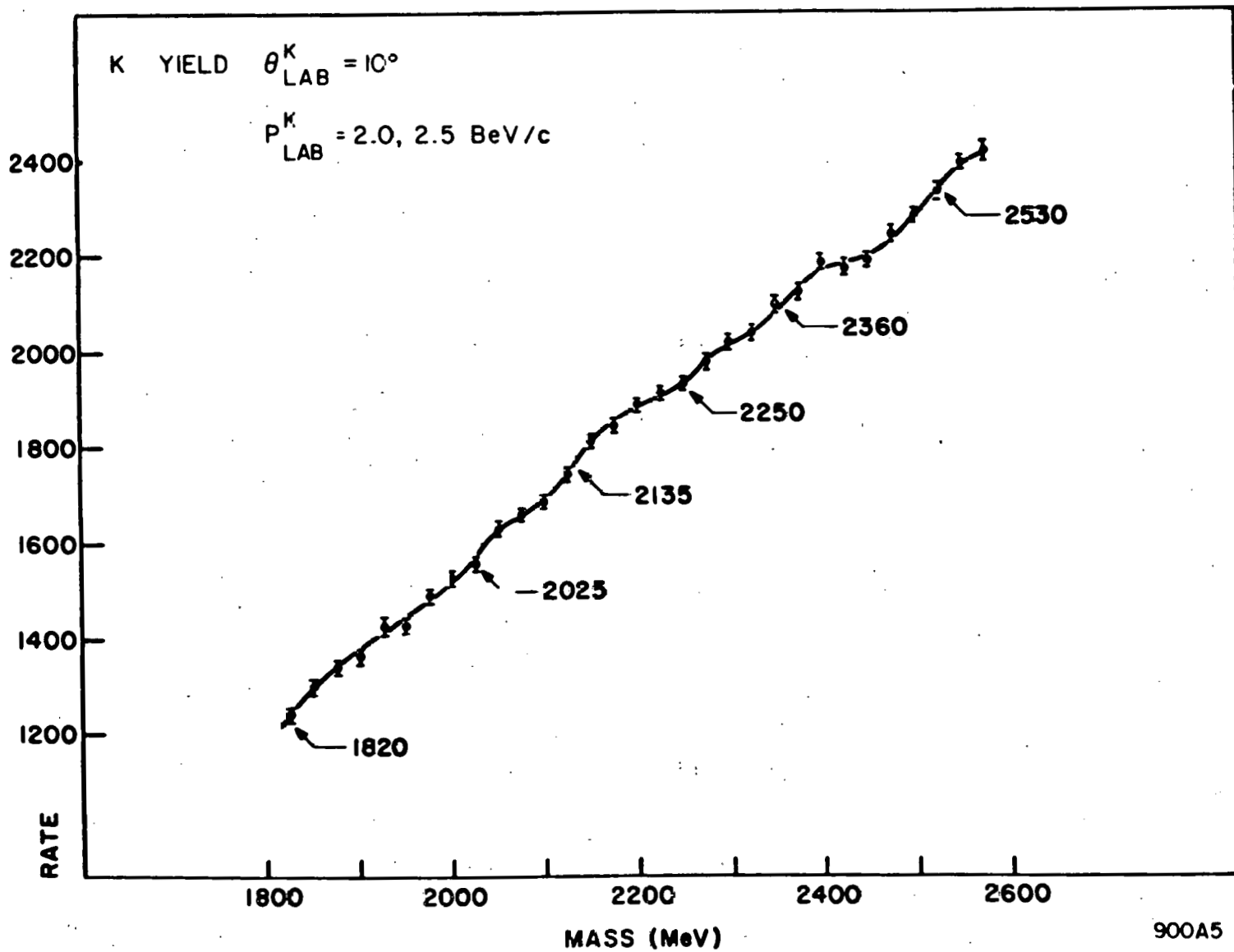
Fig. 1.5-4 K$^+$ excitation curve; data is normalized per equivalent quantum. All data taken at 2.5 BeV/c and 2.0 BeV/c spectrometer settings have been combined on a missing mass scale. (From Ref. No. 23)
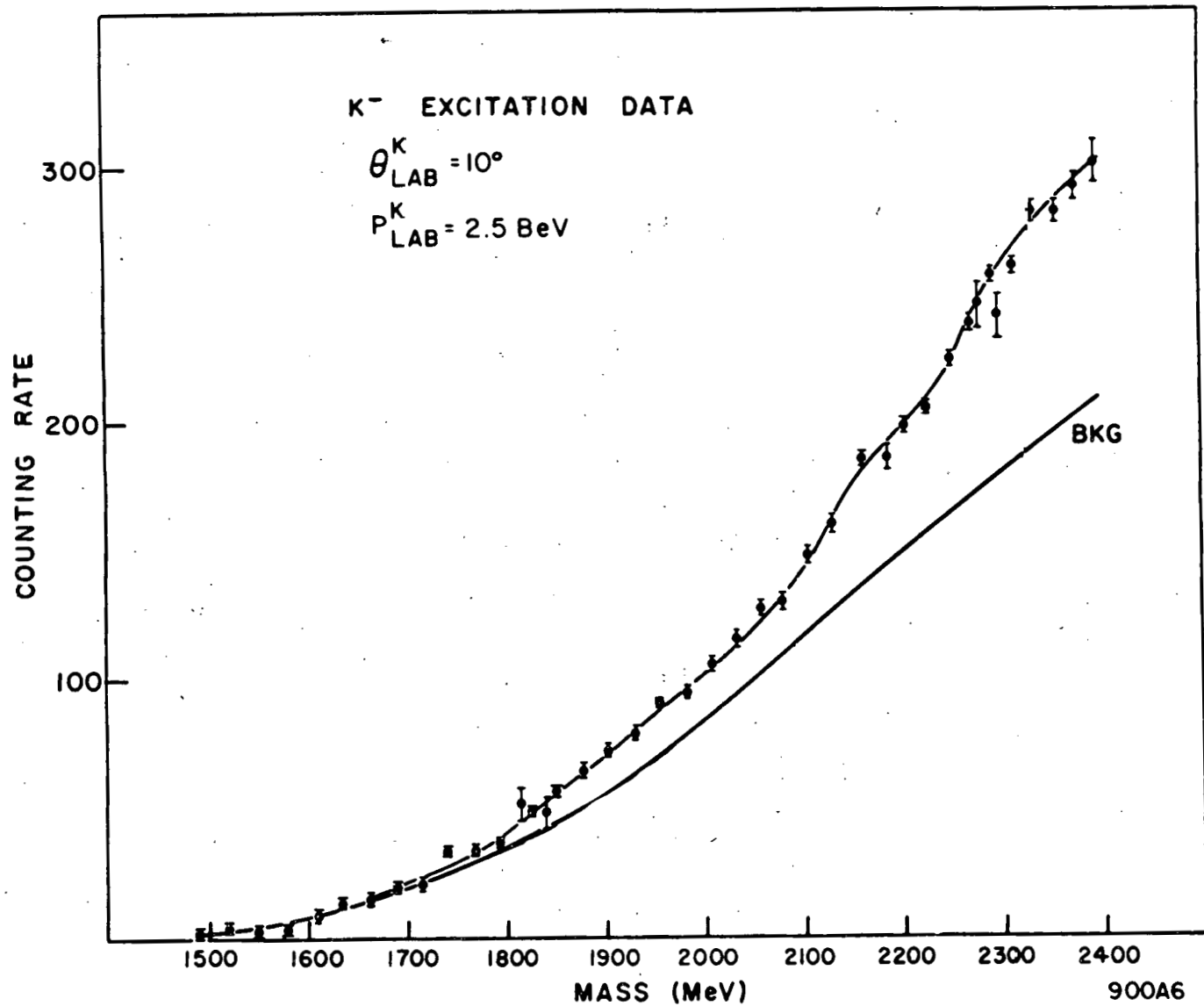
Fig. 1.5-5 K⁻ excitation curve; data is normalized per equivalent quantum.
The solid curve shows estimated background from multiparticle
reactions. (From Ref. No. 23)

A comparable structure in the K^- yield curve would then indicate the photoproduction of doubly charged strangeness +1 particles.

Fig. 1.5-5 may or may not be regarded as evidence for the existence of $S = + 1$ baryons. Because of the seriousness of the problem posed to the quark model by the possible existence of such states, more direct proof is obviously needed (like σ_{tot} (K^+p) measurements, which have been giving similar, but inconclusive, indications). Probably the most extensive use which has been made of the process $\gamma N + KB$ has been the photoproduction of K^0 beams at high-energy accelerators. This is a very important tool of kaon physics, since it provides fairly copious neutral K beams without the curse of heavy neutron contaminations - which are essentially unavoidable around proton accelerators. The K^0 beam at the Stanford Linear Accelerator is certainly one of the more attractive features of that machine. The observed yields probably come largely from the photoproduction of Φ mesons which subsequently decay into K pairs (cf. lecture 2).

1.6 Dispersion Treatment

We have looked at the low-energy data in the photoproduction of pseudoscalar mesons. We saw that simple phenomenological models have a certain amount of success in describing the salient features produced by experiment.

If we want to be more ambitious, we will try and make dynamical models for the photoproduction process. The approach through dispersion relations has had some success at low energies. In the following sections, 1.7 and 1.8, we will briefly describe some recent

successes and failures of the unitary symmetry schemes and the quark model, and some suggestions for experiments to be performed.

The dispersion treatment was the first dynamical model which was able to claim some measure of success. The classic paper of CGLN[9] described the region of the $\Delta(1238)$ isobar and has since been considerably refined (see, for an up-to-date review,(24)). The energy region above ~ 1400 MeV is hardly open to this approach, since the dispersion treatment hinges on the dominance of the highly elastic Δ (1238) state.

The basic assumption is that the relevant invariant amplitudes are analytical functions in s and t; J. Ball[25] demonstrated that we can then express the full amplitudes in terms of the imaginary part, with no additive terms, by the fixed-t, unsubtracted "dispersion relation"

$$A_i(s,t) = \text{pole terms} + \frac{1}{\pi} \int_{(m_N + m_\pi)^2}^{\infty} ds' \, \text{Im } A_i (s',t) \qquad (1.6\text{-}1)$$
$$\times \text{ kinematical factors.}$$

The knowledge of Im A_i then determines the entire reaction amplitude; Im A_i is tied up through unitarity with the intermediate states in the s and u channels; a stable state with spin 1/2 and mass M will show up as

$$\text{Im } A_i(s) \sim \delta (s - M^2) \qquad (1.6\text{-}2)$$

For $J > 1/2$, additional kinematic factors will come in, and for a resonance ($\Gamma > 0$) some Breit-Wigner form will have to be substituted to describe the resonance shape. The important feature is that this treatment not only makes definite statements about the resonant ampli-

tudes, but the non-resonant amplitudes are also completely defined.
In practive, however, calculations are laborious and additional
assumptions are needed; for details we have to refer the student to
the relevant literature.

1.7 Isobars and SU(3)

The conservation or isospin in the strong interactions makes
precise statements about various decay modes of, let's say, the
$\Delta(1238)$. It predicts, e.g., the ratio of $\Delta^+ \to p\pi^0$ to $\Delta^+ \to n\pi^+$.
We can express this in the language of group theory; p and n, π^0
and π^+ belong to irreducible representations of the SU(2) group.
Transformations within the group take us from n to p, from π^+ to
π^0, etc. The practical task is that of finding the proper Clebsch -
Gordan coefficients which link up the amplitudes.

Similarly, higher symmetries can be employed to make correspond-
ing predictions. Recall that, by transformation within the SU(3)
group, we can change π into K or η, p into Λ, Σ, and so on. In the
diagram
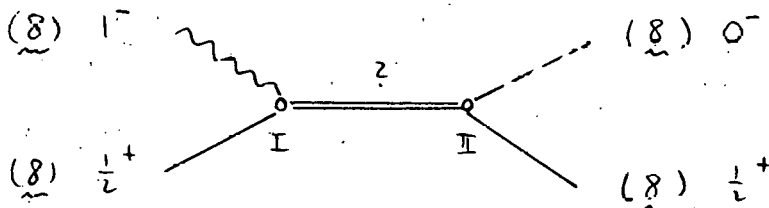
we know the SU(3) assignments for all particles in the initial and
final states (assuming that the photon is established as a U = 0

member of an octet). For nucleon isobars, we do not, in general,
know the SU(3) properties. If we want to make statements about
vertices I or II, we obviously have to establish the multiplet to
which the intermediate state belongs. We know that vertex I will
have to conserve U spin, because it is electromagnetic; vertex II
is strong, and therefore has to conserve SU(3).

If we keep these points in mind (and make the proper allowances
for kinematical effects), we can write down the C-G coefficients to
check against experiment, and maybe decide a posteriori to which
irreducible representation the B^* in question belongs.

Starting from vertex I, U spin conservation postulates that we
photo-excite only U = 1/2 isobars.

$$\gamma p \rightarrow N^* \; (U = \tfrac{1}{2}) \qquad\qquad (1.7\text{-}1)$$

This means that the usual 8 x 8 decomposition

$$8 \times 8 \rightarrow 1 + 8_a + 8_s + 10 + \overline{10} + 27 \qquad\qquad (1.7\text{-}2)$$

has to be scanned for the proper U spin content. This leaves

$$\gamma p \rightarrow 8_a, \; 8_s, \; 10, \; 27$$
$$\gamma p \not\rightarrow 1, \; \overline{10}$$

Let's now specialize to the particular case $\gamma p \rightarrow F_{15}(1688) \rightarrow \eta p$.
Vertex II, $F_{15} \rightarrow \eta p$, has to conserve I spin, which yields (the final
state has I = 1/2) $F_{15} \subset 8_a, \; 8_s, \; 27,$ and excludes 10.

We can now write down the proper CG coefficients for the SU(3)
invariant couplings, and put in appropriate kinematical factors.
This gives a prediction for the ratio

$$R = \frac{\Gamma(F_{15} \to p\eta)}{\Gamma(F_{15} \to p\pi^{o})} = \frac{1}{3} \times \begin{cases} 3 & \text{if } F_{15} \in \underset{\sim}{27} \\ \frac{1}{3}(3 - 4\alpha)^2 & \text{if } F_{15} \in \underset{\sim}{8} \end{cases} \qquad (1.7\text{-}4)$$

(where α is a parameter describing the ratio of $\underset{\sim a}{8}$ to $\underset{\sim s}{8}$).

Experiment then decides that $F_{15} \in \underset{\sim}{27}$ is excluded, $F_{15} \in \underset{\sim}{8}$ is indicated with an α parameter of about 0.6.[22]

We have chosen this example because it shows how the apparent absence of the F_{15} isobar in η photoproduction (cf. previous section) can be accounted for in terms of SU(3) - invariant couplings. Similar arguments can then be used to explain why its decay into $K\Lambda$ also seems to be suppressed. If we assign the $S_{11}(1570)$ to an octet, we can also explain its strong decay into ηp vs. a weaker πp mode, by appropriately choosing the α parameter for this coupling; however, eq.1.7-4 shows that a $\underset{\sim}{27}$ assignment may not be fully excluded because of the copious decay S_{11} (1570) $\to N\eta$.

A special case is the P_{11} (1400), which has so far not been clearly identified in photoproduction. Neither do recent electroproduction data from the SLAC indicate such a photoexcitation[26] in the process $ep \to e' N^{*}$.

This may be due to analysis difficulties which mask the state's appearance, or to the absence of the vertex $\gamma p \to P_{11}$ (1400) altogether (cf. next section). However, there may be some evidence[100] that while $\gamma p \to P_{11}$ is absent, $\gamma n \to P_{11}$ occurs more freely. If this proves to be true, we will have to assign the P_{11} to a $\underset{\sim}{\overline{10}}$ representation of SU(3), since U spin conservation tells us that

$$\gamma p \not\to \underset{\sim}{\overline{10}}; \quad \gamma n \to \underset{\sim}{\overline{10}} . \qquad (1.7\text{-}5)$$

Fuller data on angular distributions and polarization parameters will be needed to decide this question. The simple quark model does not allow for the formation of a low-mass $\underline{\overline{10}}$, so the question is of importance.

1.8 Isobars in the Non-Relativistic Quark Model

Let us assume that we can group low-mass baryons into three-quark configurations with well-defined wave functions. Dalitz showed[27] that we can assign them to L = 0,1,2 (L = total quark angular momentum) states.

The nucleon and Δ are then L = 0 (s) states with the same totally anti-symmetric space wave functions, differing only in the spin and isospin parts.

The photoexcitation $\gamma N \to \Delta$ can then proceed only through the magnetic dipole, isovector excitation of the nucleon. This checks with our results in section 1.3.

Now take L = 1 ("p states"); we find[27] negative-parity states which form octets ^2p_J (where we identify the non-strange states with the nucleon isobar $S_{11}(1570)$ and D_{13} (1527)) and ^4p_J (with which we associate the S_{11} (1709), an unidentified D_{13}, and D_{15} (1670)). The superscripts 2, 4 indicate total quark spin 1/2, 3/2; the subscript J denotes total quark angular momentum, i.e., the spin of the baryon.

Thus, if we calculate[28] the transition matrix elements for the photoexcitation

$$^2s_{1/2} \to {}^2p_J \qquad\qquad (1.8-1)$$

$$^2s_{1/2} \to {}^4p_J \qquad\qquad (1.8-2)$$

we find that process (1.8-1) can proceed freely. For (1.8-2), the transition from quark spin 1/2 to 3/2 cannot be effected by the charge or current operator, but only by the magnetic moment operator.

Sandwiching the operator

$$M = \sum_{1}^{3} \mu_i \, \vec{\sigma}_i \cdot (\vec{k} \times \vec{\epsilon}) \, e^{i\vec{k} \cdot \vec{r}_i} \qquad (1.8\text{-}3)$$

between the appropriate wave functions, Moorhouse[28] showed that the matrix element vanishes for this photoexcitation of protons. For neutrons, no such statement can be made. The prediction is then that

$$\gamma p, n \rightarrow {}^2p_J \qquad \text{is allowed}$$

$$\gamma p \rightarrow {}^4p_J \qquad \text{is forbidden} \qquad (1.8\text{-}4)$$

$$\gamma n \rightarrow {}^4p_J \qquad \text{is allowed}$$

As we showed in sections 1.3 and 1.5, experimental evidence indicates that

$$\gamma p \rightarrow ({}^2p_J) \; S_{11} \; (1570), \; D_{13} \; (1527) \text{ is definitely observed;}$$

$$\gamma p \rightarrow ({}^4p_J) \; S_{11} \; (1709), \; D_{15} \; (1670) \text{ has not been established.}$$

The limits on the latter statement are not reliable, and η production may modify our evidence on the photoexcitation of S_{11} (1709).

We can treat the L = 2 states similarly, and show that the F_{15} (1688) may be freely excited in this model.

What about the P_{11} (1400)? It is usually assigned to a ${}^2s_{1/2}$ configuration with totally symmetric space wave-function.[27] In this case, the transition $\gamma N \rightarrow P_{11}$ can be brought about only by a magnetic dipole. But the matrix element corresponding to this

excitation vanishes because the totally antisymmetric nucleon wave
function is orthogonal to the P_{11} space part.

Should further experiments in π and η production confirm the
absence of the P_{11}, then we can understand it in these terms. Should
we find, however, that $\gamma n \rightarrow P_{11}$ exists while $\gamma p \rightarrow P_{11}$ does not, so
that we have to assign this state to a $\underline{\overline{10}}$ in SU(3), then the frame-
work of this chapter does not apply anyway, because the qqq configur-
ation leads only to $\underline{1}$, $\underline{8}$, and $\underline{10}$ representations.

We will close this lecture by remarking that the study of the
photoexcitation of nucleon isobars still leaves a number of open
questions. Their solution will have an important bearing on our
understanding of some aspects of the strong interactions, and on the
credibility of various models used to describe them.

Lecture 2 Photoproduction of Vector Mesons.

2.1 Models for the Photoproduction of Vector Mesons.

We now turn to the photoproduction of mesons with spin-parity
quantum numbers 1^-. We will restrict our attention to the production
of vector mesons of hypercharge zero (S=Y=0), ρ, ω, Φ. Recall from
section 1.1 that the general production diagram for the neutral Y=0
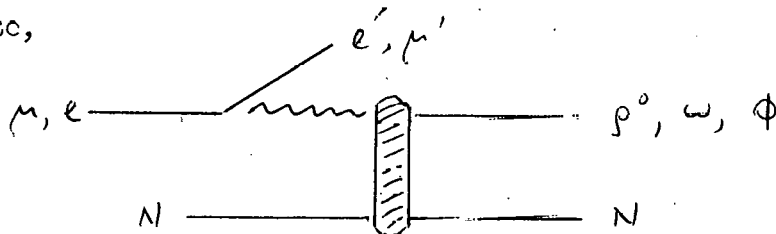vector mesons is distinguished by the fact that no quantum numbers
need be exchanged between the top and bottom line of
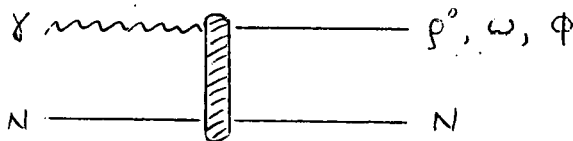
For incoming real photons, with helicity ± 1, we have to heed the
massiveness of the 1^- mesons and an additional possibility of spin
orientation (helicity 0, ± 1). For virtual photons in the initial
state,

the photon-vector meson analogy is obviously more complete
($\lambda_k = 0, \pm 1$). Recently, a fair amount of experimental material on
cross-sections, and some on polarization parameters, has become
available. Before we review this in sections 2.2-2.4, let us take
a brief look at the possible mechanisms for the process $\gamma N \to NV$.

1. Decay of isobars.

Analogous to the isobar diagrams which dominate low-energy π
photoproduction, we expect diagrams like
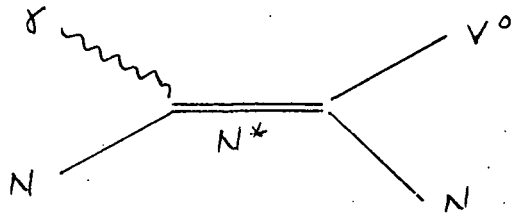
to exist in vector production. However, the lowest-mass isobar whose rest mass will permit the decay $N^* \to N\rho$ is the Δ (1920). For isobars of masses > 2 BeV, two-body decay modes are probably not dominant. (In section 2.6, we will look at attempts to link up the $N\rho$ and $N\gamma$ decays of isobars, connecting the two vertices which make up the mechanism for $\gamma N \to N^* \to N\rho$).

As in π production, characteristic angular distributions are expected from the decays of isobars of given J. Moreover, the isospin decomposition of the ρN system, $|I, I_3 > (\rho,N)$:

$$| 1, o > | \tfrac{1}{2}, \tfrac{1}{2} > = \sqrt{\tfrac{2}{3}} | \tfrac{3}{2}, \tfrac{1}{2} > - \sqrt{\tfrac{1}{3}} | \tfrac{1}{2}, \tfrac{1}{2} > \qquad (2.1\text{-}1)$$

makes us look for the decay of I = 3/2 resonces (Δ's) into ρN, rather than that of I = 1/2 states. Δ(1920) and Δ(2420) are obvious candidates.

2. One pion exchange (OPE).

The experimentally observed decay $V \to \gamma\pi$ indicates that the diagram
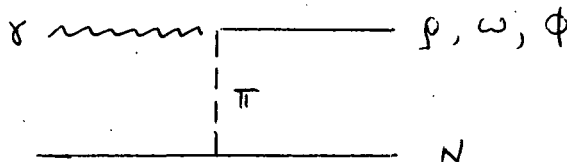
will play a part in vector meson production, and we can link the upper vertex to the radiative decay widths $\Gamma(\rho, \omega, \Phi \to \pi\gamma)$. If we neglect kinematical corrections due to the mass differences, and in the absence of absorption corrections, we expect a cross-section ratio for the photoproduction of the vector mesons:

$$\sigma(\rho) : \sigma(\omega) : \sigma(\Phi) = g^2_{\rho\pi\gamma} : g^2_{\omega\pi\gamma} : g^2_{\Phi\pi\gamma} \qquad (2.1-2)$$

Then the usual assignment of the photon as the $U = 0$ member of an $SU(3)$ octet, the conventional mixing of the $I = 0$ vector mesons according to

$$|\omega\rangle = \cos\Theta \,|\omega_1\rangle - \sin\Theta \,|\Phi_8\rangle$$

$$|\Phi\rangle = \sin\Theta \,|\omega_1\rangle + \cos\Theta \,|\Phi_8\rangle \qquad (2.1-3)$$

(with $|\omega_1\rangle, |\Phi_8\rangle$ the pure singlet and octet $I = 0$ states), plus the assumption that the $V\pi\gamma$ vertices conserve $SU(3)$, yield a sum rule for the coupling constants:

$$\sqrt{3}\, g_{\rho\pi\gamma} = \sqrt{\frac{2}{3}}\, g_{\Phi\pi\gamma} + \sqrt{\frac{1}{3}}\, g_{\omega\pi\gamma} \qquad (2.1-4)$$

Here, we have taken mixing angles from the Gell-Mann-Okubo mass formula, $\cos^2 \Theta = \frac{2}{3}$.

Experimentally, the decay $\Phi \to \pi\gamma$ has not been observed. Several arguments have been presented to explain this feature; the most straight-forward comes from the quark model: if the electromagnetic transition proceeds via emission of a photon by one quark, then the quark structure of the Φ (which consists of two strange quarks, $\lambda\bar{\lambda}$) forbids the vertex $\Phi\pi\gamma$ (two non-strange quarks make

up the π).

This leaves us with the distinctive OPE prediction that $g^2_{\omega\pi\gamma} = 9g^2_{\rho\pi\gamma}$ and therefore

$$\sigma\,(\omega)_{OPE} = 9\,\sigma\,(\rho)_{OPE} \qquad\qquad (2.1\text{-}5)$$

We also expect, from $g^2_{\Phi\pi\gamma} \approx 0$, that $\sigma(\Phi)_{OPE} \ll \sigma(\rho,\omega)_{OPE}$.

3. Diffraction mechanism.

We note that the diagram
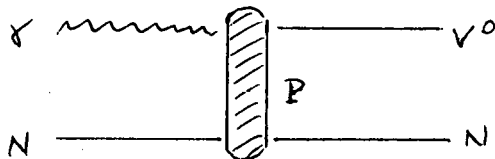
may proceed through the exchange of a system P with the quantum numbers of the vacuum. This can then be viewed in strict analogy with high-energy elastic scattering of π's or K's off protons. We therefore expect a diffraction-like picture to ensue at high energies. The distinctive features of diffractive processes like these are then the following, known from high-energy $\pi^{\pm} p \to \pi^{\pm} p$.

I) $\dfrac{d\sigma}{dt} \approx a\,e^{bt}$ where $\begin{cases} \dfrac{d\sigma}{dt}\Big|_{t\,=\,0,} = a \\ b \text{ is of order 8-10 } (\text{GeV}/c)^{-2} \end{cases}$

and $\quad \dfrac{d\sigma}{d\Omega}\,(0^{\circ}) \propto k^2$

II) $\sigma_{tot} \to$ const. at high energies,

III) The forward amplitude is purely imaginary. (cf. eq. 2.1-7)

We also expect diffractive photoproduction to proceed coherently on nuclei, with a corresponding dependence of the parameter a

on the atomic number A of order $a \sim A^{>1}$.

The characteristic diffraction peak can be seen as resulting from a coherence condition[29] at high energies: the process most likely to occur in high-energy γN collisions is inelastic meson production. Elastic scattering, whenever appreciably large, is essentially shadow scattering due to the existence of these inelastic channels. It can therefore be approximately described in terms of sums over inelastic processes (running either way). In fact, the forward peak is then due to the coherence criterion that each inelastic channel, f_{an}, return to the initial state, a, via the amplitude f_{na}; this yields for the "shadow" amplitude:

$$\text{Im } f_{aa} = \sum_n f_{an} \, f_{na}^* \, \delta^4(p_n - p_a)$$

$$= \sum_n (f_{an})^2 \, \delta^4(p_n - p_a)$$

(2.1-6)

In terms of a Regge pole analysis, we look at the exchanged object in the diffraction diagram as the vacuum trajectory P. This, the Pomeranchuk trajectory, has, for forward scattering, the angular momentum $\alpha(t = 0) = 1$. We therefore find for the amplitude

$$A(t) \sim i \, s^{\alpha(t)}$$

$$A(t \to 0) \sim i \, s \quad (\alpha(t \to 0) \approx 1) \qquad (2.1-7)$$

Then, if the trajectory $\alpha_p(t)$ has a positive slope, we expect for the physical region, $t < 0$,

$$\alpha(t < 0) \, / \, \alpha(0) < 1. \qquad (2.1-8)$$

This leads to the well-known shrinkage of the diffraction peak. Failure of the data to produce evidence for this shrinkage has to be taken as evidence that either the P trajectory has a small slope (or zero slope: fixed pole at $J = 1$); or that other trajectories contribute in addition.

In the context of SU(3), P is a unitary singlet. Then with the assumptions on the symmetry properties of photon and V^O's as above, SU(3) predicts the cross-section relation

$$\sigma(\rho)_{diff.} : \sigma(\omega)_{diff.} : \sigma(\Phi)_{diff.} = 3 : \sin^2 \theta : \cos^2 \theta$$

$$= 9 : 1 : 2 \qquad (2.1\text{-}9)$$

Notice that the prediction is diametrically opposed to the OPE picture, where ω production is much more abundant than ρ^O production. For a clean test of the OPE picture, we would have to resort to a process which cannot also proceed diffractively, like $\gamma p \rightarrow V^O \Delta^+$, where we then expect

$$\frac{\sigma(\gamma p \rightarrow \Delta^+ \omega)}{\sigma(\gamma p \rightarrow \Delta^+ \rho^O)} \Bigg|_{OPE} \approx 9 \qquad (2.1\text{-}10)$$

For the total production cross-section, due to the OPE graph, we expect an energy dependence of order k^{-2} (cf. ref. 42),

The OPE and diffraction pictures leave us with some specific, and contradictory, predictions on production rates. Let us keep in mind that we had to make certain assumptions in order to arrive at these predictions.

The next three sections will present some experimental data, and in section 2.5 we will attempt to arrive at a unified picture.

2.2   ρ Photoproduction.

The isovector ρ meson $(J^{PG} = 1^{-+}, C = -1)$ has been widely studied, in photoproduction, in its neutral charge state. This is due to its ample production rate and to its simple and distinctive final state $\pi^+\pi^-$. The other charge states $(\rho^{\pm} \to \pi^{\pm}\pi^0)$ have a neutral in the final state and are therefore harder to observe. Few data exist; and since our interest lies largely in the analogy photon - (neutral) vector meson, we will restrict our treatment here to the $I_3 = 0$ state.

Although the $\pi^+\pi^-$ final state is easy to detect both in bubble chamber and in counter experiments, the presence of other mechanisms that can produce these, makes an unambiguous determination of mass and width of the ρ^0 difficult. Fig. 2.2-1 shows the total cross section, at energies up to ~ 5.5 GeV, for the process

$$\gamma p \to p\pi^+\pi^-, \qquad (2.2-1)$$

where the dominant contributions come from

$$\gamma p \to \left. \begin{matrix} \Lambda^{++}\pi^- \\ \Delta^0\pi^+ \end{matrix} \right\} \to p\pi^+\pi^-, \qquad (2.2-2)$$

$$\gamma p \to p\rho^0 \to p\pi^+\pi^-. \qquad (2.2-3)$$

In order to disentangle the total $p\pi^+\pi^-$ yield, a Dalitz plot of invariant masses $m^2(p\pi^+)$ vs. $m^2(\pi^+\pi^-)$ can be made to show that, at low energies, there are three terms to be taken into account, i.e. processes 2.2-2, 2.2-3, and a non-resonant background. Putting in
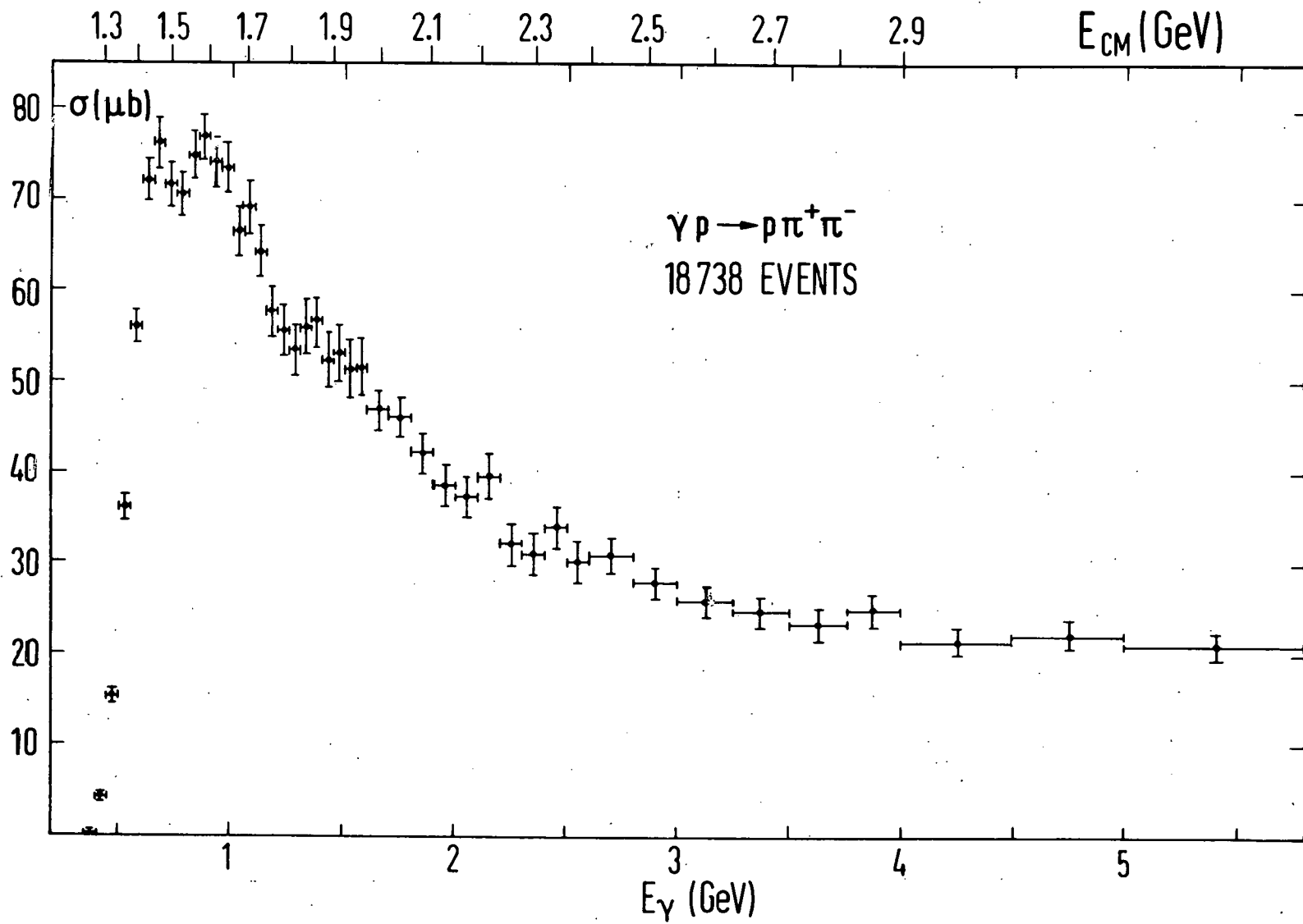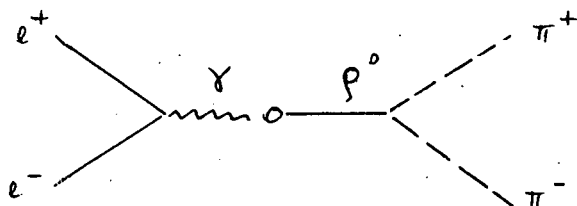
Fig. 2.2-1 Total cross-section for $\pi^+\pi^-$ photoproduction on protons. (From Ref. No. 19)

appropriate expressions for the resonance contributions, the Δ^{++} term can be separated out. The remaining problem is the discrimination of ρ production from the uncorrelated background. Fig. 2.2-2 shows the ρ yield as a function of photon energy, using three different fitting procedures. The two mass distribution functions that gave good fits to the bubble chamber data at intermediate energies $(1.5 \leq k \leq 5.5 \text{ GeV})$ are characterized by

a) A Breit-Wigner distribution multiplied by a mass-skewing factor $\left(\dfrac{m_\rho}{m_{\pi\pi}}\right)^4$ from the diffraction dissociation model of Ross and Stodolsky[30]; it ought to be stressed that this factor is <u>not</u> a necessary ingredient of the diffraction picture.

b) A Breit-Wigner distribution with energy-dependent width interfering with a background of slowly varying phase[31]. This model also assumes a purely imaginary forward amplitude for ρ^0 production, as in the diffraction mechanism.

Both of these fits tend to lower the resulting mass value for the ρ. It is important to keep in mind that the mass and width parameters for the ρ are strongly dependent on the fitting process chosen, and therefore differ appreciably between various experiments. The most reliable experimental results on m_ρ, Γ_ρ were recently quoted by Auslander et al.,[32] who used e^+e^- collisions to study the process
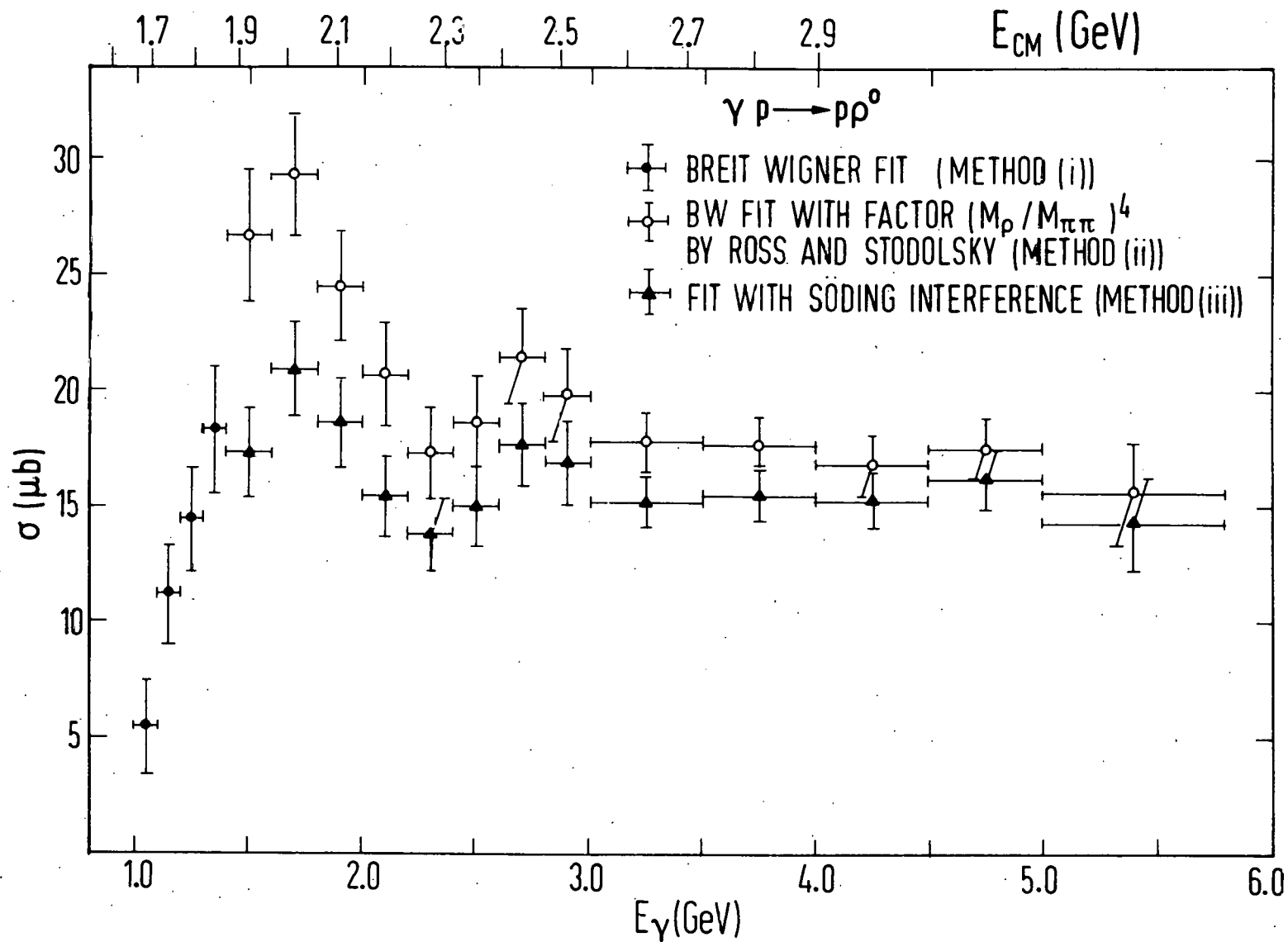
Fig. 2.2-2 Total cross-section for the process $\gamma p \to p\rho^0$. Values vary according to
fit employed for separation of these data from those shown in Fig. 2.2-1.
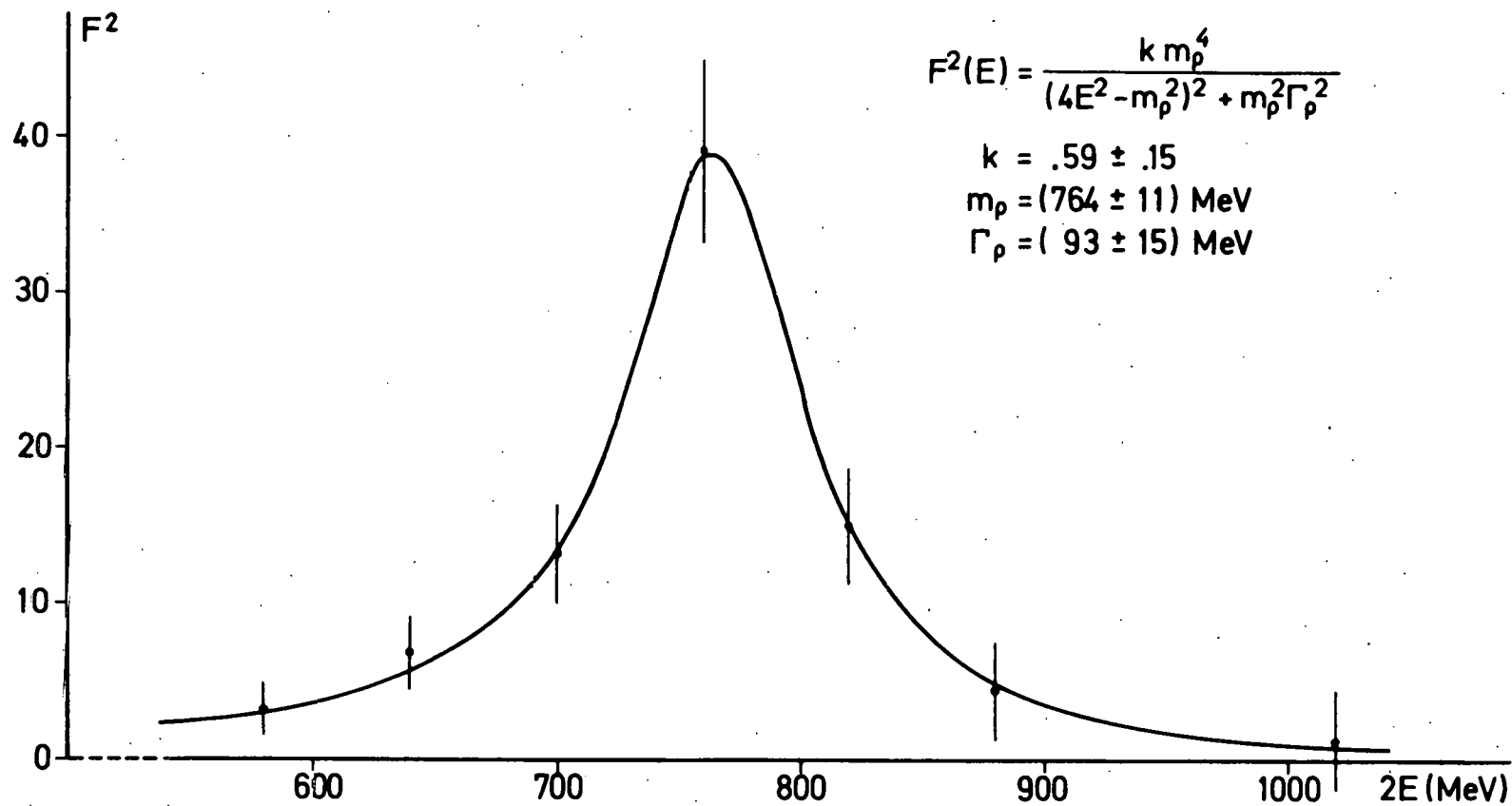Bubble chamber data. (From Ref. No. 19)

and found (cf. Fig. 2.2-3) $m_\rho = 764 \pm 11$ MeV, $\Gamma_\rho = 93 \pm 15$ MeV. This compares with photoproduction results of $m_\rho \approx 770$ MeV, $\Gamma_\rho \approx 150$ MeV. There is at present no full understanding for the difference in these parameters as resulting from e^+e^- annihilation and photon-hadron or hadron-hadron collisions.[33] However, it is certainly not surprising that the width parameter of a particle with the lifetime of the ρ should be sensitive to the difference between strong and electromagnetic formation processes.

The results of the bubble chamber data at DESY and CEA can be summarized as follows:

1. At lower energies, $k \leq 2.8$ GeV, there is some structure in the cross-section. The differential cross-section $\frac{d\sigma}{dt}$ shows some diffraction-type behavior (Fig. 2.2-4) plus more isotropic contributions, presumably from isobar decay (cf. section 2.1). We can take out events in the forward, diffraction-peak, region, and look at the remaining events. Fig. 2.2-5 shows a suggestive peak at the location of the $\Delta(2420)$ isobar, and an enhancement below 2 GeV which may be due to $\Delta(1920)$ decay and/or an OPE contribution.

2. At high energies, the diffraction picture appears to describe the experiment well. The forward cross-section can easily be fitted by an expression of the type

$$\frac{d\sigma}{dt}(\gamma p \to p \rho^0) = a\, e^{bt}$$

$$\text{with} \left\{ \begin{array}{l} a \approx 140 \ \mu b/GeV^2 \\ b \approx 8 \ GeV^{-2} \end{array} \right\} \qquad (2.2\text{-}4)$$

$$F^2(E) = \frac{k\, m_\rho^4}{(4E^2 - m_\rho^2)^2 + m_\rho^2 \Gamma_\rho^2}$$

$$k = .59 \pm .15$$
$$m_\rho = (764 \pm 11)\ \text{MeV}$$
$$\Gamma_\rho = (93 \pm 15)\ \text{MeV}$$

Experimental values of $F^2(E)$ approximated by the Breit-Wigner formula

<u>Fig. 2.2-3</u> ρ resonance shape as observed in first storage ring experiment $e^+ e^- \to \rho^0$, in Novosibirsk. (From Ref. No. 32)
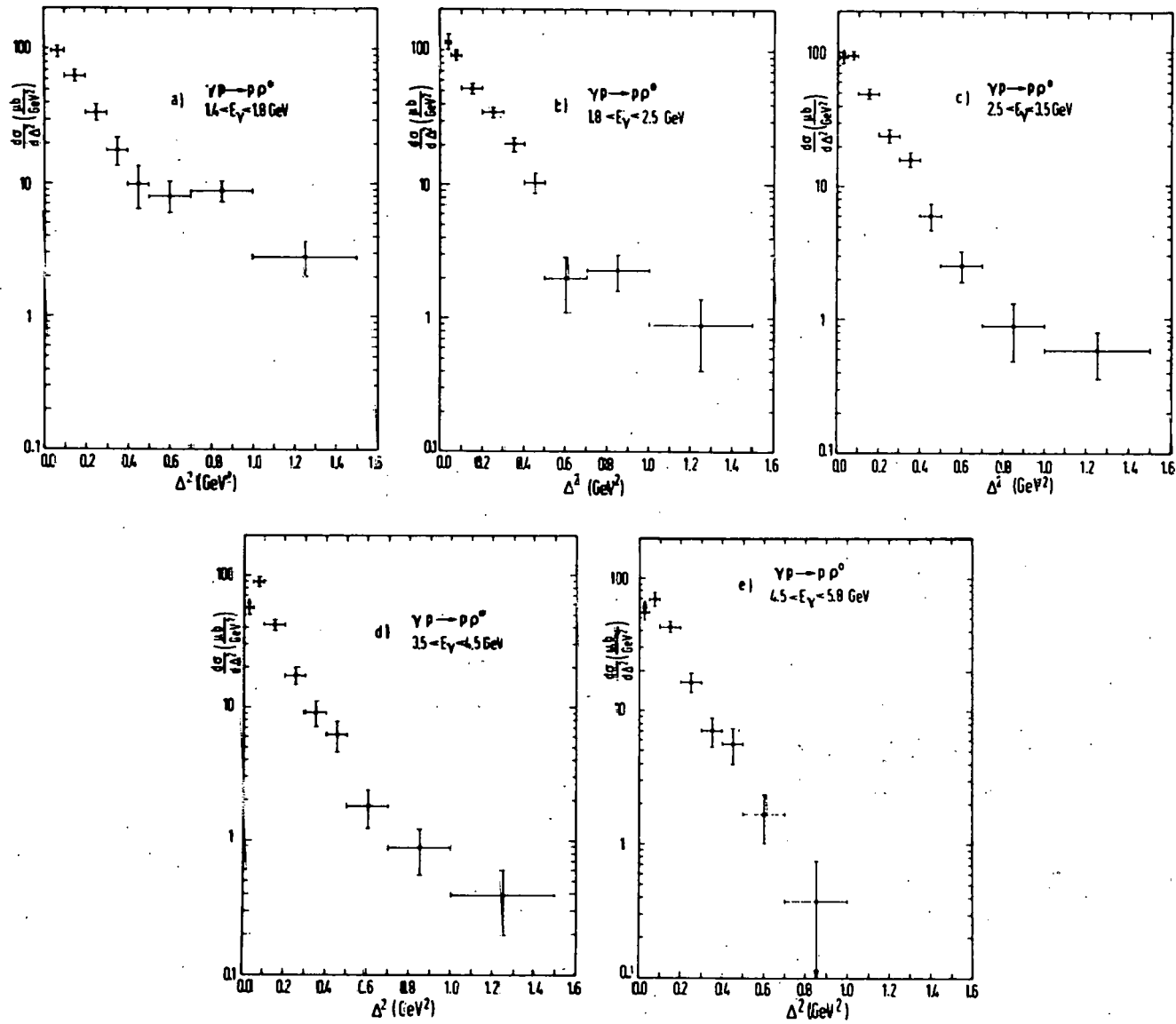
Fig. 2.2-4 Differential cross-sections $\frac{d\sigma}{d\Omega}$ for ρ photoproduction. Bubble chamber data. (From Ref. No. 19)
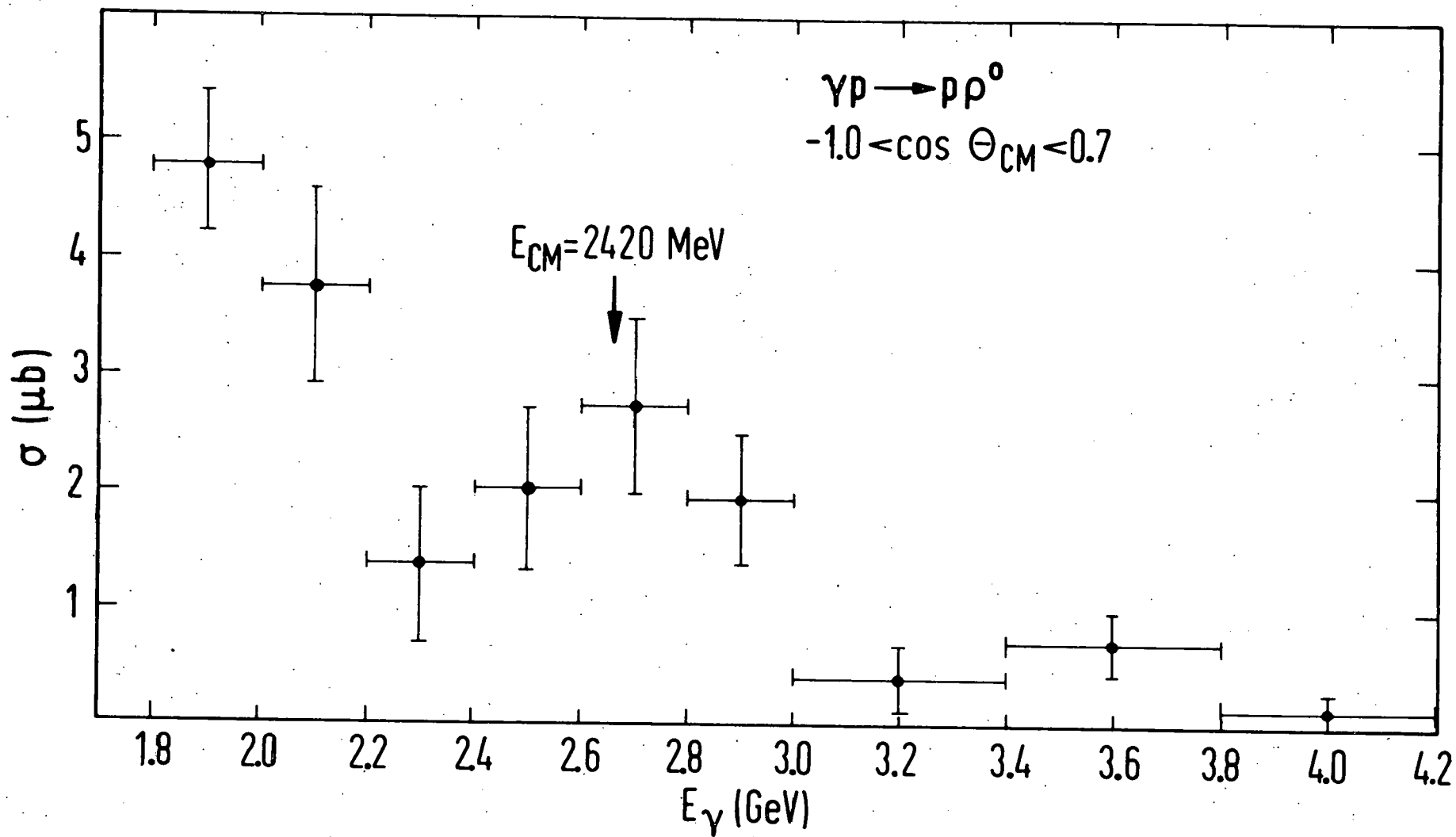
Fig. 2.2-5 Total cross-section for $\gamma p \to p\rho^{o}$, excluding forward (diffraction) production. (From Ref. No. 19)

For precise numbers, cf. Table I. The total cross-section remains roughly constant at 15 μb between 3 and 6 GeV.

3. The decay angular distributions are (conveniently expressed in terms of the helicity density-matrix elements ρ_{ik} of the ρ's) such that one cannot draw any strong conclusions as to the models proposed. In particular, predictions of the "strong absorption model" used by the CEA group[34], incorporating diffraction scattering off a spin-independent potential, seem to be at best partially met (for details we have to refer to the relevant literature[34, 19, 35]).

There are several recent counter experiments reporting ρ^o photoproduction results to complement this picture. Since they employed very different techniques to detect the $p\pi^+\pi^-$ final state, let's have a short look at them.

1. Closest in technique to the bubble chamber experiment is the observation of three-charged-prong events in a streamer chamber, recently reported from SLAC by Davier et. al.[36]. A thin hydrogen-filled reaction tube inside a large streamer chamber allowed the determination of the kinematics fairly completely. This is a new technique, distinguished from the bubble chamber approach by the possibility of triggering the detection system selectively. Although, in this first experiment with such an instrument, there still remain some problems and possible biases, several interesting features result from the analysis of $\approx$ 850 $p\pi^+\pi^-$ events, at photon energies from 6.5 to 17.8 GeV:

Table I. Data on Vector Mesons - Photoproduction and Decay Widths

Parameters (units)	ρ^O	ω	Φ	Experiment at E_γ (GeV)
m (MeV)	764 ± 11	783 ± 0.7	1019 ± 0.6	(Rosenfeld tables)
Γ (MeV)	100 ± 12	14.0 ± 2.4	4.2 ± 0.9	$e^+e^- \to V^O$ (Orsay)
	130 to 150	12.2 ± 1.3	3.4 ± 0.8	hadronic interactions
$\frac{d\sigma}{dt}$ $(\gamma p \to pV^O) = a\,e^{bt}$ a (μb GeV^{-2})	140 ± 12	28.4 ± 5.2	1.6 ± 0.6	} bubble chamber < 6
	125 ± 15			
	140 ± 50			counter, spark chamber < 6
	$\approx 80 \pm 30$			spectrometer
b (GeV^{-2})	8 ± 0.7	7.6 ± 1.2	3.5 ± 0.9	bubble chamber < 6
	8.1 ± 1.5			counter, spark chamber
	≈ 10			
	≈ 8.5			} spectrometer 6 - 18
σ_{tot} $(\gamma p \to pV^O)$ (μb)	17.8 ± 2.0	4.8 ± 0.8	0.41 ± 0.14	} bubble chamber
	15.0 ± 2.0	3.1 ± 0.7	0.45 ± 0.13	
	14.6 ± 1.8			spark chamber
		diffraction part: $\approx 1.7 \pm 0.9$		from bubble chamber data
σ_{tot} $(V^Op \to all)$ (mb)	31.7 ± 2.3		$13.4 \pm$	from bubble chamber < 6
			9.7 ± 2.0	and
			$7.2 \pm$	from spectrometer data [13, 16]
	28	28	11.5 ± 1.5	from quark model, πN, KN data
Γ $(V^O \to e^+e^-)$ (keV)	6.4 ± 0.72	1.1 ± 0.25	1.3 ± 0.21	Orsay $e^+e^- \to V^O$
	(similar values from many other experiments)		1.1 ± 0.33	DESY $V^O \to e^+e^-$
		0.49 ± 0.19	2.1 ± 0.9	CERN $V^O \to e^+e^-$

Note that the quoted results are neither complete nor given for all energy intervals.

To fit the $\pi^+\pi^-$ mass distribution well, a ρ Breit-Wigner form has to be multiplied by the mass-skewing factor $\left(\dfrac{m_\rho}{m_{\pi\pi}}\right)^4$, as mentioned above.

Above 6 GeV, a diffraction picture describes the data best, with the ρ decay angular distribution such that it may agree with the strong absorption model mentioned above.

At energies above $\approx$ 6 GeV, the $p\pi^+\pi^-$ final state appears to be completely dominated by $\rho^0 p$ production, with other resonant $\pi^+\pi^-$ states assigned an upper limit of 0.2 µb.

2. Blechschmidt et. al.[37] at DESY used a large magnet-spark chamber system in conjunction with a photon tagging facility to study ρ^0 production. They were thus able to have information on incoming photon energies good to $\pm$ 50 MeV. Taking data from 3.2 to 4.9 GeV on three target materials (H, C, Aℓ), they studied the A dependence of the diffraction-type behavior. Their results indicate:

They find ρ masses of $\sim$ 770 MeV, including the $\left(\dfrac{m_\rho}{m_{\pi\pi}}\right)^4$ factor, with a width of order 120 MeV.

Fitting the data to the form $\dfrac{d\sigma}{dt} = a\,e^{bt}$, they find a dependence on the mass number A of

$$a \sim A^{1.68} \qquad\qquad (2.2\text{-}5)$$

$$b \sim A^{2/3} \qquad\qquad (2.2\text{-}6)$$

confirming the diffraction picture. For a completely opaque nucleus, we would expect $a \sim A^{4/3}$ while a transparent nucleus would lead to $a \sim A^2$. Assuming that the exponential can be used to determine the total cross-section, they quote

$$\sigma_{tot} \ (\gamma p \to \rho p) = 14.6 \pm 1.8 \ \mu b \qquad (2.2\text{-}7)$$

3. Asbury et al[38] (DESY - Columbia) used a two-arm spectro-
meter to look for the charged π pairs from the process

$$\gamma + A \to A + \pi^+\pi^- \qquad (2.2\text{-}8)$$

using target materials A = Be, C, Al, Cu, A, Pb. Studying forward
production with their highly selective detection system, they found
no $\pi^+\pi^-$ enhancement other than the ρ^o at invariant masses between
0.35 and 1.2 GeV/c^2. According to the diffraction model, the forward
coherent production cross-section for nuclei can be written as

$$\frac{d\sigma}{d\Omega}\bigg|_0 = C(A) \times p_\rho^2 \times f'\ (p_\rho) \times f_T\ (R,t,\sigma_{\rho N}) \qquad (2.2\text{-}9)$$

where C is a constant, f' is proportional to the total πN cross-
section $\sigma_{\pi N}$, and f_T is a function of the nuclear radius $r = r_o A^{1/3}$,
the momentum transfer, and the ρN total cross-section. If we assume
coherent production in the forward direction, and a uniform nuclear
density inside a sphere of radius R, we can extract the nuclear
radius r_o and the ρN total cross-section $\sigma_{\rho N}$ from the experimental
data. We just have to measure $\frac{d\sigma}{dt}$ as a function of one of the known
dependencies on A, t, or p, the others being kept constant.
Fig. 2.2-6 shows the A dependence (normalized to Be), at three
energies, of the cross-section per nucleon. The resulting best values
for r_o and $\sigma_{\rho N}$ are

$$r_o = 1.29 \pm 0.4 \ f, \qquad (2.2\text{-}10)$$

$$\sigma_{\rho N} = 31.7 \pm 2.3 \ mb. \qquad (2.2\text{-}11)$$

$$\left(\frac{1}{A}\frac{d\sigma}{d\Omega}\right)\Bigg/\left(\frac{1}{9}\frac{d\sigma}{d\Omega}\right)_{Be}$$

2.0

1.8

1.6

1.4

1.2

1.0

0.8

P = 4.500 GeV/c
r_0 = 1.35 ± 0.04
$\sigma_{\rho N}$ = 30.7 ± 5.3 mb
χ^2 = 3.6   DF = 3

P = 3.500 GeV/c
r_0 = 1.20 ± 0.12 f
$\sigma_{\rho N}$ = 35.2 ± 9.4 mb
χ^2 = 1.6   DF = 2

P = 2.700 GeV/c
r_0 = 1.23 ± 0.06 f
$\sigma_{\rho N}$ = 31.0 ± 2.6 mb
χ^2 = 1.6   DF = 3

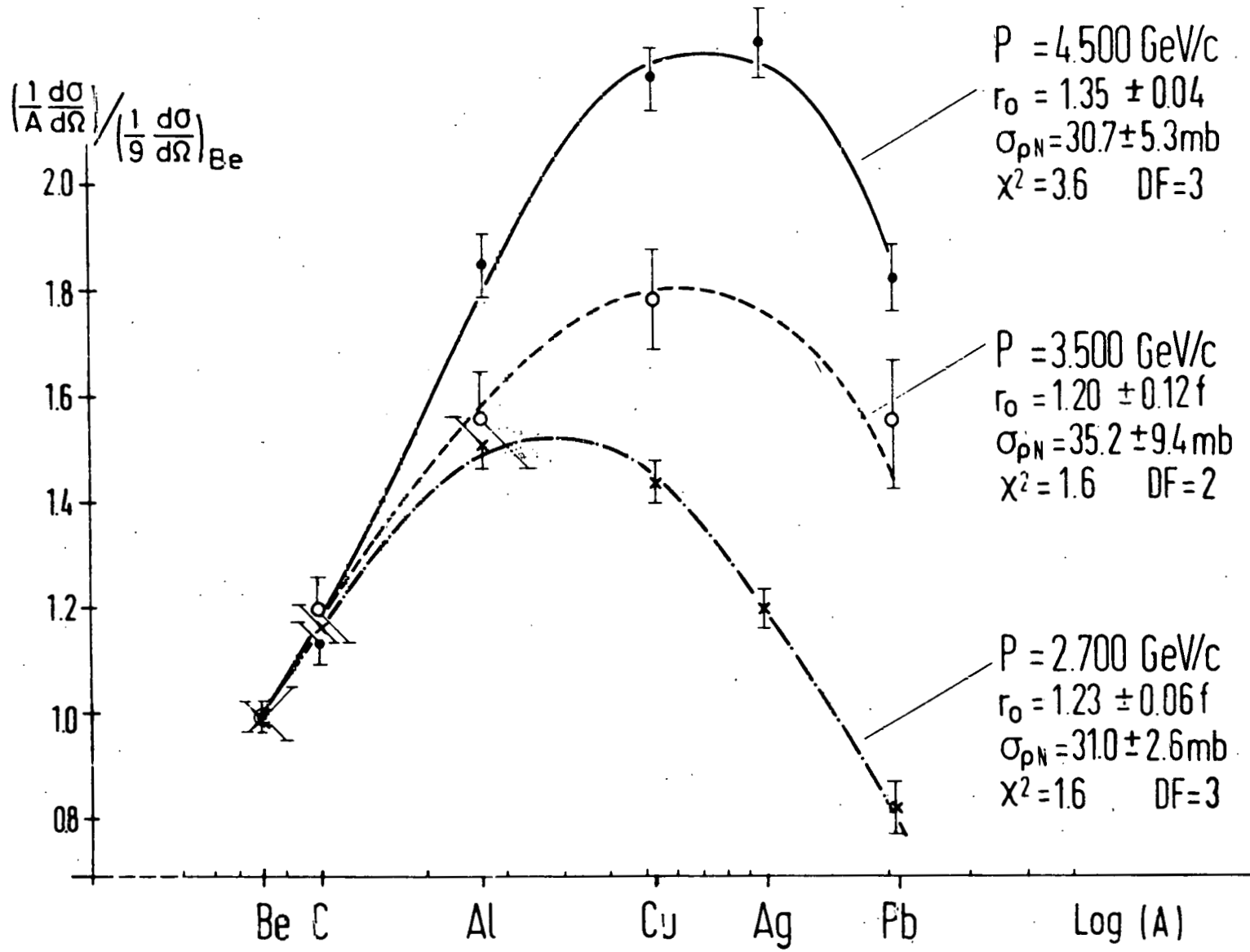Be C   Al   Cu   Ag   Pb   Log (A)

Fig. 2.2-6 Coherent photoproduction of ρ^0 mesons: Dependence of forward differential cross-section per nucleon on the mass number A. Parameters r_0, $\sigma_{\rho N}$ result from fits according to Drell and Trefil. (From Ref. No. 30)

This value for $\sigma_{\rho N}$ compares well with the πN total cross-section, which in the quark model should be the same: at these energies, $\sigma_{\pi N} \approx 30$ mb. The momentum transfer dependence is given in Fig. 2.2-7), for various elements. Again, the diffraction character appears. There may even be diffraction minima and maxima indicated outside the forward peak. Corresponding optical-model calculations by Fleischer[39] have given good agreement. The bottom graph of Fig. 2.2-7 shows the ratio of the πN and ρN forward cross-sections to be constant as a function of momentum.

The forward peak, described by $\frac{d\sigma}{dt} = a \, e^{bt}$, again yields a $b(A)$ dependence of $b = b_o A^{2/3}$ (cf. eq. 2.2-6), with $b_o = 10.5$. Since the diffraction model appears to give credible agreement with experimental features, the forward prediction was also used to get a check on the $\pi\pi$ mass distribution

$$\frac{d^2\sigma}{d\Omega \, dm} = C(A) \, 2m \, R(m) \, f_T \, f' \, (p_\rho) \, p_\rho^2 \qquad (2.2\text{-}12)$$

or, at high energy and small t,

$$\frac{d^2\sigma}{d\Omega \, dm} \approx C(A) \, 2m \, R(m) \, p_\rho^2 \, e^{a(t)}. \qquad (2.2\text{-}13)$$
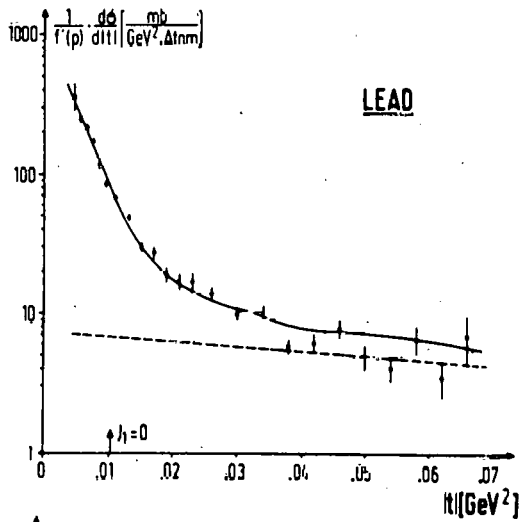
The resulting mass spectra are shown in Fig. 2.2-8, where the best fits again involve the mass-skewing factor $\left(\frac{m_\rho}{m_{\pi\pi}}\right)^4$, a Breit-Wigner distribution, and an empirical background. Best values for the resulting mass and width are $m_\rho = 765 \pm 5$ MeV, $\Gamma_o = 130 \pm 5$ MeV. The width is smaller than the 140 - 150 MeV quoted as bubble chamber results[19].
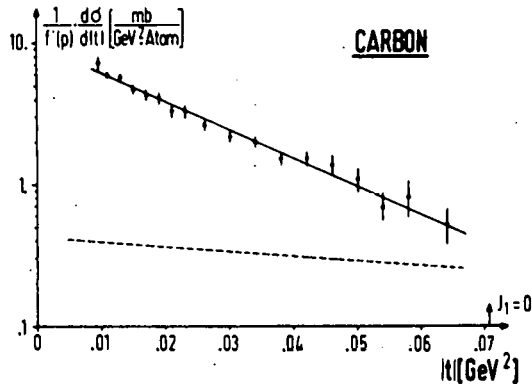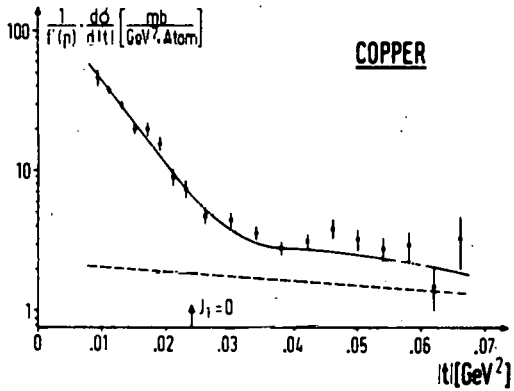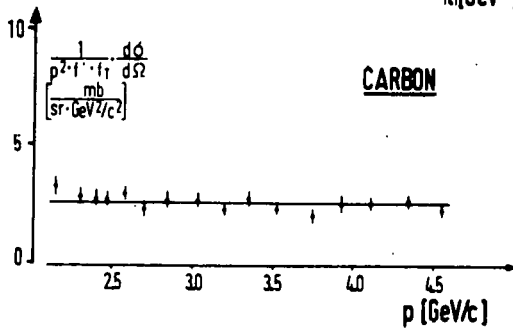
Fig. 2.2-7 Momentum transfer dependence of differential cross-section $\gamma A \rightarrow A\rho^{0}$. $f'(\alpha_{\sigma_{\pi N}})$ has been divided cut. Fit according to Ref. 30. Graph d) compares momentum dependence of $\gamma A \rightarrow A\rho$ and $\pi N \rightarrow \pi N$. (From Ref. No. 38)
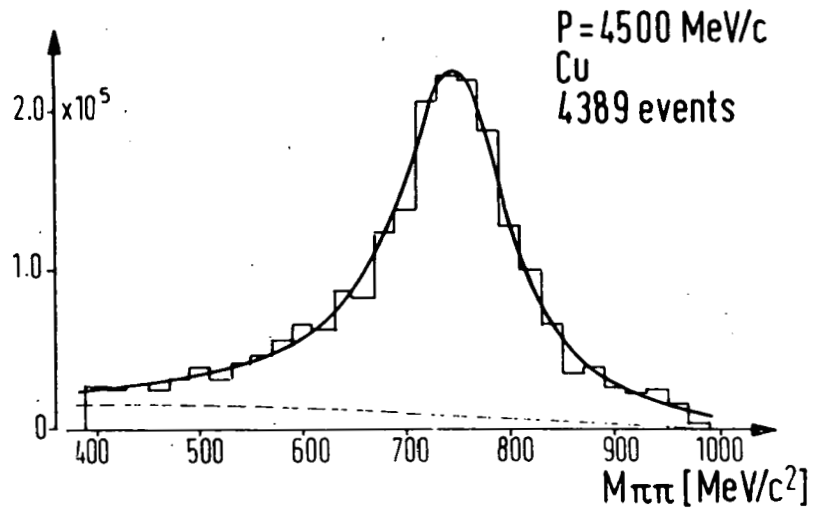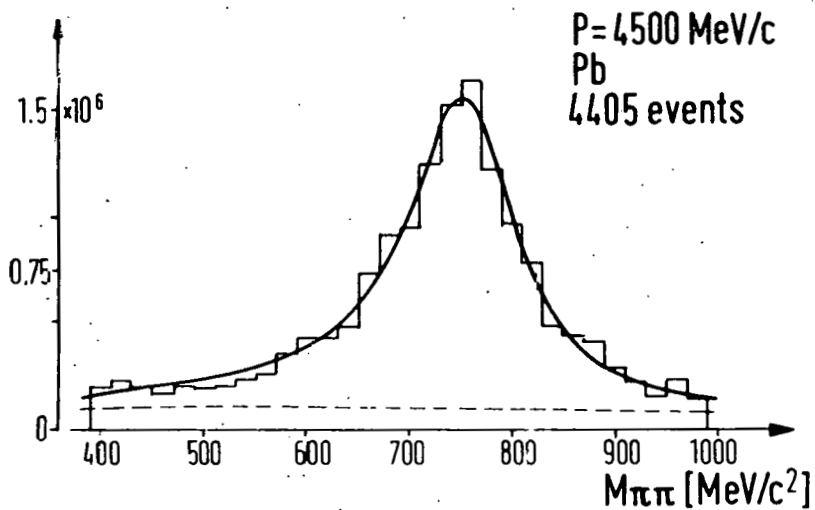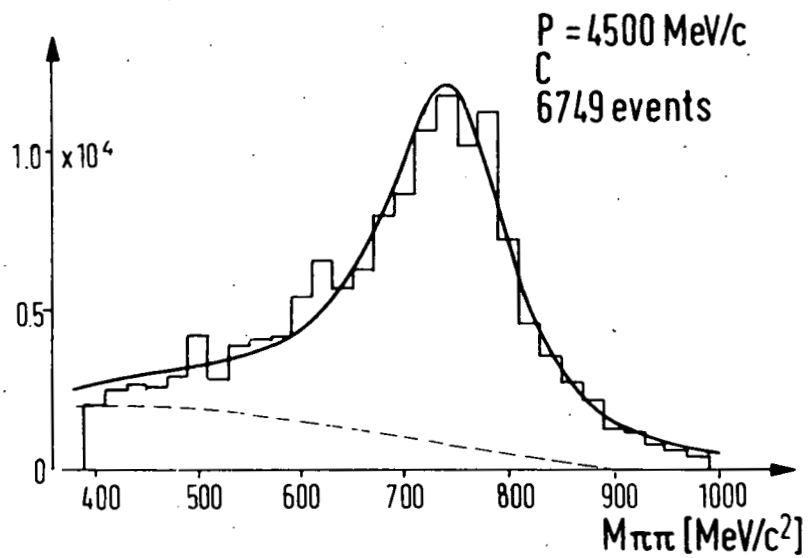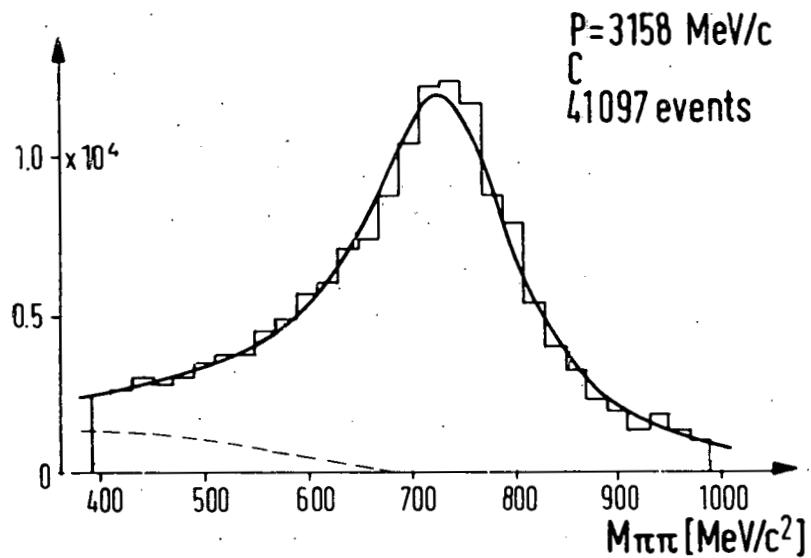
Fig. 2.2-8 $\pi^+\pi^-$ invariant mass spectra for various target elements and momenta. Fits according to eq. 2.2-12. Dashed curves indicate estimates of non-resonant backgrounds. (From Ref. No. 38)

4. Recently, at the Stanford Linear Accelerator, Jones et.al.[40] have used a single-arm spectrometer to look at excitation functions for information on the photoproduction of neutral mesons. With the good flux and bad duty cycle characteristics of the Linac, this approach becomes desirable if difficult.

In the process $\gamma p \to p m^o$, precise momentum analysis of the final-state proton will yield information on the mass spectrum for m^o. If we hold everything constant but vary the angle subtended by the spectrometer, a typical excitation function like in Fig. 2.2-9 results. As mentioned for the $K\Lambda$ - $K\Sigma^o$ case on page 29, a two-body final state (m^o sharp) will show up as a sharp step, within the resolution of the detection system. Resonances of finite width, and three-or-more-body final states, put less of a kinematical constraint on the detected proton, and will show up as more gradual rises. Fig. 2.2-9 shows that there are background protons below the lowest production threshold (for the π^o). There is a π^o step at the appropriate threshold value, a strong rise associated with ρ^o production (from which we cannot separate the ω's); we also expect steps superimposed at the η and Φ thresholds, although they do not definitely show up here. This method is open to errors stemming from background fitting, and the proper way to pick resonance parameters. The quoted results for photoproduction of ρ^o on protons are the following, between 6.5 and 17.8 GeV: Taking m_ρ = 770 MeV/c^2, Γ_ρ = 125 from their best fits, they found that inclusion of the mass-skewing factor did not improve these fits. Fig. 2.2-10 shows their
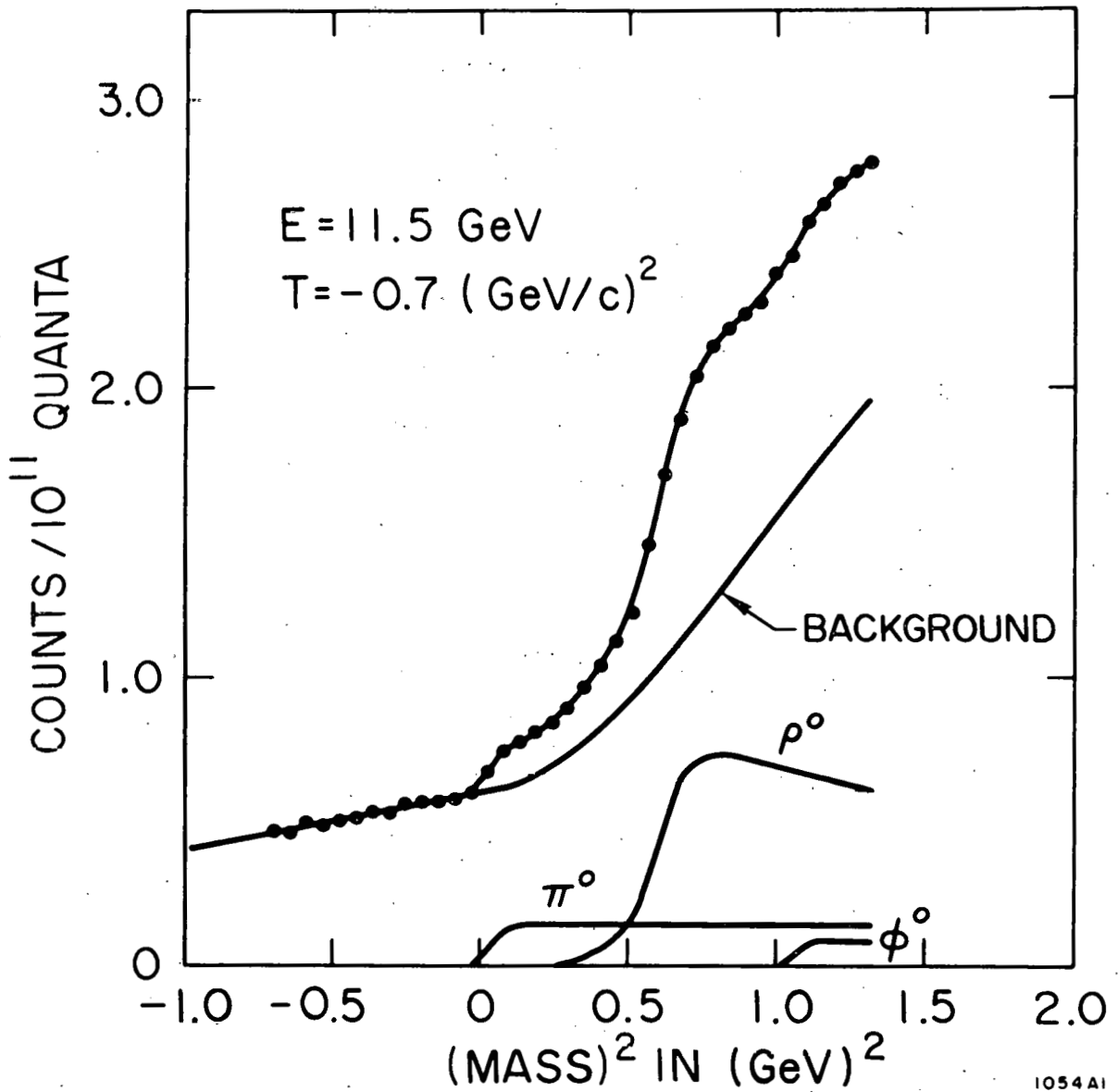
Fig. 2.2-9 Excitation function for the process $\gamma p \to p X^o$. Counting rates of proton recoils, at given E_γ and t, plotted vs. mass^2 of produced boson. (From Ref. No. 40)

differential cross sections $\frac{d\sigma}{dt}$ between momentum transfer values

$0.2 < -t < 0.9$ $(GeV/c)^2$. Evidently these results are consistent

with the diffraction picture, with a <u>non-shrinking</u> diffraction

peak going as $e^{8.5t}$. At energies lower than 10 GeV, there may be

some non-diffractive admixture, since between $t = 0.7$ and 0.9 $(GeV/c)^2$

there is a factor-of-two drop in cross-section between 6.5 and 10 GeV;

if so, it dies out quickly and is no longer visible at $\sim$ 10 GeV.

(Recall that we expect OPE contributions to decrease as $1/k^2$).

It has to be kept in mind that the measured cross-section has

to be extracted from the data through a difficult fitting procedure,

where a typical error of $\pm$ 30% is quoted for the background shape

(see <u>Fig. 2.2-9</u>). In addition, because of the non-separation of

ρ and ω, an SU(3)-suggested ratio $\sigma(\rho)/\sigma(\omega) = 9$ was assumed, so that

the apparent yield was simply reduced by 10%. Parameters for fits

according to $\frac{d\sigma}{dt} = a\ e^{bt + ct^2}$ are quoted in <u>Fig. 2.2-10</u>.

We have seen, in conclusion, that on the whole, ρ^0 photoproduction

appears to be well described in terms of the diffraction picture.

Relevant experimental numbers have been summarized in Table I.

2.3 ω Photoproduction

Due to the three-body decay of the ω with a neutral in the final

state, we have no counter experiments detecting the $p\ \omega$ final state.

Not even the one-arm spectrometer, excitation function method is

applicable, because the more copious production of ρ's masks ω

production within the present resolution of such systems. In principle,

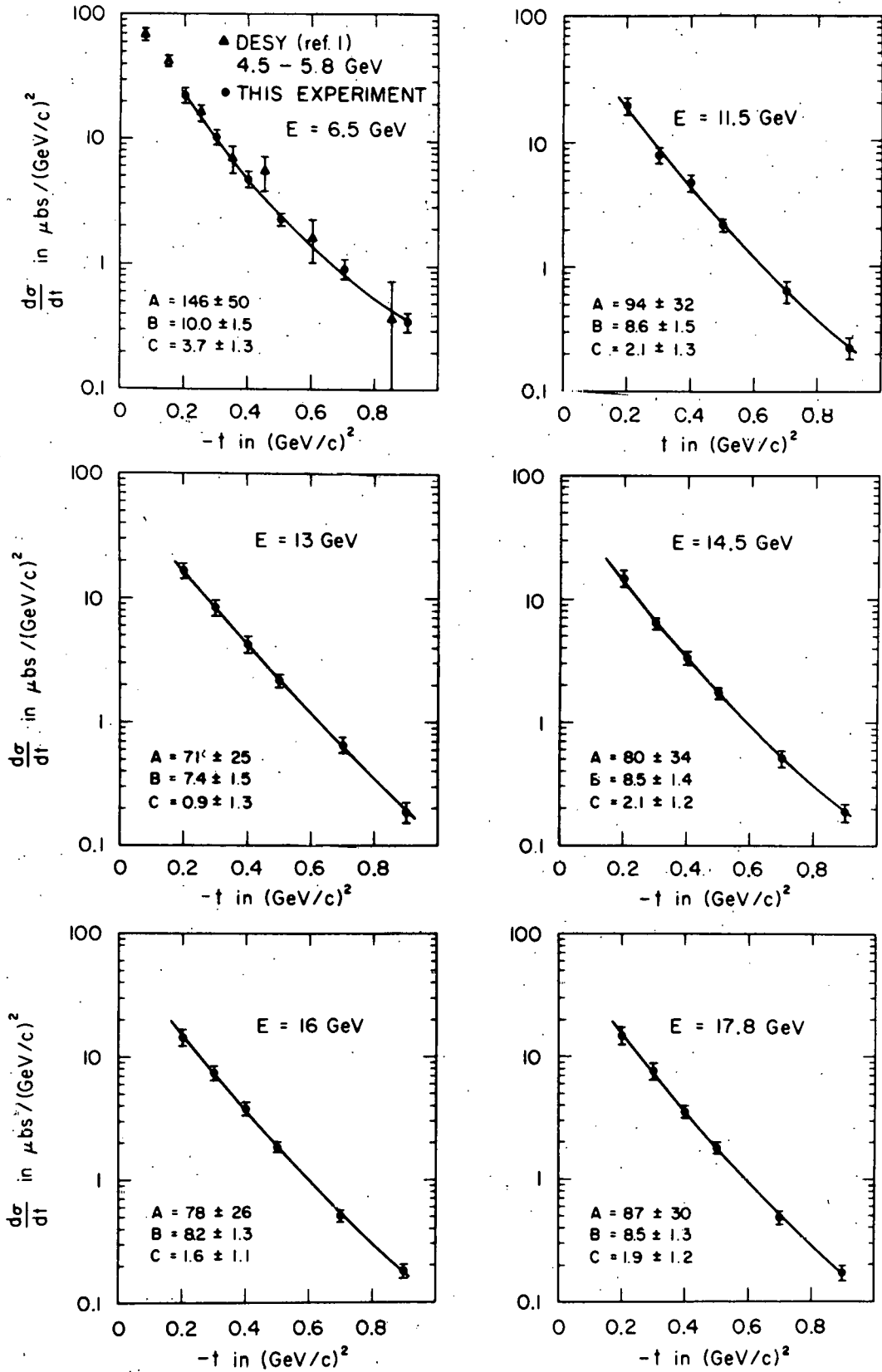this could be overcome by measuring the G-parity violating $\omega \to \pi^+\pi^-$

Fig. 2.2-10 High-energy photoproduction of ρ^0. Differential cross-sections fitted according to $\frac{d\sigma}{dt} = a\ e^{bt + ct^2}$. (From Ref. No. 40)

mode which has a branching ratio of less than 1%. No such data
exist, but a double-arm spectrometer like that of reference (38)
may soon be used for a similar investigation; however, the
expected rates are very low. The bubble chamber results on ω photo-
production are shown in __Figs. 2.3-1 and 2.3-2.__ They show, for the
total cross section, a sharp rise above threshold, to ~8μb, then a
sloping off toward a value of ~ 3 mb, not displaying the constant
cross-section behavior expected for diffraction production, but
rather a picture suggestive of a considerable OPE contribution
(which we expect to decrease with ~ $1/k^2$). The angular dependence
$\frac{d\sigma}{dt}$ displays a forward peak and a more isotropic component, with the
peak becoming more pronounced with increasing energy. The best fit
to the total cross-section data has an OPE-type term and a
diffraction-like term with very small energy-dependence:

$$\sigma_{tot} \ (\gamma p \to p\omega) \approx A E_\gamma^{-1.6} + B \ E_\gamma^{-0.08}, \qquad (2.3-1)$$

The OPE exponent -1.6 is, according to a compilation by Morrison[42],
typical of many OPE processes, and the diffraction-term has an
exponent taken from ρ production.

A thorough investigation of this OPE-plus-diffraction picture[41]
led to a value for the radiative decay width of the ω of $\Gamma(\omega \to \pi\gamma)$ =
(0.7 ± 0.3) MeV. Parameters for the exponential dependence
$\frac{d\sigma}{dt}$ (t) α e^{bt} are again given in Table I.

Using eq. 2.3-1, we can tentatively separate out the diffractive
contribution to σ_{tot} $(\gamma p \to p\omega)$. For k $\lesssim$ 6 GeV, we find $\sigma_{diff}(\gamma p \to p\omega)$
≈ 1.7 ± 0.9 μb. Note that this gives good agreement with the ratio

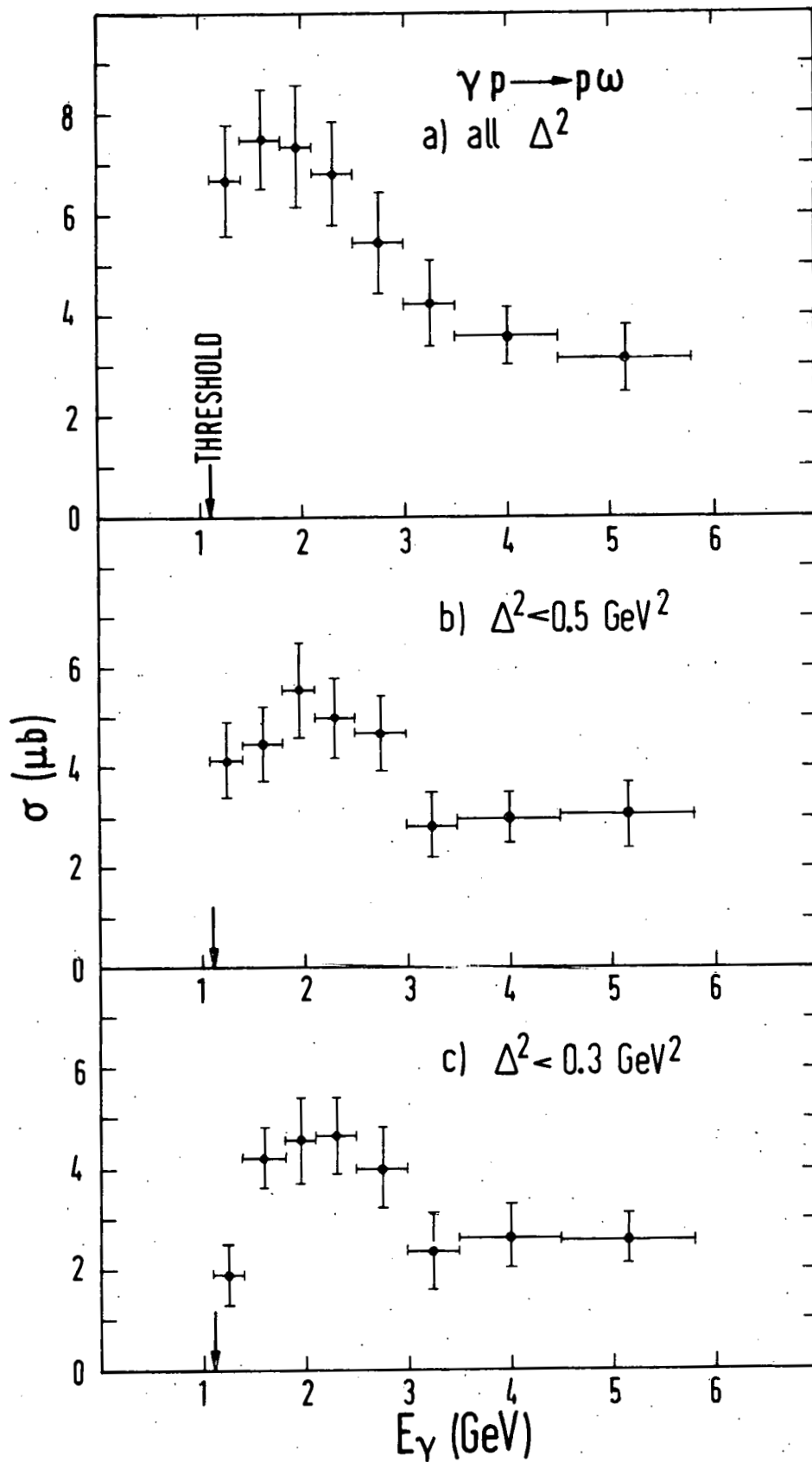Fig. 2.3-1 Total cross-sections for $\gamma p \to p\omega$ with various cutoffs on $|t|$ ($\equiv \Delta^2$). (From Ref. No. 19)

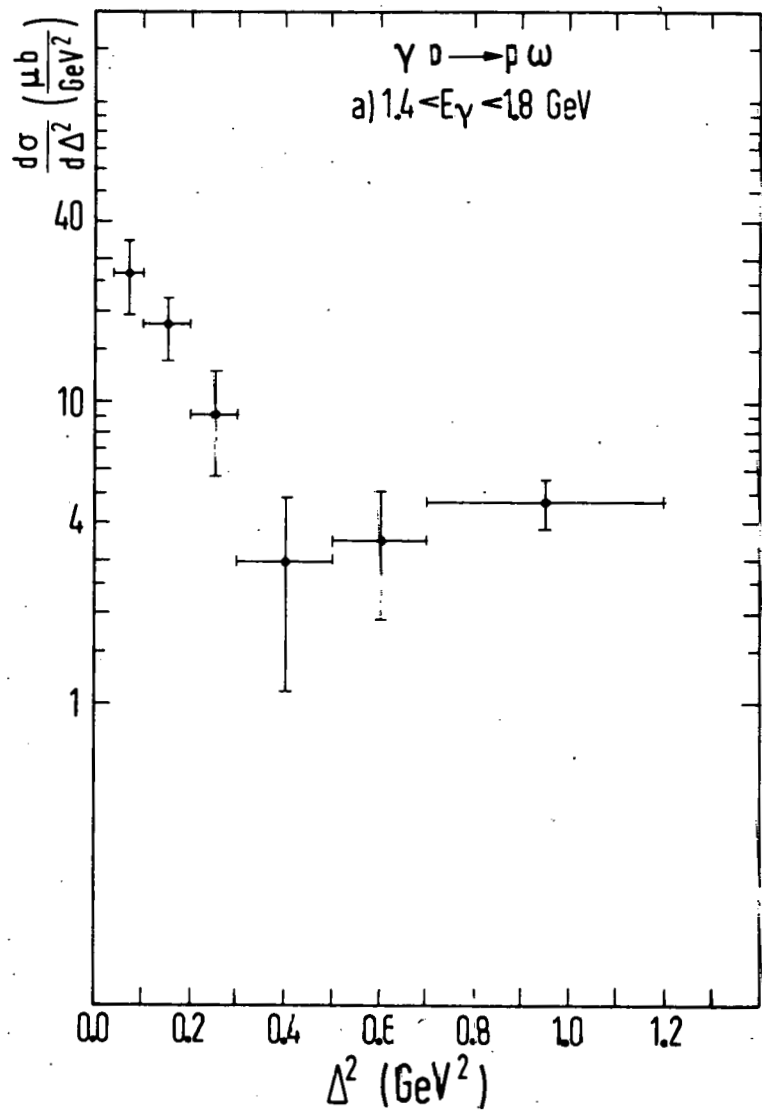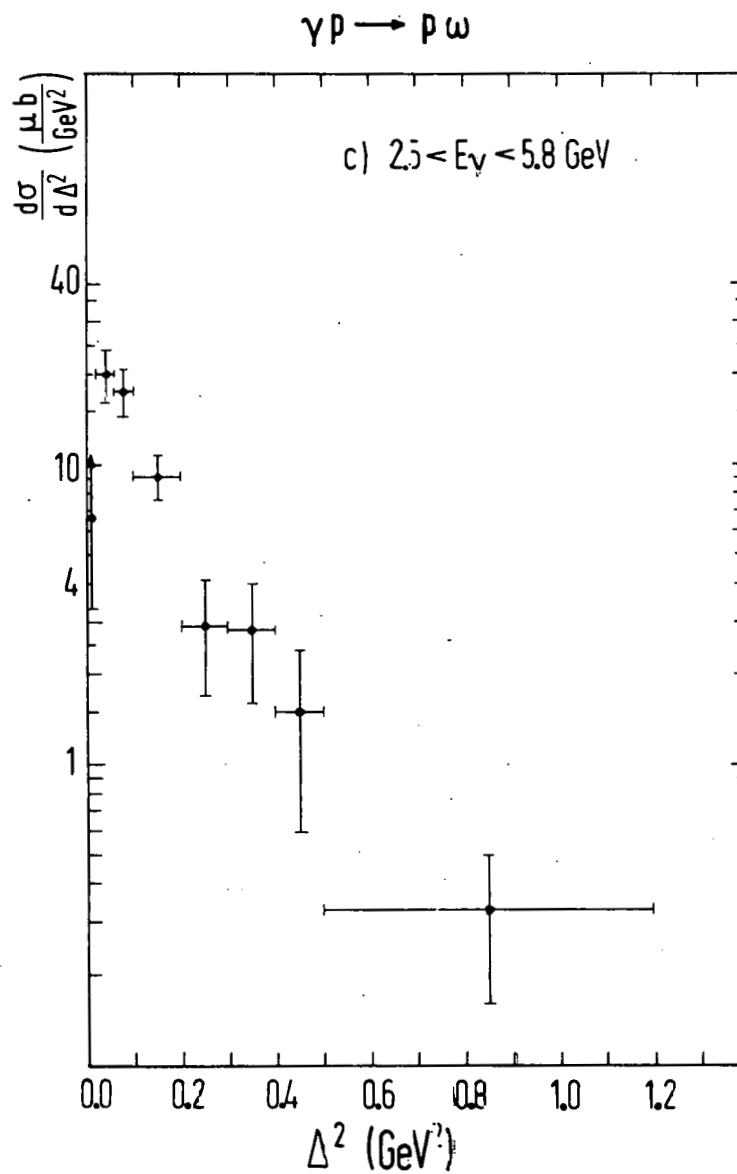Fig. 2.3-2(a) Differential cross-section $\frac{d\sigma}{dt}$ ($\gamma p \to p\omega$) for $1.4 \leq k \leq 1.8$ GeV/c. (From Ref. No. 19)

Fig. 2.3-2(b) Differential cross section $\frac{d\sigma}{dt}$ ($\gamma p \to p\omega$) for $2.5 \leq k \leq 5.8$ GeV/c. (From Ref. No. 19)

$\sigma_{diff.}(\gamma p \to p\omega)/\sigma_{diff.}(\gamma p \to p\rho^o) \approx \frac{1}{9}$ predicted by the diffraction picture combined with the usual SU(3) assumptions (eq. 2.1-9).

2.4 Φ Photoproduction.

The detection of Φ mesons can in principle proceed along precisely the same lines as that of ρ's, since the dominant decay mode is K^+K^- ($\sim 47\%$) with the added feature that $\Gamma_\Phi \ll \Gamma_\rho$, so that the background subtractions do not lead to serious problems. However, the Φ gets photoproduced only at a very small rate, so that there are comparatively few data. The bubble chamber results up to ~ 6 GeV are given in Figs. 2.4-1 and 2.4-2. The resulting features, within the errors quoted, are these: the total cross-section $\gamma p \to p\Phi$ does not rise as sharply at threshold as that for ρ or ω production. No structure is discernible, possibly due to poor resolution and statistics. $\frac{d\sigma}{dt}$ is compatible with diffractive behavior, especially for the high-energy interval, with a best fit $\frac{d\sigma}{dt}(t) \propto e^{(3.5 \pm 0.9)t}$, a slope much smaller than what we find for ρ and ω photoproduction.

Asbury et al.[43] at DESY have used their double-arm spectrometer to detect K^+K^- pairs in the same manner as $\pi^+\pi^-$ pairs from ρ decay, measuring Φ forward coherent production on nuclei. Mass distributions are given for K pairs in Fig. 2.4-3. For all elements studied, they are seen to be strongly peaked in the mass region of the Φ (1020 MeV/c^2). Analysis of the A dependence similar to that for the ρ case (section 2.2) yielded a total cross section $\sigma_{\Phi N} \approx 13.4$ mb. In addition, a study of the decay angular distribution yields a result consistent with a purely transverse polarization of the Φ mesons.
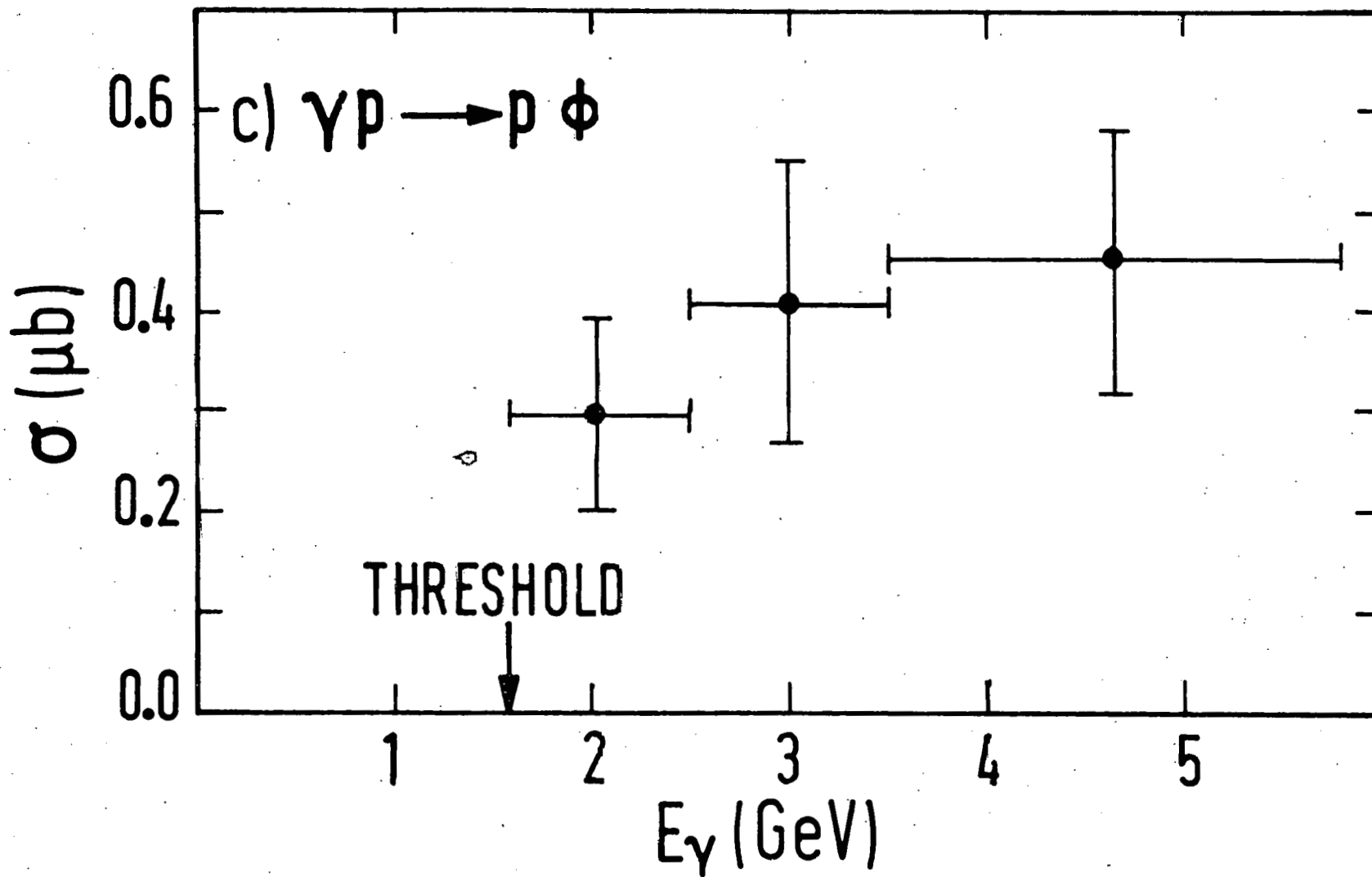
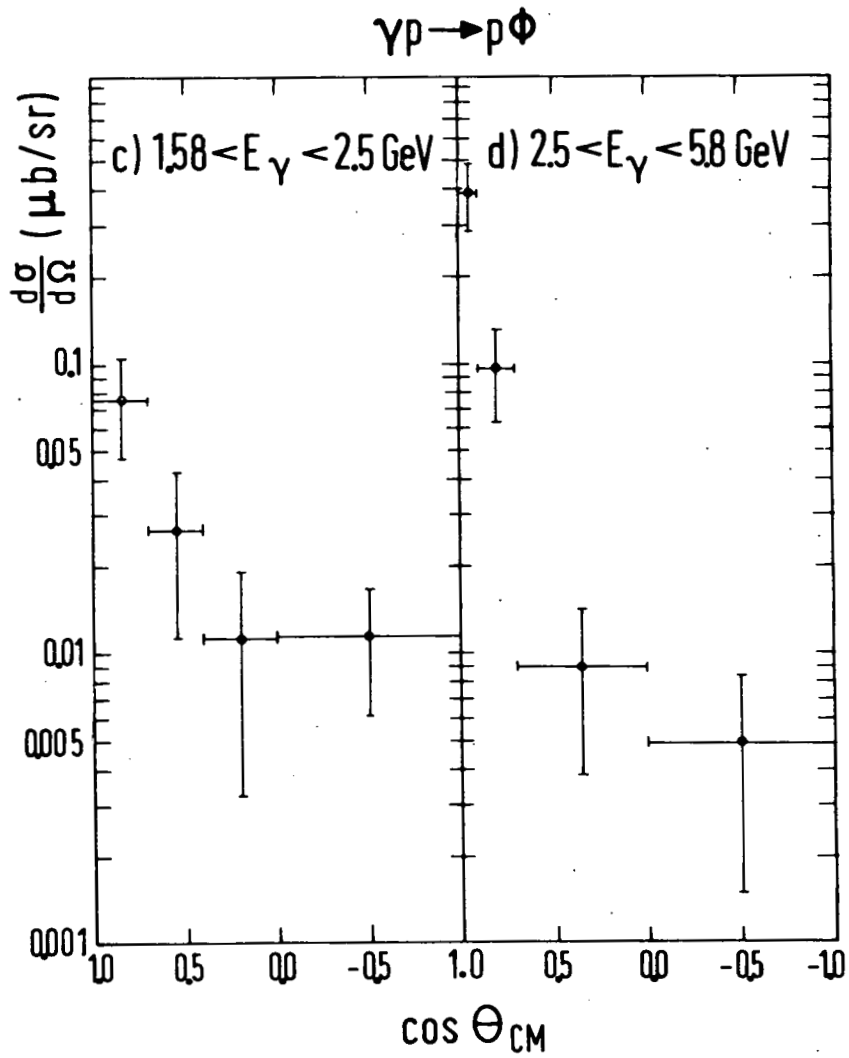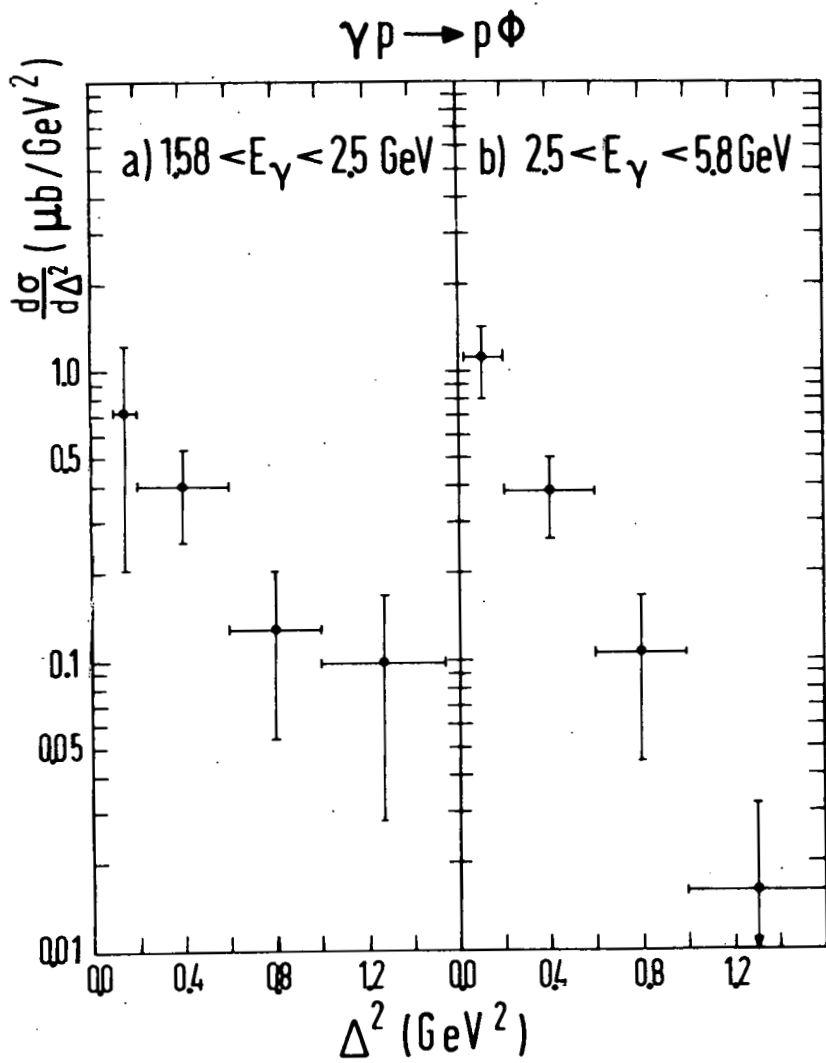Fig. 2.4-1 Total cross-section for $\gamma p \rightarrow p\Phi$. Bubble chamber data. (From Ref. No. 19)

Fig. 2.4-2 Differential cross-sections for $\gamma p \to p\Phi$ for two energy intervals. (From Ref. No. 19)
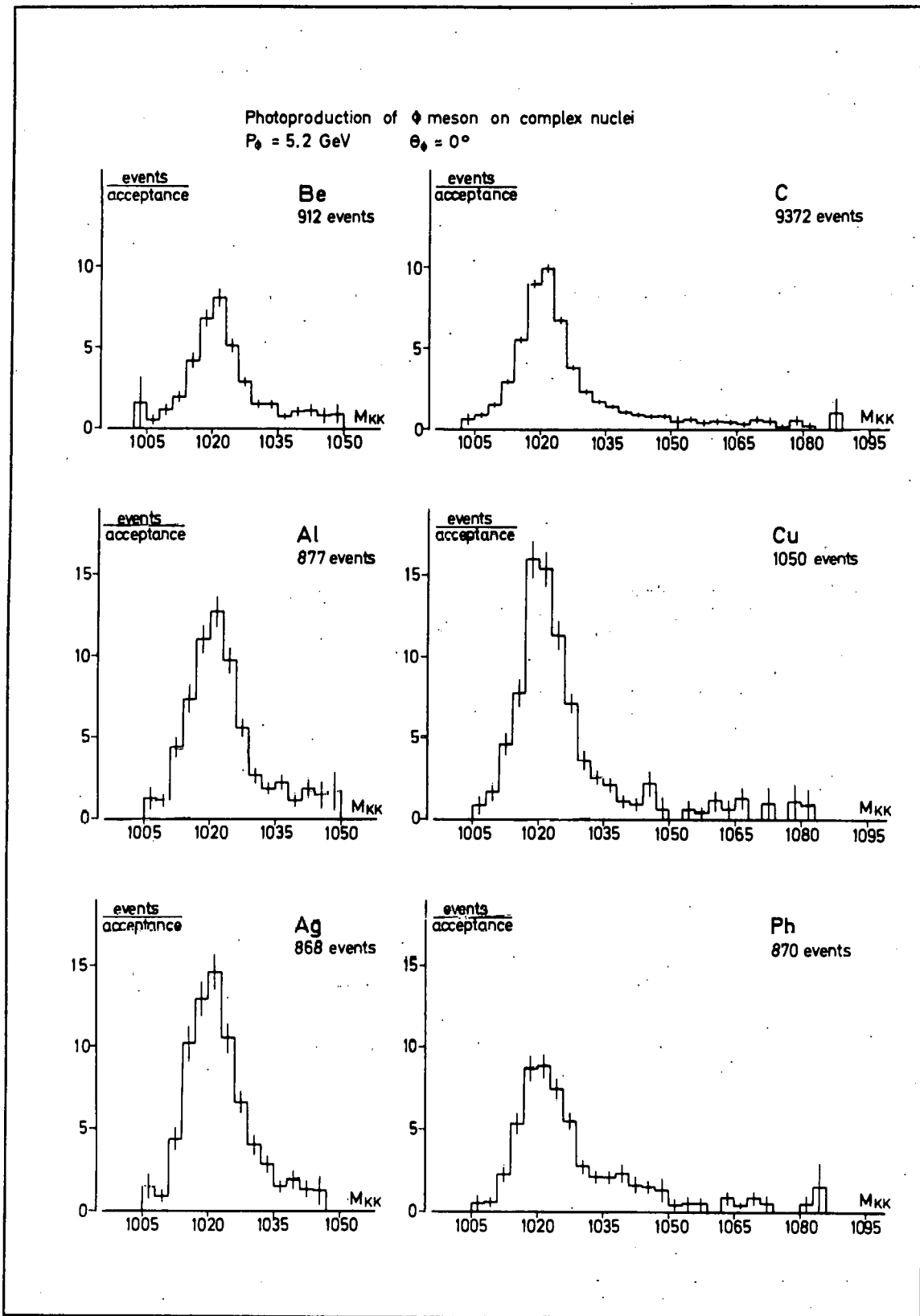
Fig. 2.4-3 K^+K^- invariant mass spectra for various target elements.
(From Ref. No. 43)

The extension of the data to higher energies is particularly important for a study of the diffraction mechanism . Two of the beam survey experiments at SLAC were used to study the production of $K^{\pm}$ close to the forward direction, on Be[44] and hydrogen targets[45]. Relating the K yield to the Φ production cross-section by assuming that all K's stem from Φ decays, upper limits were given for $\sigma(\Phi)$. Using various assumptions on backgrounds and t dependence, $\sigma(\Phi)$ at 7-8 GeV was estimated to be between 0.5 and 1.0 μb.

The recent single-arm experiments of Jones et al.[40] looking for excitation functions in single-neutral-meson production observed clearly discernible steps in the yield function (see Fig. 2.2-9) at Φ threshold. By following a suitable subtraction procedure, they quote a cross-section behavior according to $\frac{d\sigma}{dt}$ $(\gamma p \to p\Phi) \approx a\ e^{bt}$ with $b \approx 4.5$ $(GeV/c)^{-2}$. Their measured values are at $|t|$-values > 0.3 $(GeV/c)^{2}$ only, so an extrapolation to small t may be problematic. However, if we believe the quoted t dependence as governing the entire cross-section behavior, then we can use the forward amplitude and the optical theorem to estimate the total cross-section for ΦN scattering (see next section) from the vector dominance model; the resulting values are $\sigma_{tot}(\Phi p) = 9.7 \pm 2.0$ mb at 13 GeV, 7.2 ± 1.9 at 16 GeV. Together with the 6 GeV values of ~ 13.4 mb quoted by Asbury et al.[43], this looks like a definitely decreasing trend, in disagreement with expectations of the diffraction model. (Fig.2.4-4).
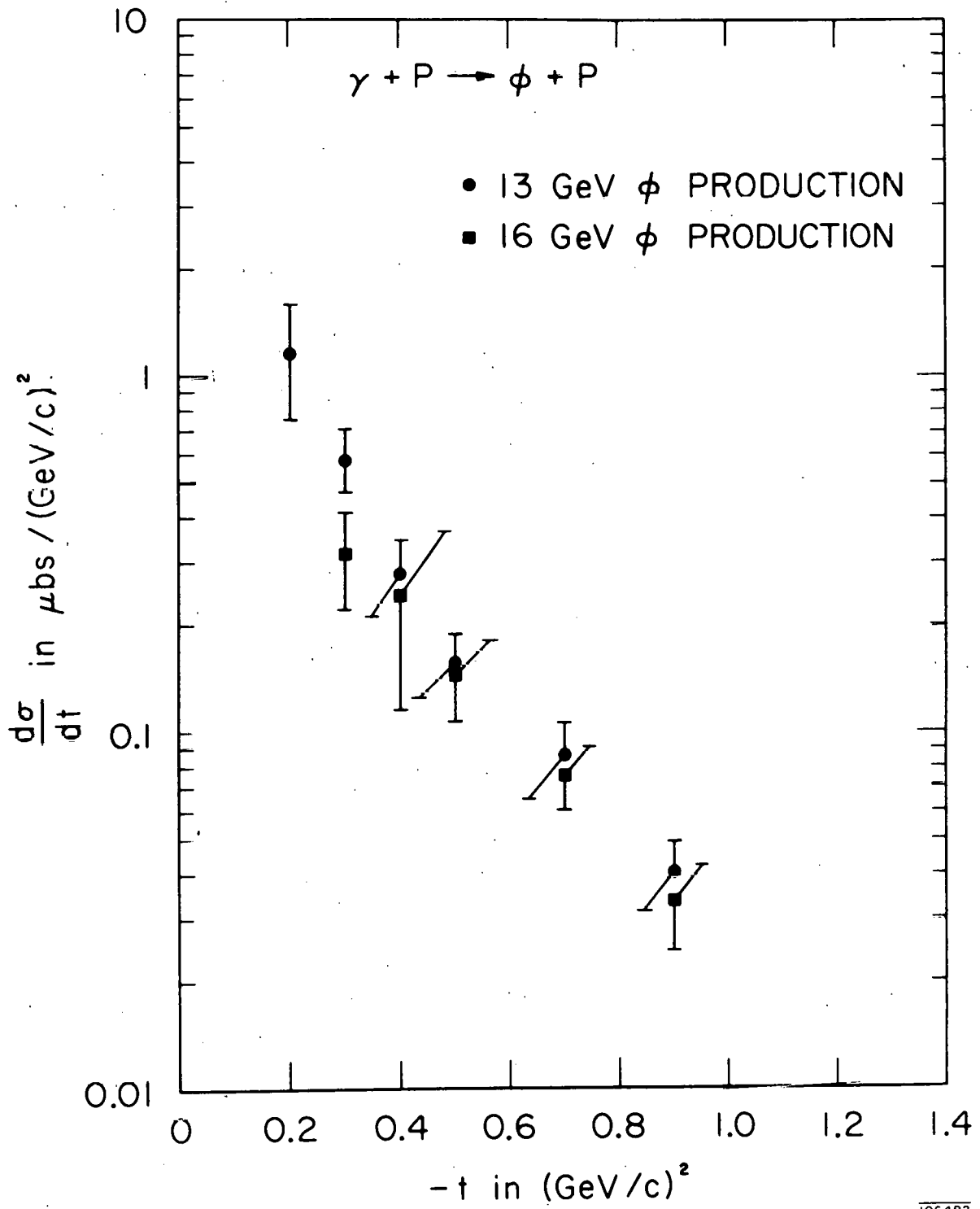
Fig. 2.4-4 Differential cross-sections for $\gamma p \to p\Phi$ at high
energies. (From Ref. No. 40)

2.5 The Vector Dominance Model

The experimental information on vector meson photoproduction is
briefly summarized in Table I. If we go back to the considerations
of section 2.1 and try to decide on the dominant mechanisms for the
process $\gamma p \rightarrow p V^o$, we find that (if, for the time being, we leave
isobar formation out of the picture), neither the OPE nor the
diffraction model yields satisfactory comparisons. The OPE prediction
(2.1-5) that $\sigma(\omega) \approx 9\sigma(\rho)$ is obviously not satisfied. But the fit
(2.3-1) to the ω data suggests that there is an OPE contribution for
the ω which accounts for the distinctly non-diffractive behavior
of ω production at lower energies. If we separate out the presumable
diffraction part, the diffraction model prediction (2.1-9) $\sigma(\rho)$:$\sigma(\omega)$:
$\sigma(\Phi) = 9{:}1{:}2$ does appear to reproduce the ρ/ω ratio reasonably.
However, the observed Φ rate is much too low (by a factor of order 10).
Let us see how we can patch up this discrepancy. The predicted ratio
from the graph
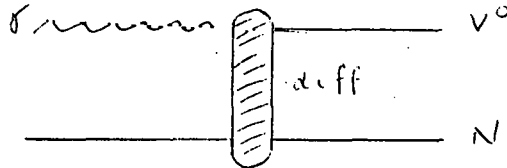
assumed SU(3) symmetry, and P trajectory exchange, where P is a unitary
singlet of $J^P = 0^+$. Meshkov and Ponzini[46] argue in the framework
of the collinear group SU(6)$_W$ that high energy forward elastic
scattering data make the unitary singlet exchange illusory, and that
higher representations have to be exchanged. Their method has an
attractive feature that is not an ad hoc construction, but fails to

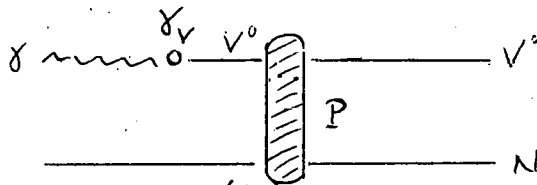reproduce the Φ rate by a factor of 2.

The most obvious remedy is to introduce symmetry breaking. This comes most naturally in the framework of the vector dominance model, where we write the above graph somewhat differently, introducing a direct photon-vector meson coupling:

The vector dominance model[47] essentially assumes that we can write the hadronic electromagnetic current as a linear combination of phenomenological vector meson currents

$$j_\mu(x) = -\left[\frac{m_\rho^2}{2\gamma_\rho^2}\,\rho^0_\mu(x) + \frac{m_\omega^2}{2\gamma_\omega^2}\,\omega_\mu(x) + \frac{m_\Phi^2}{2\gamma_\Phi^2}\,\Phi_\mu(x)\right] \qquad . \quad (2.5\text{-}1)$$

With the usual SU(3) assumptions we can then write the incident photon as

$$|\gamma\rangle = \frac{\sqrt{3}}{2}\left(|\rho^0\rangle + \frac{1}{3}|\omega\rangle - \frac{\sqrt{2}}{3}|\Phi\rangle\right) \qquad (2.5\text{-}2)$$

which gives us a relation between photon-induced and vector-meson-induced reactions according to

$$\sigma(\gamma a \to bc) = \sum_i \frac{\alpha\pi}{\gamma_i^2}\,\sigma_{tr}(V^0 a \to bc) \qquad (2.5\text{-}3)$$

(where σ_{tr} means that we specify helicity states ± 1 for the vector mesons.)

We now apply eq. 2.5-3 to the diffraction process $\gamma p \to p V^0$, noting that we can write the direct γV^0 coupling in terms of the

leptonic decay widths

$$\Gamma(V \rightarrow e^+e^-) = \frac{\alpha^2}{12} \frac{4\pi}{\gamma_V^2} m_V + \text{small terms} \qquad (2.5\text{-}4)$$

Table I shows the experimental information on the leptonic decay widths. We then write the critical ratio

$$\frac{\sigma(\gamma p \rightarrow \Phi p)}{\sigma(\gamma p \rightarrow \rho^o p)} = \frac{m_\rho}{m_\Phi} \frac{\Gamma(\Phi \rightarrow e^+e^-)}{\Gamma(\rho^o \rightarrow e^+e^-)} \frac{\sigma_{e\ell}(\Phi p)}{\sigma_{e\ell}(\rho^o p)} \qquad (2.5\text{-}5)$$

with the recent results from DESY[48] on the $\Phi \rightarrow e^+e^-$ decay width of 1.1 ± 0.2 eV and the accepted $\rho \rightarrow e^+e^-$ width of ~ 6 keV. We then insert, using the optical theorem,

$$\frac{\sigma_{e\ell}(\Phi p)}{\sigma_{e\ell}(\rho^o p)} = \left| \frac{\sigma_{tot}(\Phi p)}{\sigma_{tot}(\rho^o p)} \right|^2 \qquad (2.5\text{-}6)$$

the σ_{tot} values from the preceding chapter or Table I, and find all quantities in (2.5-5) experimentally determined. The numerical check is:

$$\text{Left-hand side} \approx \frac{1}{40} \qquad \text{Right-hand side} \approx \frac{1}{60}$$

Preliminary numbers of 2.1 ± 0.9 keV for the radiative decay width of the Φ, as reported by a CERN group[49], or of 1.30 ± 0.21 keV, as deduced from an $e^+e^- \rightarrow \Phi$ experiment at the Orsay electron storage ring[101], improve the numerical agreement somewhat. (Recall the SU(3) prediction $\Gamma(\rho \rightarrow e^+e^-): \Gamma(\omega \rightarrow e^+e^-): \Gamma(\Phi \rightarrow e^+e^-)$ = 9: 1: 2: or, with some symmetry-breaking introduced into the γV vertex[50], 9: 0.65: 1.30).

Let's recapitulate then: we essentially keep SU(3) symmetry in the γV vertex, introduce symmetry-breaking in the VVP vertex, where the P is still a unitary singlet. This symmetry-breaking can easily be introduced in terms of the quark model[51]: from the relations for the total cross-sections

$$\sigma(\rho p) = \sigma(\omega p) = \frac{1}{2} \left(\sigma(\pi^- p) + \sigma(\pi^+ p) \right), \qquad (2.5\text{-}7)$$

$$\sigma(\Phi p) = 2\sigma(K^+ p) + \sigma(\pi^- p) - 2\sigma(\pi^+ p), \qquad (2.5\text{-}8)$$

where we insert experimental results on the RHS, we obtain $\sigma(\rho p) = \sigma(\omega p) = 28$ mb, $\sigma(\Phi p) = 11.5 \pm 1.5$, in fair agreement with the direct experimental numbers quoted in Table I.

If we try to play the same game with ω production, we have the difficulty that only two preliminary (and discrepant) numbers exist for $\Gamma(\omega \to e^+ e^-)$: a CERN experiment[49] on $\omega \to e^+ e^-$ giving a value of 0.49 ± 0.19 keV, and the Orsay storage ring experiment[101] $e^+ e^- \to \omega$, yielding $\Gamma(\omega \to e^+ e^-) = 1.1 \pm 0.25$ keV. Moreover, it is not trivial to extract the diffraction part from the total cross-section for $\gamma p \to p\omega$. Taking the "best guess" values (see Table I), we find

$$\frac{\sigma(\gamma p \to p\omega)}{\sigma(\gamma p \to p\rho^0)} = \frac{m_\rho}{m_\omega} \frac{\Gamma(\omega \to e^+ e^-)}{\Gamma(\rho^0 \to e^+ e^-)} \left(\frac{\sigma_{tot}(\omega p)}{\sigma_{tot}(\rho^0 p)} \right)^2 \qquad (2.5\text{-}9)$$

The first and third factors on the RHS are ≈ 1 (in the absence of direct information on $\sigma_{tot}(\omega N)$, we take the quark model value), and we find

Lefthand side $= \dfrac{1}{10}$ Righthand side $= \begin{cases} \dfrac{1}{13} \text{ taking CERN value for } \Gamma(\omega \to e^+e^-) \\[2ex] \dfrac{1}{6} \text{ taking ORSAY value for } \Gamma(\omega \to e^+e^-) \end{cases}$

In view of the poor input material, we will not take this as a strong endorsement. Still, the VDM appears to make the overall experimental picture of photoproduction of vector mesons consistent with our present theoretical understanding, at moderate energies ($\leq$ 6 GeV). Before we worry about the apparent decrease of the Φ cross-section above 6 GeV[40], let us wait for more complete data.

2.6 Some Specific Tests of the Vector Dominance Model.

Without wanting to prejudge other attempts to account for the initially inconsistent picture in Φ photoproduction, we take the apparent success of the VDM as an indication for the relevance of eq. (2.5-3). The only direct test of the direct coupling hypothesis would be a comparison of decay modes like $\omega \to \pi\gamma$ and $\omega \to \pi\rho$ (which does not work energy-wise); $A_1 \to \pi\gamma$, $A_1 \to \pi\rho$ (where the experimental number is not clear, and we have to disentangle transverse and longitudinal ρ's); or $A_2 \to \pi\gamma$, $A_2 \to \pi\rho$ (where the $J^P = 2^+$ value allows only transverse ρ's). We would predict the radiative decay width to be $\sim$ 1 MeV; unfortunately, no direct experimental information exists on this decay. Some recent analysis of somewhat less direct experimental evidence has yielded a consistently favorable picture.

We can, for instance, analyze photoproduction cross-sections and check for consistency with π production of vector mesons:

$$\gamma p \to N\pi \quad \longleftrightarrow \quad \bar{\pi}p \to V^0 n \qquad\qquad (2.6\text{-}1)$$

The corresponding amplitudes are connected by the VDM model and time-reversal invariance, if we separate out the proper helicity and isospin amplitudes. Dar et al.[52] have shown several combinations of cross-sections which are accessible to such checks. Fig. 2.6-1 shows the agreement between the two sides of the relation

$$\frac{d\sigma}{dt} (\gamma p \to p\pi^0) \sim \frac{1}{2} \left\{ \frac{\pi\alpha}{\gamma_\rho^2} \left[\frac{d\sigma}{dt} (\pi^0 p \to \rho^0_{tr} p) \right] + \frac{\pi\alpha}{\gamma_\omega^2} \left[\frac{d\sigma}{dt}(\pi^0 p \to \omega_{tr} p) \right] \right\} \quad (2.6\text{-}2)$$

where the π^0-initiated amplitudes on the RHS can be obtained by isospin invariance from π^- and π^+ data. A corresponding prediction for $\gamma n \to \pi^0 n$ is drawn into the picture, and awaits experimental check.

A particularly suitable case is presented by a comparison of the reactions $\gamma p \to \pi^+ n$ and $\pi^- p \to \rho^0 n$
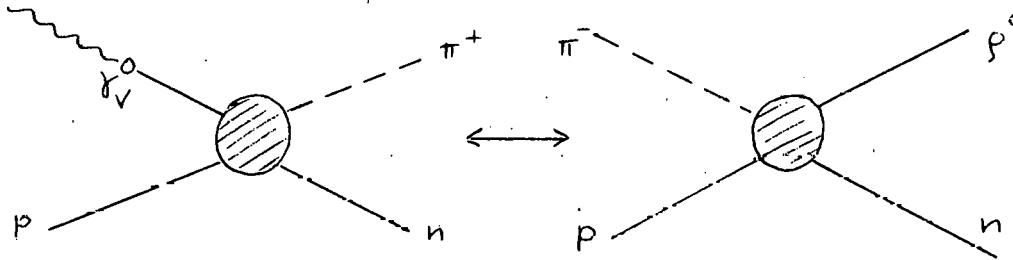
They are linked up by the VDM and by I and T invariance. A detailed comparison is possible for the data on either side of the relationship

$$\frac{d\sigma}{dt}(\gamma p \to \pi^+ n) \approx \frac{\pi\alpha}{\gamma_\rho^2} \rho_{11}(t) \frac{d\sigma}{dt} (\pi^- p \to \rho^0 n) + \omega\Phi \text{ terms} + \text{interference terms} \quad (2.6\text{-}3)$$

where $\rho_{11}(t)$ is the helicity density matrix element giving the fraction of transversely polarized ρ's (since we want to compare
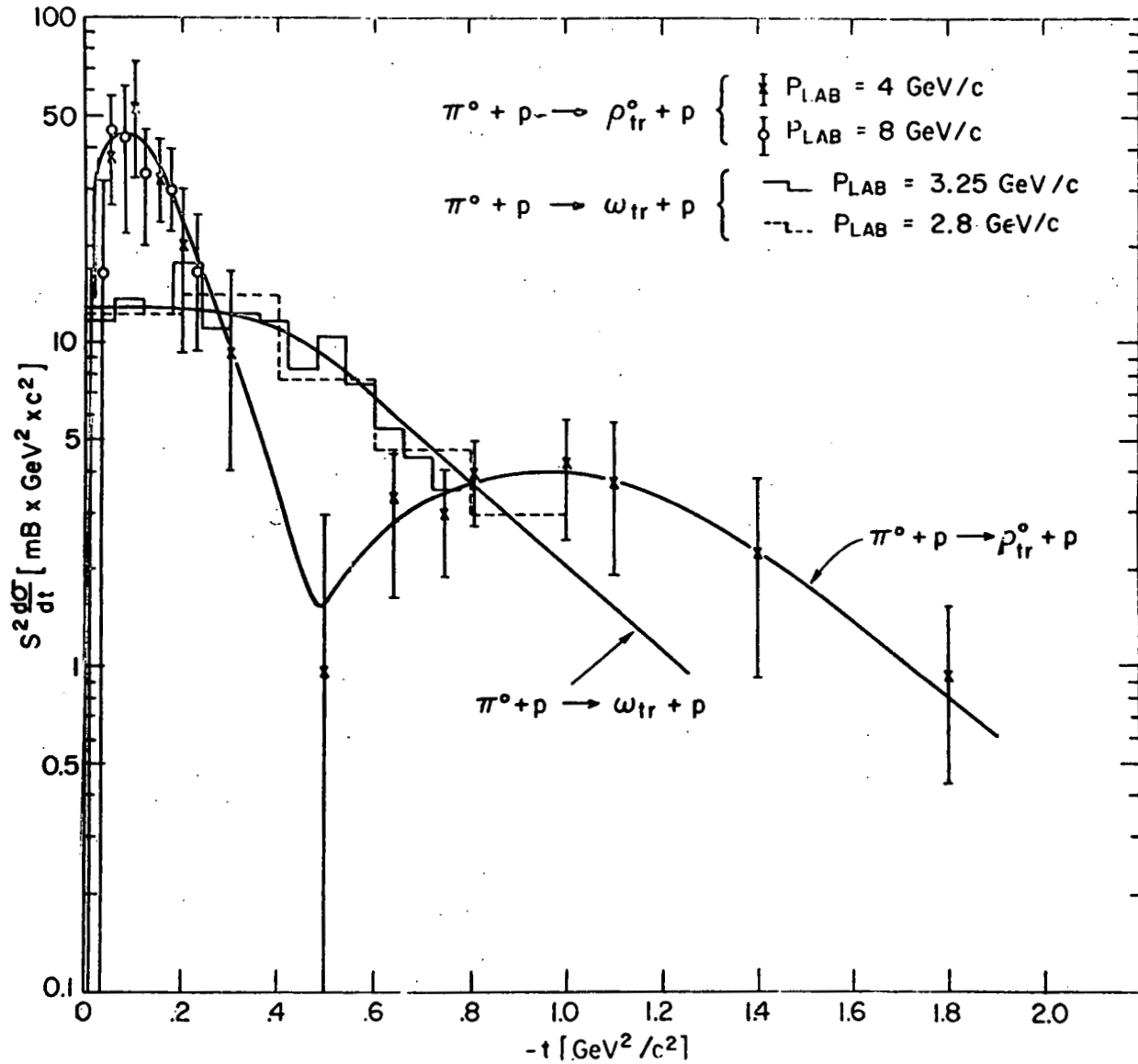
Fig. 2.6-1 Prediction for π^o photoproduction (solid curve: off protons; dashed curve: off neutrons) according to vector dominance model. Data points are for process $\gamma p \to p\pi^o$. (From Ref. No. 52)

the same helicity states for photons and ρ's[53]). The material
presented in section 2.5 suggests that we may disregard ω and Φ;
and evaluate the RHS with ρ's alone. Various authors[54,55,102]
have recently given quantitative evaluations of eq. (2.6-3) at
several energies, carefully checking the helicity density matrix
element ρ_{11} and the background difficulties inherent in the RHS exper-
imental data. <u>Fig. 2.6-2</u> gives examples at 4 and 8 GeV/c from ref.(54):
at small t, good agreement is apparent. The disagreement at larger t
can be accounted for by considering the interference effect of the
contribution of the ω contribution to the vector line. Isospin
invariance then implies that we should not use $\sigma(\gamma p \to n\pi^+)$ for the
comparison, but rather a linear combination of cross sections which
will make the interference terms cancel. We therefore recall that we
can break up the photoproduction amplitudes into isovector- and
isoscalar-photon initiated parts, A_S and A_V, yielding

$$\frac{d\sigma}{dt} (\gamma p \to \pi^+ n) = |A_V + A_S|^2$$

$$\frac{d\sigma}{dt} (\gamma n \to \pi^- p) = |A_V - A_S|^2$$

(2.6-4)

and replace $\sigma(\gamma p \to n\pi^+)$ by $\frac{1+R}{2} \sigma(\gamma p \to n\pi^+)$; R is the π^-/π^+ ratio,
which is experimentally known from π photoproduction off deuterium
(cf. section 3.6). Agreement then becomes quite satisfactory.

Another test of the VDM hypothesis was reported by Asbury et al.[56],
who use coherent vector production on nuclei to compare the two sides of

$$\frac{d\sigma}{dt} (\gamma A \to \rho^0 A) \bigg|_{t=0} = \frac{1}{16} \frac{k}{p_\rho} \frac{\alpha}{\gamma_\rho^2} \sigma_{tot}^2 (\rho A \to \rho A)$$
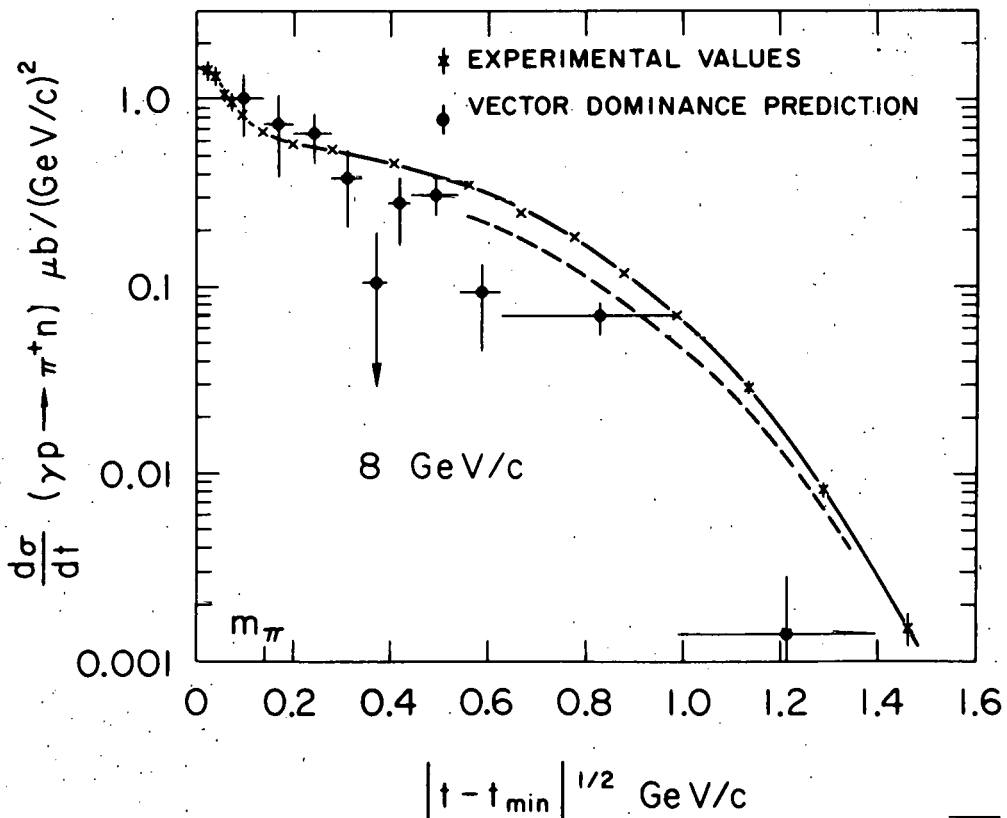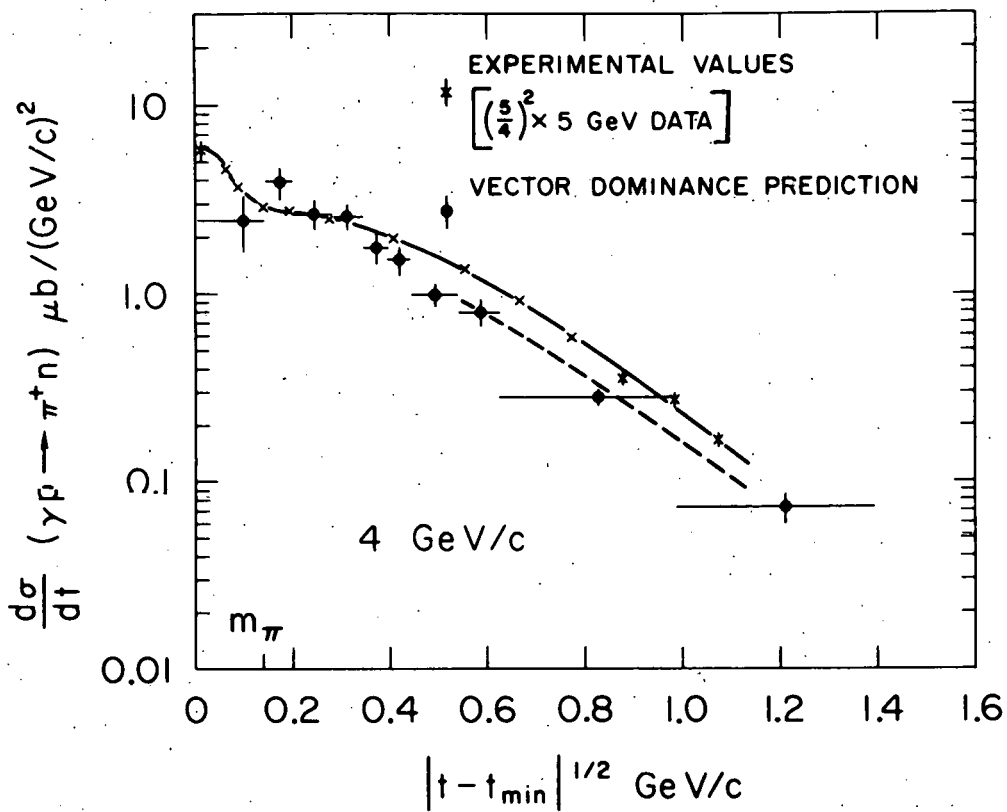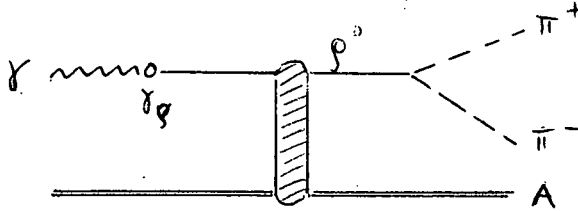
(2.6-5)

Fig. 2.6-2   Data check of π^+ photoproduction cross-sections predicted by VDM from $\pi^- p \to \rho^0 n$ data. Dashed curves incorporate correction due to $\rho\omega$ interference. (From Ref. No. 54)

in order to check the validity of the VDM-suggested diagram

They studied the ρ^0 photoproduction cross-section at small t values
between 0.004 and 0.06 $(GeV/c)^2$ and obtained the LHS of eq. (2.6-5)
by extrapolating to t ≈ 0. The RHS was calculated by computing
$\sigma_{tot}(\rho A \to \rho A)$ from the total ρN cross-section, as determined from the
relative photoproduction yield on various nuclei[38]. The resulting
numerical value for $\frac{\gamma_\rho^2}{4\pi} \approx 0.42 \pm 0.1$ compares well with its direct
determination from $\rho \to e^+ e^-$ decays and $e^+ e^- \to \rho$ annihilation. The
good numerical agreement should then be taken as evidence for the
validity of the graph studied here.

A further application of the VDM was recently proposed by
H. Joos[57] who suggests a comparison of nucleon isobar decays
$\Delta \to N\rho$ and $\Delta \to N\gamma$. For the I = 3/2 isobars $\Delta(1920)$ and $\Lambda(2420)$ a
rough estimate for the $N\gamma\Delta$ vertex is possible from the structure
observed at corresponding energies in π^0 backward photoproduction[69].
Thus, estimates for the ρN decay widths are made according to

$$\Gamma(\Delta \to \rho^0 N) = K \ \frac{\alpha\pi}{\gamma_\rho^2} \ \Gamma(\Delta \to \gamma N) \tag{2.6-6}$$

where K is a kinematical factor. Correspondingly, the graph
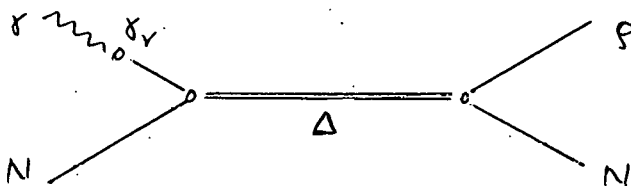
can be evaluated to give a value for the photoproduction cross-section at resonance peak energy (cf. Fig. 2.2-5). The cross-section for $\gamma p \to \Delta$ (2720) $\to p\rho^o$ is 0.6 μb; the observed value, uncorrected for helicity $\pm$ 1 only, 2 ± 1 μb. We regard this as a reasonable initial agreement. (Δ(1920) is too hard to separate uniquely out of OPE and diffraction contributions).

2.7 Total Cross Section $\sigma(\gamma p)$

More tests of the VDM can be thought up. We will here stop with the treatment of the total electromagnetic cross-section for hadrons. We have, as mentioned in 2.2 and 2.4, some experimental information on the cross-sections $\sigma(\rho N)$ and $\sigma(\Phi N)$. We can use the VDM then to predict the total γ-hadronic cross-section.

The high-energy behavior of the photon-proton total cross-section is of considerable interest. In the high-energy limit, the forward Compton graph, when viewed as a simple diffraction process as discussed in the previous sections for vector mesons,

has to vanish for real photons. Suppose we have a right-handed photon coming in: the P exchange graph will leave its helicity, $\lambda_k = +1$, unchanged. When we now cross into the t-channel, the time-reversed photon remains right-handed, but its momentum is reversed; we then have combined incoming helicity $\lambda_{k_1} = +1 - (-1) = +2$. The direct-channel pole P would have to carry two units of helicity. In simple

Regge language (cf. section 3.3): if $\sigma_{tot}(s \to \infty) =$ constant, we expect a "Regge pole" P with angular momentum $\alpha_P(t = 0) = 1$, which behaves like a vector under three-dimensional rotations. It therefore cannot couple to two photons (just as a spin-one object cannot decay into two photons). Thus, the optical theorem will postulate $\sigma_{tot}(\gamma p) \to 0$ as $E \to \infty$.

If we want to salvage the situation, we can either assume $\alpha_P(0) < 1$, which would lose the main reason why the "Pomeranchon" P was invented; or we can invoke a residue function with a singularity at $t = 0$ to cancel the "nonsense zero"; or we can assume a fixed pole at $J = 1$.

On the other hand, the forward production of vector mesons is, as we pointed out, also ascribed to P exchange in the diffraction picture; for the massive mesons, crossing into the t-channel does not lead to the helicity - 2 assignment for the P; the asymptotic cross-section for some inelastic processes is therefore not expected to be suppressed. In future high-energy experiments on $\sigma_{tot}(\gamma p)$, we will particularly have to try to use photon beams of longitudinal as well as transverse polarization (e.g. using virtual photons from electro-production) in order to understand the process; for helicity - 0 (virtual) photons, the nonsense zero obviously does not exist.

If we want to make specific predictions for the magnitude of $\sigma_{tot}(\gamma p)$, we can use the VDM to link up $\sigma p \to$ anything and $V^o p \to$ anything. The most simple-minded prediction then neglects the ω and Φ parts of eq. 2.5-3, and we write

$$\sigma(\gamma_V A \to B) = \frac{\alpha\pi}{\gamma_\rho^2} \sigma(\rho^O A \to B) \qquad (2.7\text{-}1)$$

where γ_V is an isovector photon. This leads to a prediction of $\sigma_{tot}(\gamma_V p) \approx 100$ µb, taking numbers from Table I. The isoscalar contributions will be considerably smaller; in the energy region where data exist on $\sigma_{tot}(VN)$, from 3 - 5.5 GeV, we expect a value of $\sigma_{tot}(\gamma p) \approx 110$ µb on these grounds.

Another estimate uses the VDM in the specific form of the diffraction dissociation model[30], making use of the experimental information on the forward cross-sections, $\sigma(\gamma p \to V^O p)|_{t=0}$. Inserting the best values into the relation[58]

$$\sigma_{tot}(\gamma p) = \sqrt{16\pi}\left[\frac{e}{\gamma_\rho}\frac{d\sigma}{dt}^{1/2}(\rho) + \frac{e\sin\theta_y}{2f_y}\frac{d\sigma}{dt}^{1/2}(\omega) + \frac{e\cos\theta_y}{2f_y}\frac{d\sigma}{dt}^{1/2}(\Phi)\right]$$

$$(2.7\text{-}2)$$

where the weighted couplings have the mentioned ratio 9:0.65:1.3. We again find a prediction of $\sigma_{tot}(\gamma p) \approx 100$ µb. It is not easy to assign errors to these predictions, since we have to take the diffractive part of the forward cross-sections alone. They ought to be good to $\sim \pm 10\%$.

2.8. Measurement of the Total Cross-Section $\sigma(\gamma p)$.

The experimental problems involved in the measurement of $\sigma(\gamma p)$ are obvious; above all, it is a very difficult task to separate hadronic from purely electromagnetic events. Moreover, if we try to look at all final-state particles in order to make up for the lack of initial-state information (due to the usually poor definition of

photon energies), we run into the problems associated with the
detection of neutrals $(\gamma, \pi^O, K^O, n, \ldots)$.

Therefore, one of the main experimental tasks will be an
adequate definition of the initial-state energy, and possibly of the
initial-state polarization parameters. We will attempt to use
polarized photons to initiate the process. This can be done in a
number of ways; practically, the problem is being tacked with

    a) the photon tagging method,

    b) the electroproduction mechanism.

In addition, there are plans to use a

    c) backscattered laser photon beam

for a bubble chamber experiment proposed at the high-current SLAC.
Methods b and c are able to also provide polarization parameters for
the ingoing channel, a is not.

A beautiful, very recent experiment[59] used the photon-tagging
scheme at the 7.5 DESY synchrotron, in conjunction with a hydrogen
buble chamber, to measure $\gamma p \rightarrow$ hadrons up to 5 GeV photon energies.

They obtain a bremsstrahlung γ beam of known energy by having
a low-intensity electron beam hit a thin radiator, and momentum-
analyzing the electrons which underwent a bremsstrahlung process.
A counter hodoscope detects these electrons, covering a range of
0.5 to 5 GeV with a resolution of ~ 0.1 GeV.

The electron beam is swept over the radiator by a pulsed magnet
such that the bremsstrahlung photons will hit different sections of
the bubble-chamber depending on their time of arrival. Digitizing

electron momentum, pulsed field, and time-of-arrival, then fully

determines the photon energy (if we exclude double-bremsstrahlung

processes), so that ~ 10 events can be recorded for each 1 msec beam

pulse. A careful normalization can be performed by looking at the

fully determined events $\gamma p \to p e^+ e^-$, $\gamma p \to p \pi^+ \pi^-$. We can then find

σ_{tot} simply by counting strong-interaction events.

<u>Fig. 2.8-1</u> shows the results of the Hamburg group. σ_{tot} is seen

to decrease from ~ 200 μb at 0.5 GeV to ~ 110 μb from 2 to 5 GeV.

The errors given in the figure are statistical and systematic. There

is good agreement between these numbers and those expected from eq's

2.7-1 and 2.7-2. The figure also shows, for comparison, the single

(dotted line) and double (dashed line) π production cross sections.

The agreement with the VDM predictions ought to be regarded as

impressive evidence for its value in describing photon-induced hadronic

interactions. The idea of using electro-(or muo-) production to

provide kinematical input parameters is presently being employed to

determine σ_{tot} (γp) up to much higher energies, with e and μ beams

at the SLAC, and a μ beam at the Brookhaven AGS.

The idea is that we can write the double differential cross-

section for inelastic electron or muon scattering into solid angle

element dΩ and energy bin dE' as[60]

$$\frac{d^2\sigma}{d\Omega dE'} \approx F(\sigma_T + \epsilon \sigma_S)$$

(2.8-1)

where F and ε are energy- and angle-dependent kinematical quantities.

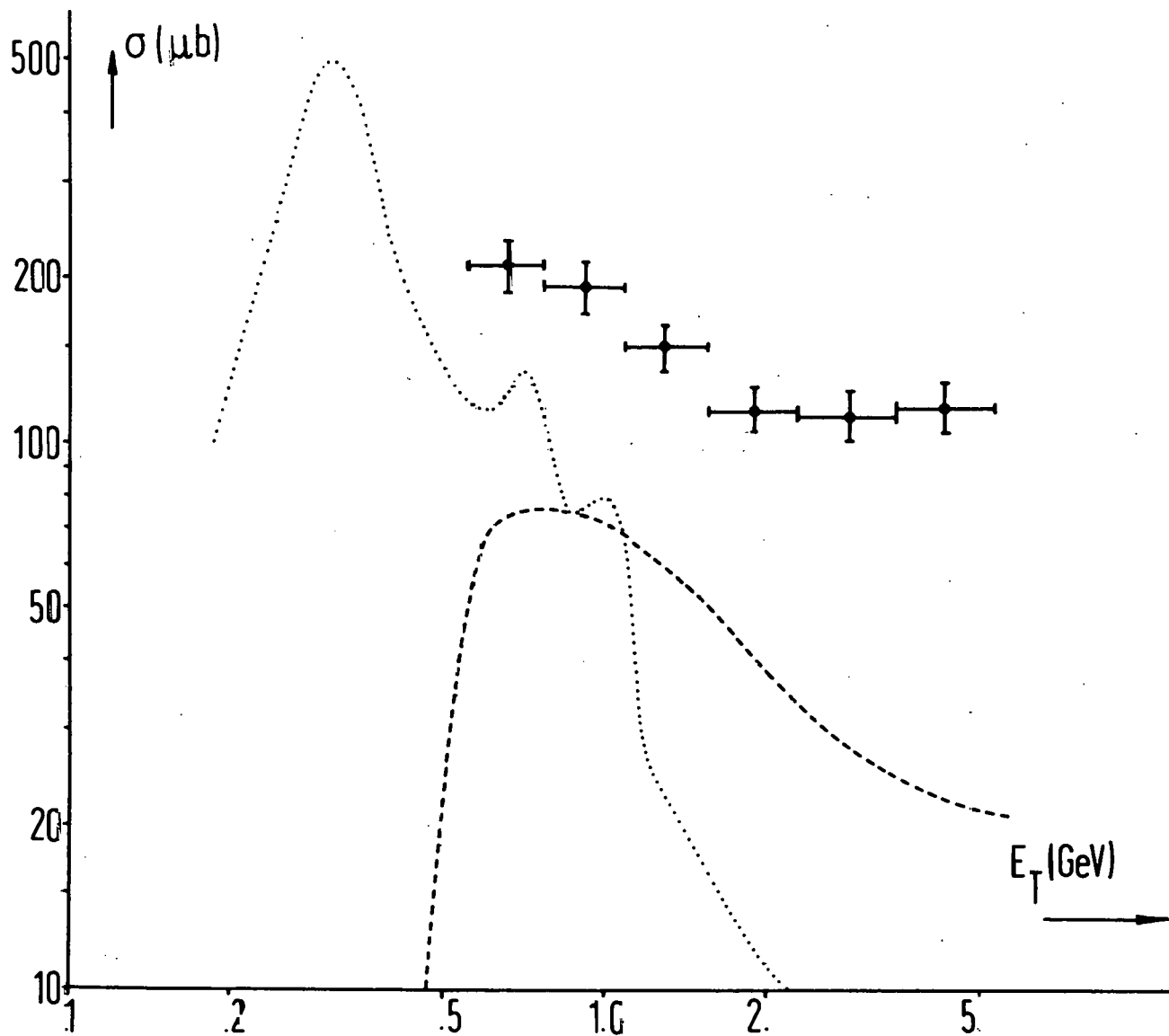It can be shown that, for small momentum transfer q^2, the "scalar"

Fig. 2.8-1 Measured values for $\sigma_{tot}(\gamma p)$. Dotted curve: single π production; dashed curve: double π production cross-section. (From Ref.No.59)

and "transverse" cross-sections σ_S, σ_T behave like

$$\sigma_S \xrightarrow[q^2 \to o]{} q^2 \left(\frac{d\sigma}{dq^2}\right)_{q^2 = o}$$

$$\sigma_T \xrightarrow[q^2 \to o]{} \sigma(\gamma p)$$

(2.8-2)

Then, if we measure electroproduction at small angles, and plot $1/F \ \frac{d^2\sigma}{d\Omega dE}$ vs. q^2 , we can hope to do a linear extrapolation to $q^2 = o$ and find $\sigma_{tot}(\gamma p)$ in this manner.

The experimental difficulty here lies in the fact that the radiative tail of the elastic scattering mechanism will dominate small-angle behavior and falsify the findings. A compromise has to be found by measuring at values of q^2 small enough so that an extrapolation to q^2 = zero appears credible, but large enough so that the radiative tail (which we believe we can evaluate well) does not completely drown out the electroproduction process.

This compromise can also be achieved at much smaller angles if we do not take electrons, but muons as incident particles. The radiative corrections are to be applied with a relative weight R[61]

$$R \approx \frac{\ln\left(\frac{-q^2}{m_\mu^2}\right) - 1}{\ln\left(\frac{-q^2}{m_e^2}\right) - 1}$$

(2.8-2)

At small momentum transfers q^2, this gives the μ experiment a considerable edge over inelastic electron scattering. For example, at

$q^2 = 0.02$, 0.2, and $1 (GeV/c)^2$, $R \approx \frac{1}{30}$, $\frac{1}{6}$, and $\frac{1}{4}$, respectively.
Although electron beams have a big advantage through their flux, we
will have to have considerable confidence in the calculation of the
radiative corrections if we want to do experiments at very small angles.
Fortunately, both μ and e experiments will be performed, and we can
look for consistency between them.

Lecture 3 Photoproduction of Pseudoscalar Mesons at High Energies

3.1 Experimental Data on t-Channel Poles.

In lecture 1, we focused our attention mainly on s-channel singularities in the photoproduction of pseudoscalars; in the 2nd lecture, after taking a close look at the data, we decided that one particular pole in the t-channel amplitude carried particular importance in the photoproduction of vector mesons. We will now look into the high-energy behavior of the photoproduction amplitudes for pseudoscalars.

We had previously noticed that the bump structure of the total cross section for processes $\gamma p \rightarrow N\pi$ appears to become less and less conspicuous with increasing energy. This is suggestive of the fact that we have to study the t- and u-channels and the influence of their singularity structure on the total amplitude; we believe that somewhere between 2 and 3 GeV, they will start being the dominant influence.

Let us look at a few relatively well-studied reactions:

a) $\gamma p \rightarrow p\pi^{o}$.

Fig. 3.1-1 shows the forward cross-section measured at DESY[62] and CEA[63], giving $\frac{d\sigma}{dt}$ at momentum transfers up to $-t = 1.8$ (GeV/c)^2. The DESY data were taken with two lead glass Čerenkov counters detecting the π^{o} decays into 2 γ's so that very small angles were accessible to measurement; the CEA experiment was performed with a spectrometer observing the recoil proton, thereby putting a cut-off on the small-t region (very slow protons cannot be detected in this way).
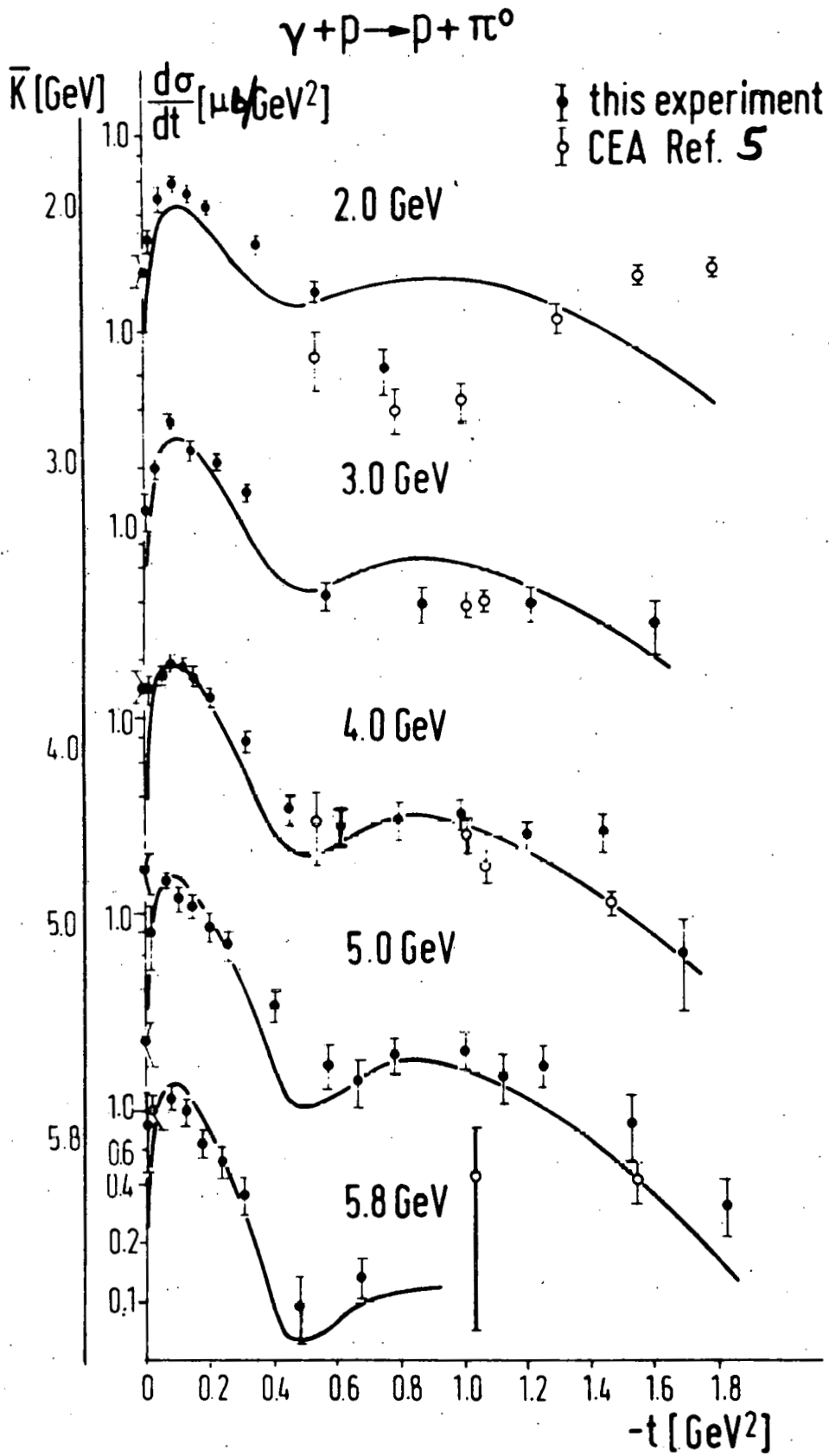
Fig. 3.1-1 Forward differential cross-section for $\gamma p \to p\pi^{o}$.
(From Ref. No. 62) Fits according to ref. 73.

We observe the following features: at high energies, 4-6 GeV, there is a very slim forward peak, poorly resolved. At all energies, a dip at moderately small t is followed by a peak at $-t \approx 0.1$ $(GeV/c)^2$; there is a secondary dip somewhere around $-t \approx 0.5$ $(GeV/c)^2$, but its position and its shape are not too constant over the energy range covered.

Fig. 3.1-2 gives a missing mass curve from the recent one-arm spectrometer experiment performed at SLAC[40] from which we earlier mentioned ρ^o and Φ yield data. Due to kinematically forbidden "ghost protons" which show up below π^o threshold, a non-trivial subtraction procedure has to be followed. The accuracy of the π^o production cross-section given in Fig. 3.1-3 is heavily dependent on this subtraction. The quoted results show nothing of the forward peak and first dip, since again there was a low-energy cut-off on the proton detection, but the cross-section at 6 GeV matches up with the 5.8 GeV data in Fig. 3.1-1. Notice, however, that the secondary dip gets less pronounced and degenerates into a shoulder between 6 and 18 GeV.

b) $\gamma p \rightarrow n\pi^+$

We have good and precise information on the forward π^+ production cross-section from DESY, CEA, and SLAC. It was taken with the aid of single-arm spectrometers (with the large SLAC spectrometer analyzing momenta up to $\sim$ 20 GeV/c); it is tricky to do very-small-angle experiments, so that we have to refer to the literature for details on their realization.
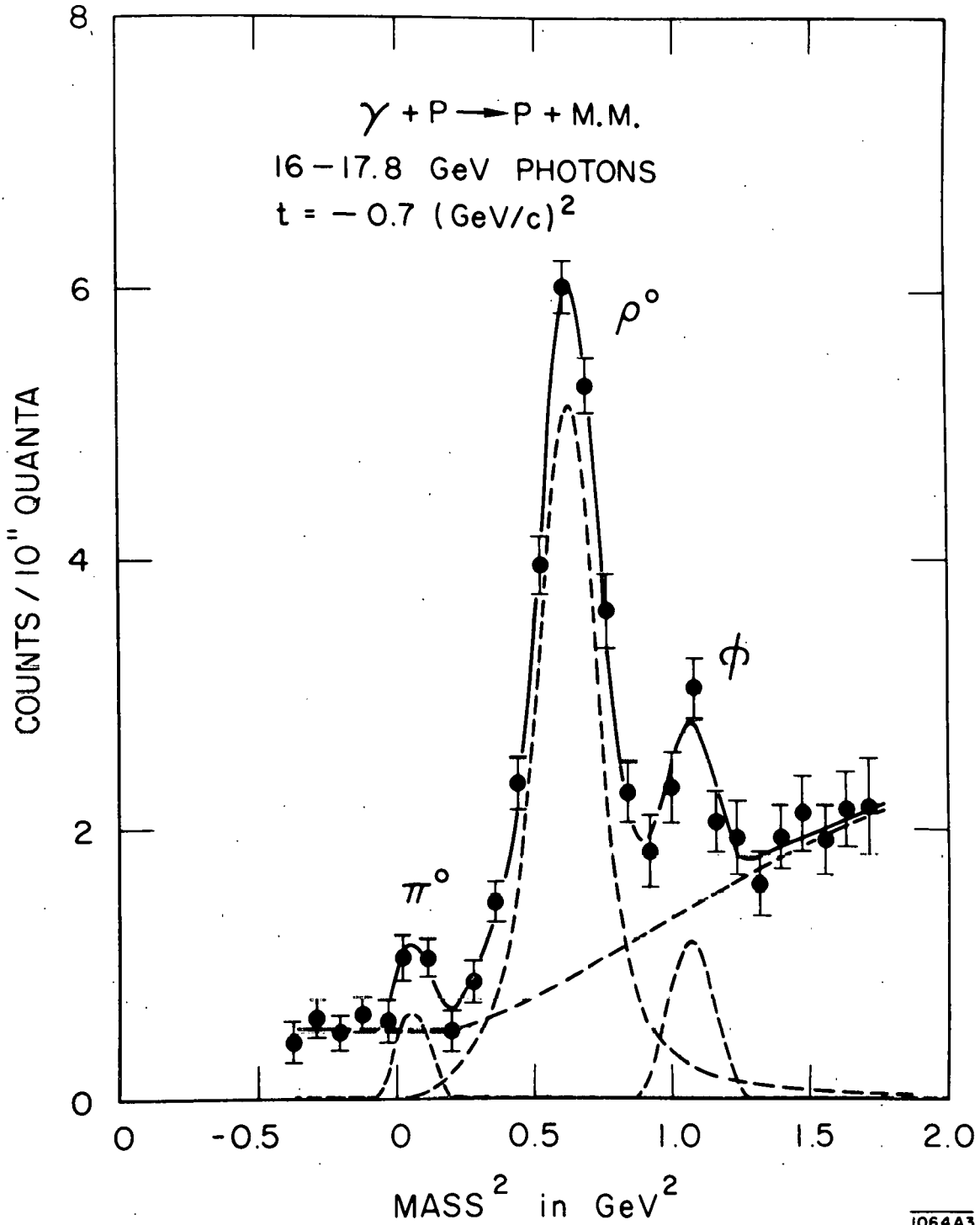
Fig. 3.1-2 Yields of recoil protons due to single boson photo-
production (cf. Fig. 2.2-9). Multiparticle back-
grounds have been subtracted out. Best fit curves
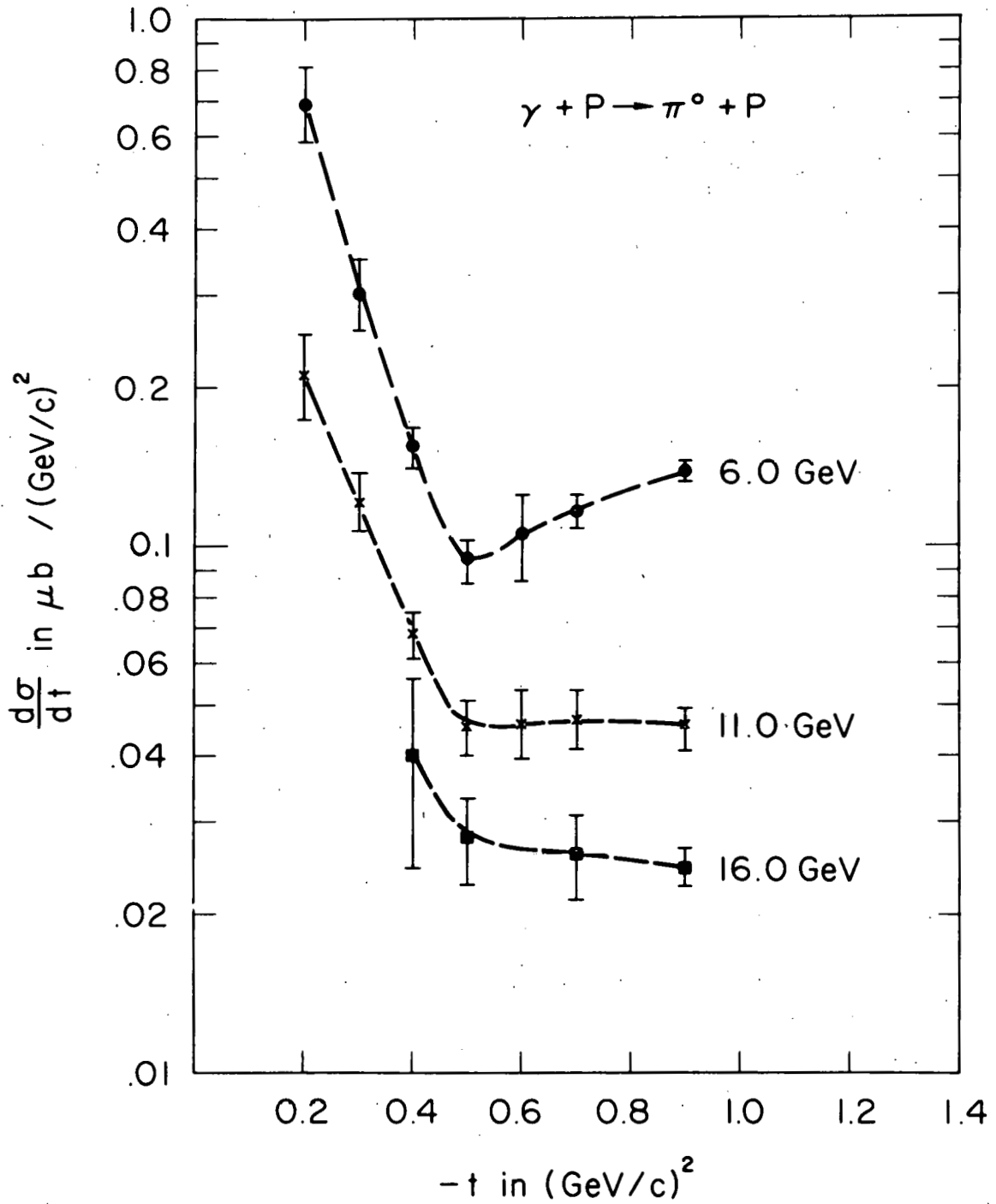are indicated. ω meson is not resolved.(From Ref. No. 40)

Fig. 3.1-3 High-energy π^{0} photoproduction: forward differential cross-sections. (From Ref. No. 40)

Fig. 3.1-4, summarizes the results of experiments below 1 $(GeV/c)^2$ momentum transfer [64,65,66]. Note the logarithmic scale. The DESY data go down to $-t = 10^{-4}$ $(GeV/c)^2$. There is consistent indication for a sharp forward peak, and none for any dip in the region $10^{-4} \leq |t| \leq 1$ $(GeV/c)^2$, $2.7 \leq k \leq 5$ GeV.

The SLAC data [67] taken at energies up to $k = 16$ GeV, confirm this result and carry it to higher energies and higher momentum transfers (up to $|t| = 2$ $(GeV/c)^2$. Moreover, the SLAC data show that outside the sharp forward peak, an exponential behavior describes the data well according to $\frac{d\sigma}{dt} \alpha\ e^{bt}$, with $b \approx 2$ for energies $k \geq 8$ GeV and momentum transfers $|t|$ between 0.07 and 0.6. At higher $|t|$ values, the exponential fall-off is steeper, with $b \approx 3.3$ $(GeV/c)^{-2}$. (Fig. 3.1-5).

c) $\gamma p \rightarrow K^+ \Lambda$

With the same apparatus as used for the high-energy π^+ detection, the Richter group at SLAC took forward photoproduction data on the process $\gamma p \rightarrow K^+ \Lambda$. The results, shown in Fig. 3.1-6, are quite dissimilar; there is a distinct dip at small angles, as we would expect from a one-particle exchange mechanism in its simplest formulation (cf. below). There is also, beyond the region of the dip, an exponential fall-off $\frac{d\sigma}{dt} \sim e^{bt}$ with $b \approx 3.1$ $(GeV/c)^{-2}$ between 5 and 10 GeV, close to the b value used to fit the π^+ data.

An obvious experimental difficulty in this context is the separation of the $K\Lambda$ and $K\Sigma^0$ final states (cf. Section 1.5). The errors on the Σ^0 cross-section are more bothersome than in the Λ case
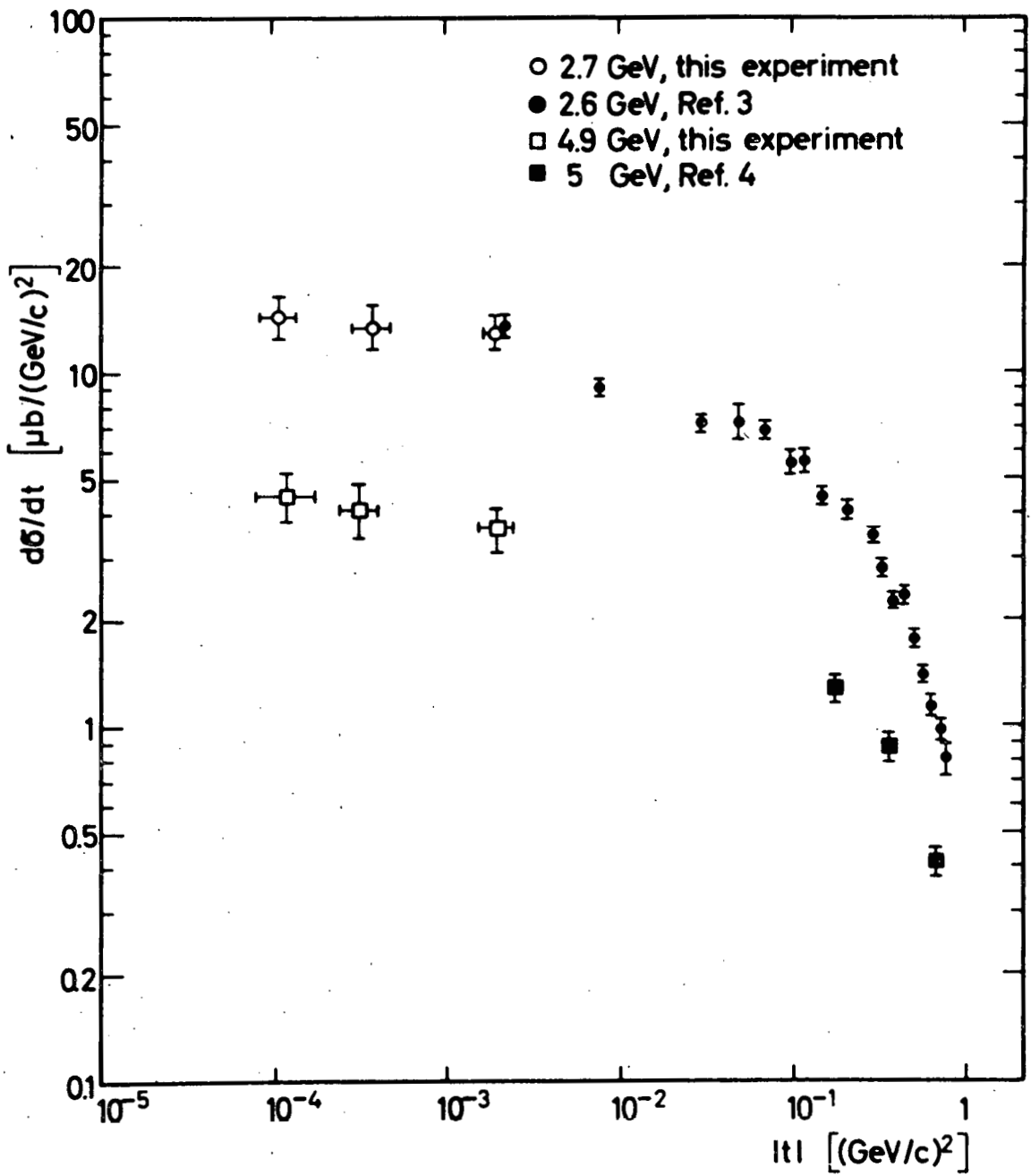
Fig. 3.1-4 Differential cross-section for $\gamma p \to n\pi^+$ at 2.7 to 5 GeV. Forward peak, on logarithmic scale, is indicated down to $|t| \approx 10^{-4}$ (GeV/c)^2. (From Ref. No. 64)

$$\gamma p \longrightarrow \pi^+ n$$
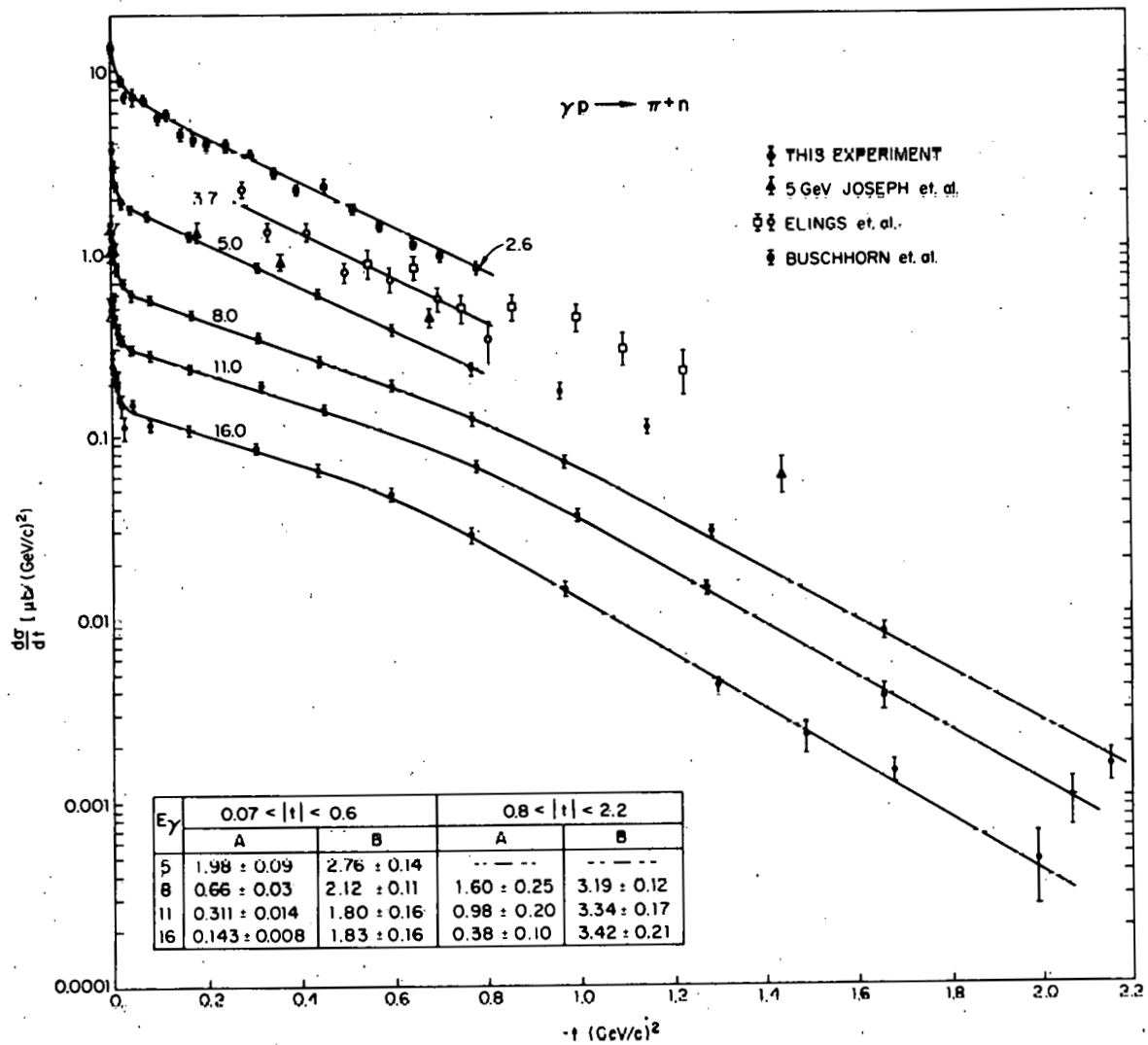
E_γ	$0.07 < |t| < 0.6$		$0.8 < |t| < 2.2$	
	A	B	A	B
5	1.98 ± 0.09	2.76 ± 0.14	-- — --	-- — --
8	0.66 ± 0.03	2.12 ± 0.11	1.60 ± 0.25	3.19 ± 0.12
11	0.311 ± 0.014	1.80 ± 0.16	0.98 ± 0.20	3.34 ± 0.17
16	0.143 ± 0.008	1.83 ± 0.16	0.38 ± 0.10	3.42 ± 0.21

Fig. 3.1-5 High-energy π^+ photoproduction. Forward peak and exponential slopes are indicated, with break in slope around -t = 0.7 (GeV/c)^2. (From Ref. No. 67)

Fig. 3.1-6 High-energy K$^+$ photoproduction differential cross-section exhibiting dip at small $|t|$. (From Ref. No.68)

because of the subtraction necessity. We'll come back to the KΛ/KΣ ratio later on (section 3.7).

3.2 Backward Photoproduction of π's.

Next, let us look at experimental information on photoproduction processes involving u-channel poles; we expect them to largely determine t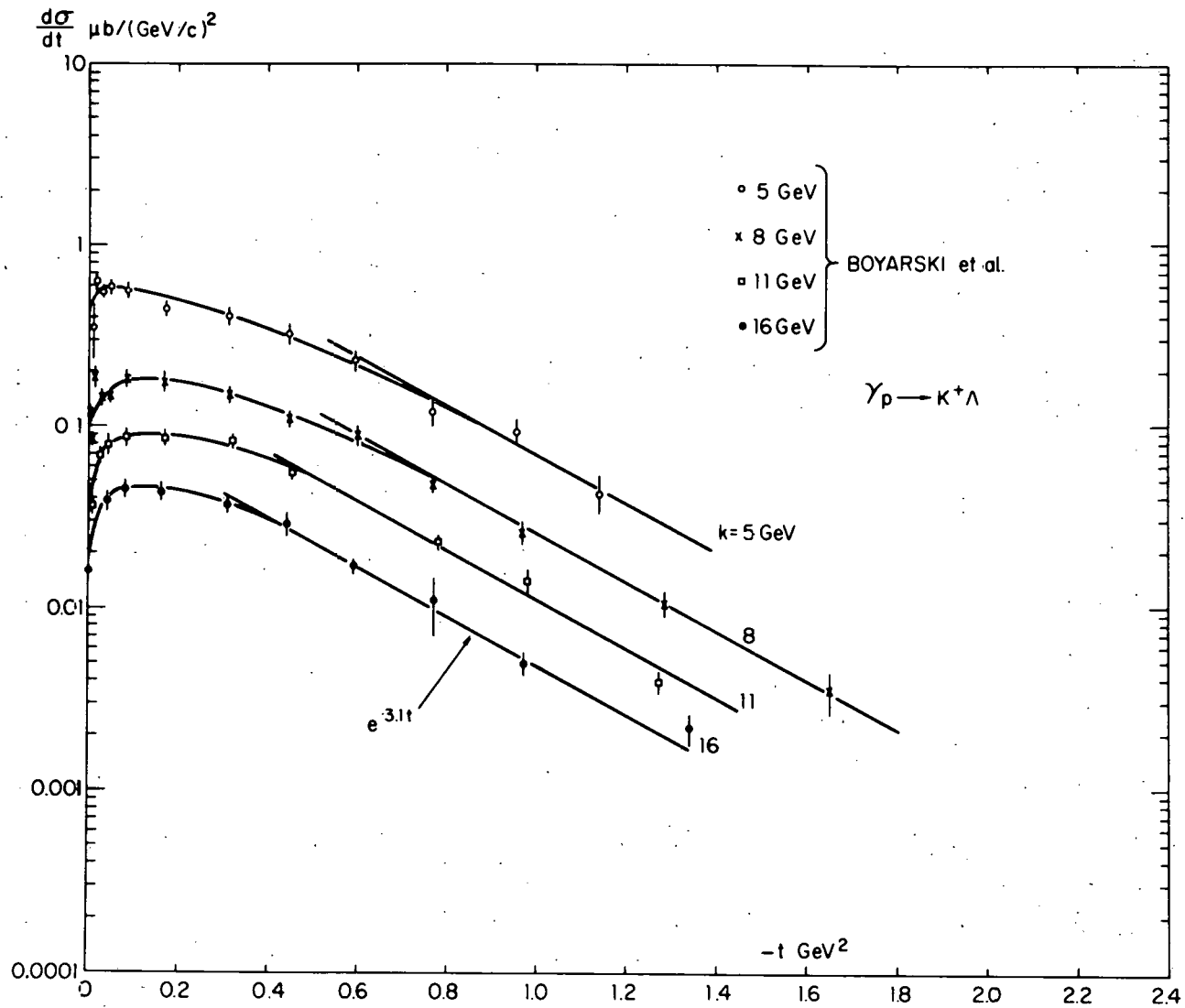he backward cross-section in the same manner in which t-channel poles are needed to account for forward phenomena. However, let us keep in mind (from section 1.3) that for the backward cross-section, only one of the four helicity amplitudes will contribute. Therefore, we also expect to see the resonance structure in this one amplitude in a very pronounced fashion, at energies ≤ 3 GeV.

a) $\gamma p \rightarrow p\pi^0$

Recent DESY data[69] display a pronounced peak-and-dip type structure, when we plot the $180°$ cross-section over the photon energy (cf.Fig. 3.2-1). It is seen that mainly the Δ resonances ($I = 3/2$) appear to show up appreciably - $\Delta(1920)$, $\Delta(2420)$, and possibly higher mass Δ's. The corresponding peaks in the production cross-section have been used to evaluate the photoexcitation of these states (cf. section 2.6). In terms of the helicity decomposition, the fact that we see these states strongly implies that the amplitude H_4 plays a strong role in their excitation, out of initial helicity 1/2 (section 1.3).

At higher energies, only very preliminary data from SLAC[70] are presently available. Fig. 3.2-2 shows the behavior of $\frac{d\sigma}{du}$ vs. u for four processes, at energies around 10 GeV, and momentum transfers
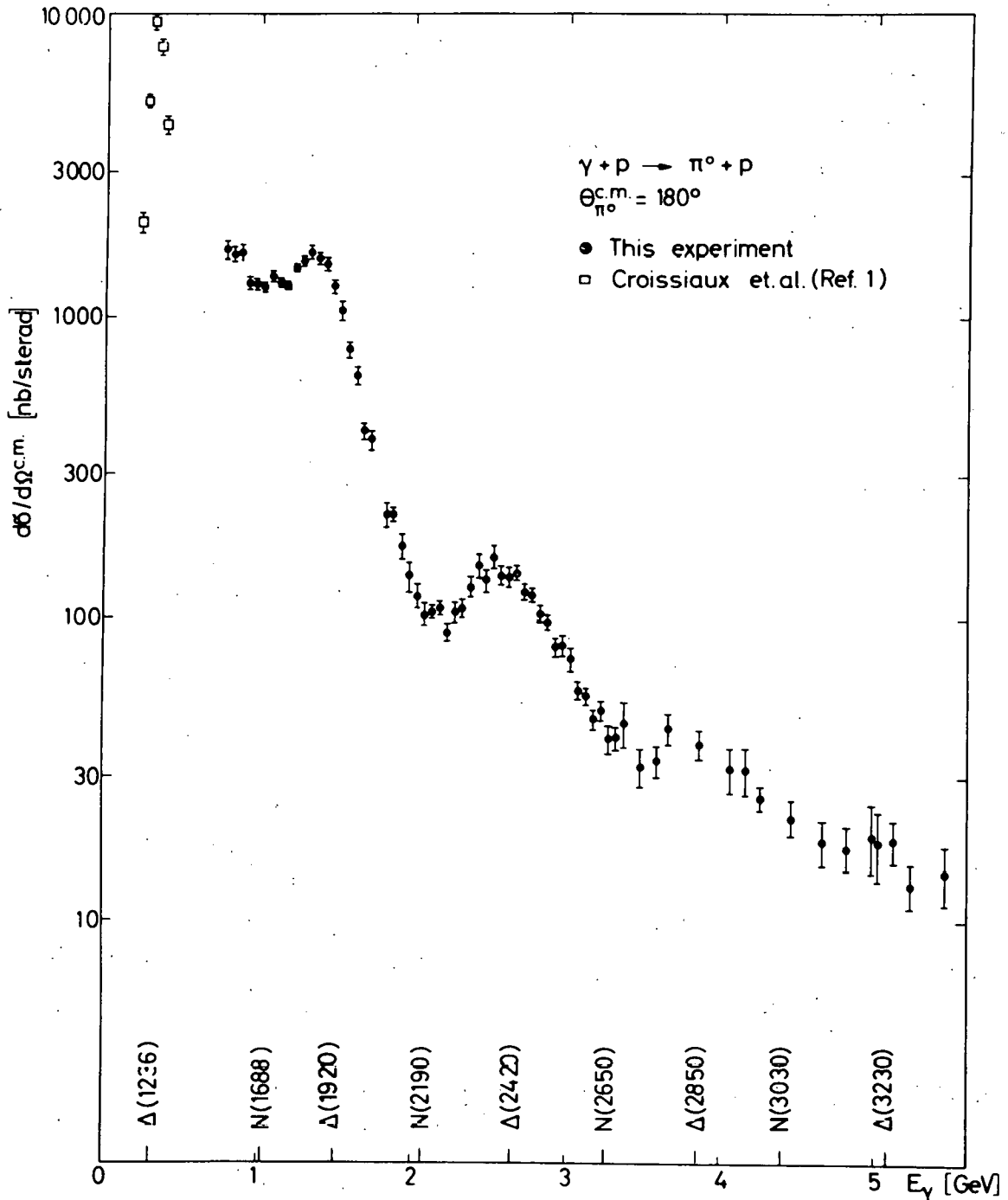
Fig. 3.2-1 180° differential cross-section for $\gamma p \to p\pi^\circ$. (From Ref. No. 69) Δ resonances appear to dominate the structure.
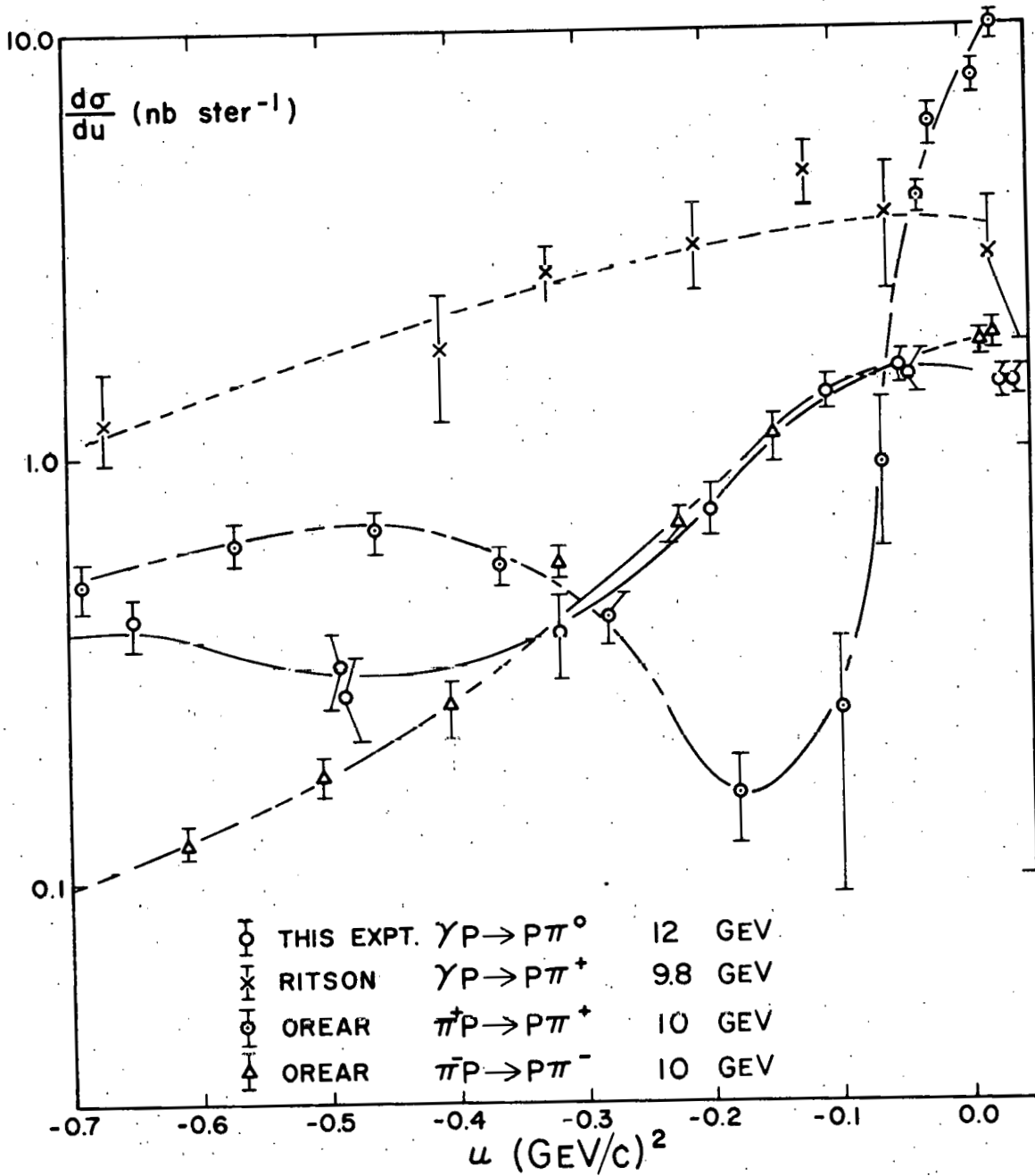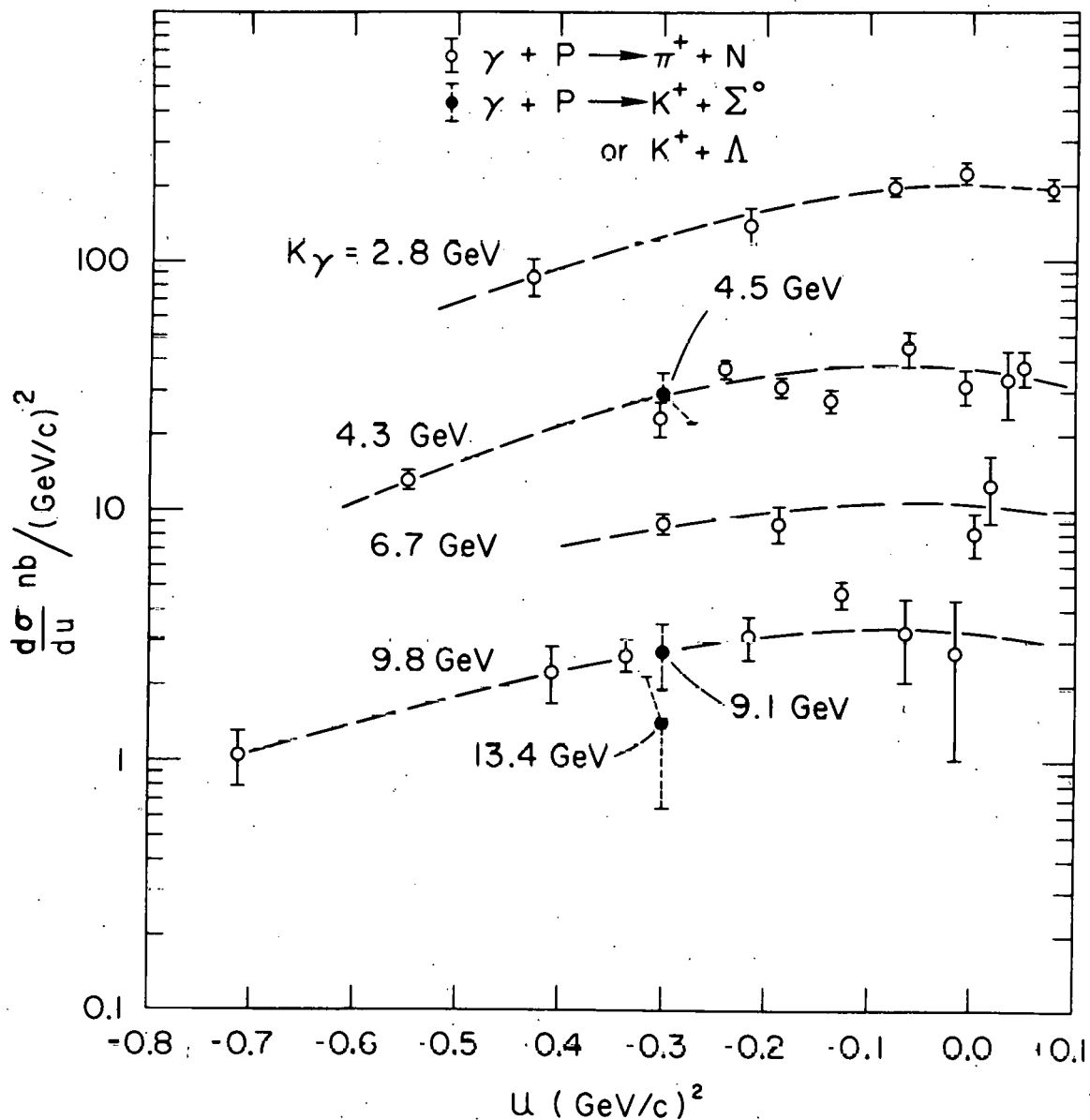
Fig. 3.2-2 Backward differential cross-section $\frac{d\sigma}{du}$ (u) for $\gamma p \to p\pi^0$.
(From Ref. No. 70) Comparison with π^+ photo-
production and $\pi^{\pm}$ p scattering is indicated.

-u between 0 and 0.7 $(GeV/c)^2$. (Note that we now are interested in momentum transfers in the <u>u-channel</u>, for backward production, quite analogously to the t channel analysis in the context of forward production.) The π^o cross-section $\frac{d\sigma}{du}$ shows no clear structure as a function of u: a slow decrease from u = 0 down, with a possible flat dip at $-u \approx 0.5$ $(GeV/c)^2$. For comparison, similar curves are plotted for $\pi^{\pm}p \rightarrow p\pi^{\pm}$ and for $\gamma p \rightarrow n\pi^+$ in the backward direction. Let's just note that the pronounced dip in $\pi^+p \rightarrow p\pi^+$ at u = -.15$(GeV/c)^2$ does not show up in photoproduction.

b) $\gamma p \rightarrow n\pi^+$

<u>Fig. 3.2-3</u> gives the angular distribution $\frac{d\sigma}{du}$ for π^+ backward production, at various energies between $2.8 \leq k \leq 9.8$ GeV. These data were taken at SLAC[71] with the 1.6 GeV/c spectrometer, again with an excitation-function technique - keeping beam energy and spectrometer angle fixed, and varying the accepted momentum for the spectrometer. As we explained in section 3.1, this method involves a difficult subtraction of backgrounds. At accepted momenta outside the allowed region for photoproduced π^+, there is still a considerable yield due to double processes in the target. In order to believe quantitatively the values given in <u>Fig. 3.2-3</u>, we have to put considerable trust in the subtraction procedure. However, the trend of $\frac{d\sigma}{du}$ vs. u appears clear - there is a smooth monotonical decrease, without any dip structure. The s-dependence of the backward cross-section is consistent with

$$\frac{d\sigma}{du}\bigg|_{fixed\ u} \quad \alpha\ s^{-2.9\ \pm\ 0.5}$$

Fig. 3.2-3 Backward differential cross-section $\frac{d\sigma}{du}$ (u) for
$\gamma p \rightarrow n\pi^+$. Three points represent same for
$\gamma p \rightarrow K^+\Lambda$ (or Σ°). (From Ref. No. 71)

between k = 2.8 and 13.4 GeV. The figure also shows a couple of points for the combined processes $\gamma p \rightarrow K^+\Lambda$ and $\gamma p \rightarrow K^+\Sigma^0$ (Λ and Σ could not be experimentally separated), in the backward direction. Since these are the only K backward data we have, let's just remark that they are roughly as large as the π^+ cross-sections at the same energies.

3.3 The Simple-Minded Regge Picture.

As we try to analyze the data shown in terms of t- and u-channel exchanges, let us recall that in relativistic scattering theory, crossing symmetry links up asymptotic high-energy behavior in the reaction a b $\rightarrow$ c d with low-energy poles in the t-channel a $\bar{c} \rightarrow \bar{b}$ d and in the u-channel a $\bar{d} \rightarrow \bar{b}$ c. In other words, the s-channel photoproduction amplitudes at high energies will be governed by low-energy singularities with the quantum numbers of the t and u channels.

It is well-known that elementary pole diagrams do not yield a successful picture; however, the concept of Regge trajectory exchanges associated with the quantum numbers of the corresponding channel has had considerable appeal.

In the simplest case, we have only one trajectory dominating the forward or backward behavior, e.g., in the parade case $\pi^- p \rightarrow \pi^0 n$, the ρ exchange diagram, where we now have the entire ρ trajectory (with angular momentum α_ρ (t) $\approx 0.6 + t$) exchanged, and nothing else is expected to contribute. Normally, there will be a spin-flip and a non-flip part of the amplitude, and we can write

$$\frac{d\sigma}{dt} \sim |A|^2 \sim (|B_{flip}(t)|^2 + |B_{non-flip}(t)|^2) \left(\frac{s}{s_o}\right)^{2\alpha(t)-2} \qquad (3.3\text{-}1)$$

The B's are associated with the residues of the poles which move with energy in the complex angular momentum plane. Then it becomes clear that for t = -0.6, α_ρ (t = -0.6) = 0, the spin-flip amplitude must have a zero (called a "nonsense zero", since it does not make physical sense that the α = 0 pole in the t channel could carry across any spin unit.) We expect then, and see, a pronounced dip in the cross-section $\frac{d\sigma}{dt}$ (t) (π^- p $\to \pi^o$n) at t $\approx$ 0.6, and we say the dip is due to a nonsense zero in the spin-flip part of the ρ trajectory amplitude. Such dips have been observed in many cases, and we will look out for them in the photoproduction cross-sections - keeping in mind that they refer to the dominance of one trajectory (or at worst, a few) in the amplitudes. Let us look at the data presented, and see whether they exhibit characteristics which can be explained in these simple terms.

a) γp $\to$ pπ^o Forward

The quantum numbers of the t channel with C = -1 suggest the ω as the leading trajectory. (We know that $\rho \to \pi\gamma$ and $\Phi \to \pi\gamma$ are small when compared with $\omega \to \pi\gamma$). The simple Regge pole model, with the exchange of the leading trajectory only, would then predict a zero cross-section at t $\approx$ 0.5 (GeV/c)^2. The lower-energy data show a dip in this region, but not a zero. To remedy the situation, an additional exchange of the $J^P = 1^+$ B meson was suggested[72,73] to fill in the dip, and Fig. 3.1-1 shows the fairly credible fits.

Some doubts remain, since the decay $B \to \pi\gamma$ has never been seen.
Above all, the leading trajectory (the ω) is expected to dominate
the situation more and more with increasing s according to eq. (3.3-1).
So, if the B meson trajectory has a slope equal to the ρ's, the dip
should become more pronounced at higher energies. The recent data
at 11 and 16 GeV suggest the opposite (Fig. 3.1-3).

One experimental remedy which can be invoked to study this aspect
is the initiation of this process by polarized photons;[74] exchange
of a natural parity object $(P = (-1)^J)$ will be observed in the pro-
duction plane only if the photons have a polarization component in
the plane. Unnatural parity exchange $(P = (-1)^{J + 1})$, like the 1^+
B meson) should be separated out by measuring the cross-section in
the dip portion, $t \approx -0.5$, with incident photons polarized perpen-
dicularly to the production plane. Very preliminary results of an
experiment to separate 1^- from 1^+ exchange in this manner[75]
(using a crystal-bremsstrahlung beam for plane polarization) indicate
that indeed the B (1^+) contribution is not what governs behavior in
the dip position. For a thorough investigation, we await final
results for this and other similar proposed investigations.

Another way to explain the peculiar behavior of the π^0 cross-
section as a function of energy and momentum transfer has been
suggested by Ross[76]. He proposes that not only the ω trajectory
exchange determines the cross-section, but that a final-state
rescatter modifies the picture such that the amplitudes due to
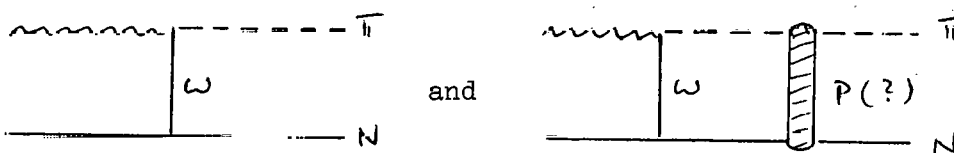
interfere in such a manner that they produce dips - which may then move and change shape with energy. Similar calculations have been successful in explaining the nucleon polarization in $\pi^- p \to \pi^0 n$, which was persistently observed experimentally, and due to the ρ's being the only exchanged trajectory in the reaction, was not expected to occur; this has been, for some time, a particularly embarrassing detail for straight-laced Reggeists.

One can tackle the problem similarly with the expedient of introducing Regge cuts in addition to poles (this is, in a way, what we did in the case of the above rescatter), or by involving fixed poles in the J plane. We regret that the frame of these lectures does not allow us to spend more time. Rather, we will eagerly wait for more experimental input -- especially from polarized γ beams.

The overall experimental picture in π^0 photoproduction is summarized in <u>Fig. 3.3-1</u>, where the features are shown on a distorted scale; a very narrow peak in the angular distribution due to the "Primakoff graph",

$$\gamma \sim\!\!\sim\!\!\sim\!\!\sim\!\!0\!-\!-\!-\!-\ \pi^0$$
$$\gamma$$
$$\underline{\hspace{5cm}}\ N$$
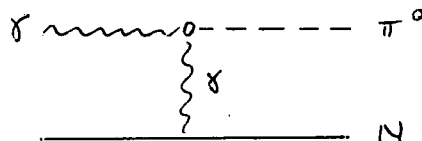
a forward dip, a peak, and secondary dip due to the t-channel ω pole and its "nonsense zero", and finally a not very steep backward peak

FORWARD PEAK DUE TO PRIMAKOFF EFFECT

FORWARD DIP OF NON-PRIMAKOFF CROSS SECTION

PEAK DUE TO t-CHANNEL EXCHANGE $(\omega?)$

BACKWARD PEAK DUE TO U-CHANNEL EXCHANGE

0° DIP (NOT RESOLVED EXPERIMENTALLY)

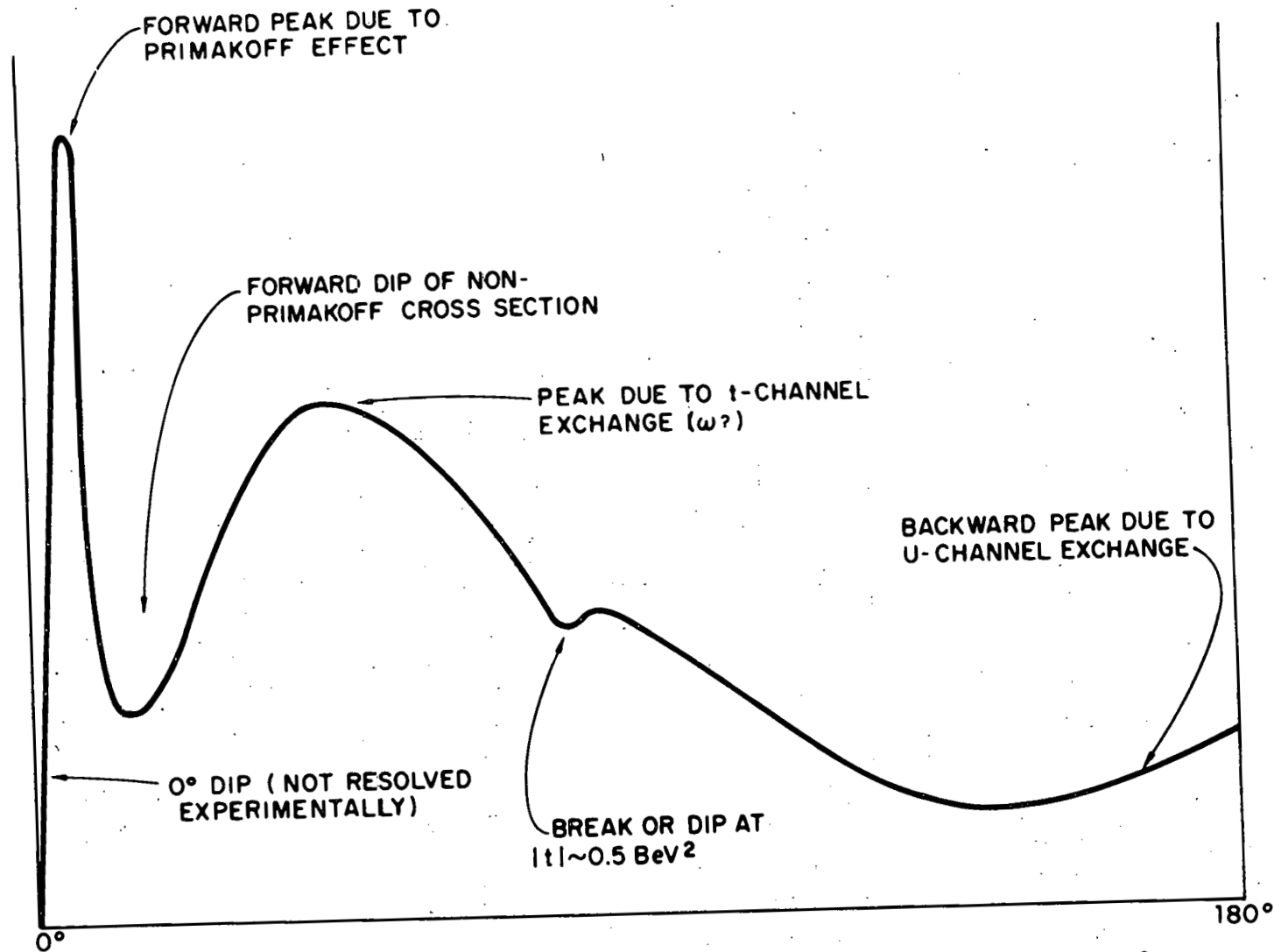BREAK OR DIP AT $|t| \sim 0.5$ BeV^2

0°

180°

Fig. 3.3-1 General characteristics of angular distributions for $\gamma + p \rightarrow \pi^0 + p$.

(From Ref. No. 12)

due to u-channel poles. <u>Fig. 3.3-2</u> compares the data, on a logarithmic scale, with the simple Regge fit (which does not include the sharp forward peak due to the Primakoff graph). The parameters adopted for the ω and B trajectories were

$$\alpha_\omega(t) = 0.56 + t$$

$$\alpha_B(t) = -0.30 + t \tag{3.3-2}$$

b) $\gamma p \to \pi^+ n$ forward

There are two features characteristic of the π^+ forward data; the sharp peak at $|t| < 0.02$ $(GeV/c)^2$, and the exponential fall-off with e^{bt} at larger $|t|$ values (<u>Fig. 3.1-5</u>). If we parametrize the latter feature in terms of eq. (3.3-1),

$$\frac{d\sigma}{dt} \alpha \ \epsilon^{\ 2\alpha(t) \ -2}$$

we find a trajectory for the leading exchange which is essentially flat with momentum transfer. <u>Fig. 3.3-3</u> shows that the ensuing values of $\alpha(t)$ are almost compatible with a fixed pole at $\alpha = 0$, very different from the trajectory naïvely expected from the lowest-mass t-channel pole
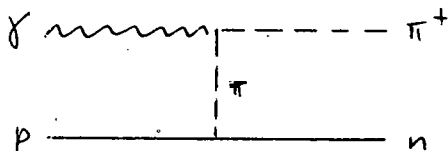
Even if $\alpha(t)$ is presumed to be due to collusion of several trajectories, it remains hard to explain, since, while the unit slope π trajectory passes through $\alpha_\pi = 0$ at $t = 0.02$ $(GeV/c)^2$, all other candidates
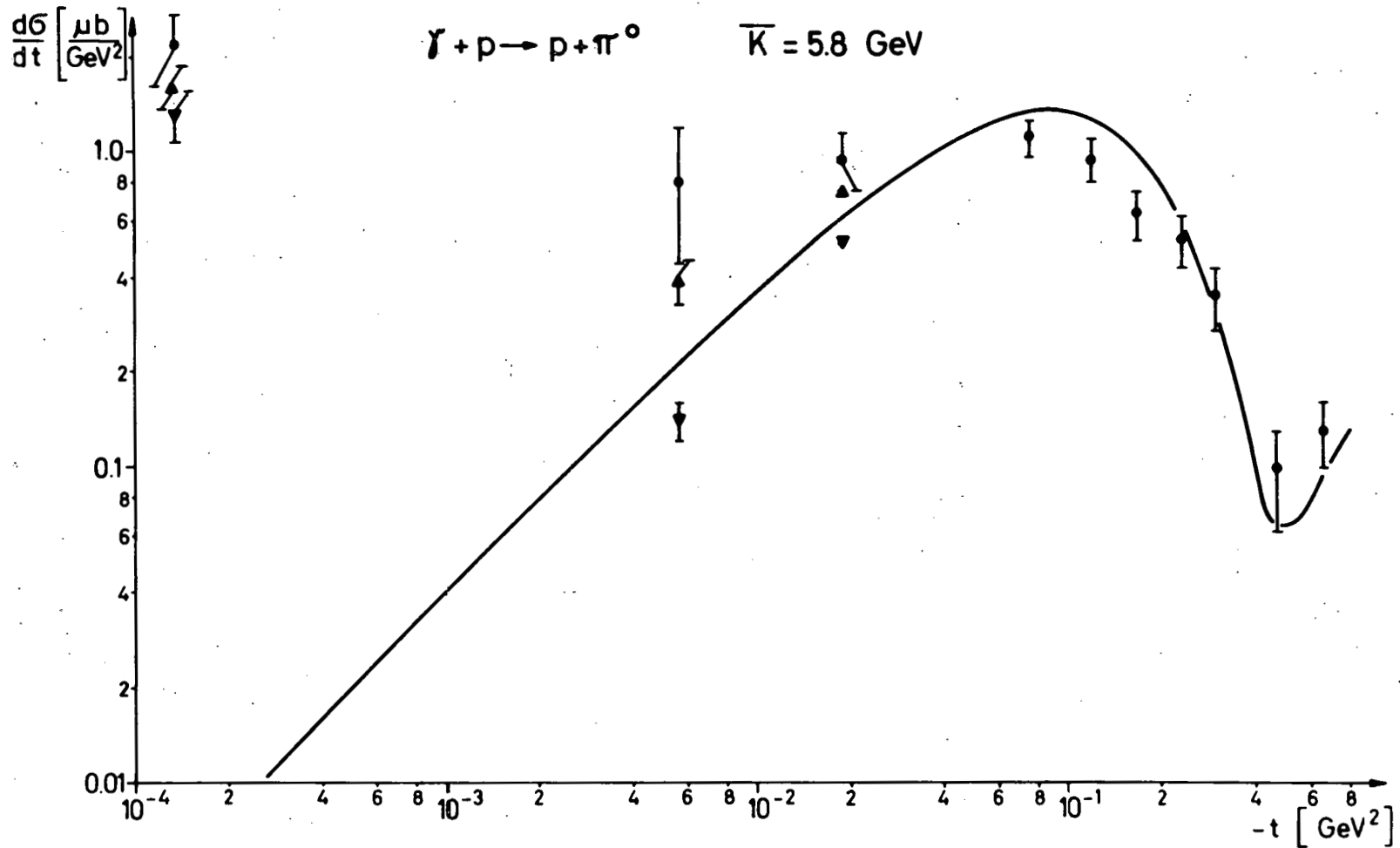
Fig. 3.3-2 Forward π^o photoproduction: fit to data (on exponential scale) using Reggeized ω and B exchange. (From Ref. No. 62)

Fig. 3.3-3 Effective leading pole parameter α(t), from t dependence
of π⁺ photoproduction. It is compatible with a fixed
pole at 0. (From Ref. No. 84)

(like the vector mesons) cross through zero at $\sim$ -0.5 $(GeV/c)^2$; however, the data indicate that $\alpha(t)$ remains close to zero, out to much larger t values.

We simply note a failure of the simple Regge picture here, and we delay the discussion of the sharp forward peak to section 3.5; it cannot be understood in terms of single-trajectory exchange alone.

   c) $\gamma p \rightarrow K^+\Lambda$ Forward

Recall that (cf. <u>Fig. 3.1-6</u>) the K^+ photoproduction data looked very similar to the π^+ results, as long as we do not look at t < 0.02, where the spectacular difference comes in between forward peak and dip. At $|t| > 0.5$, the slope is similar to that in the π^+ case, and from this $\frac{d\sigma}{dt} \alpha \, e^{3.1t}$ behavior we again deduce a flat effective trajectory $\alpha_K(t) \approx 0$, which we would naively want to associate with the charged K pole
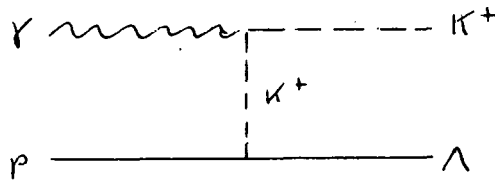
Fig. 3.3-4 shows the resulting trend for $\alpha_\pi(t)$, again compatible with a fixed pole at J = 0, over the entire t-range covered. Again, no interpretation in simple Regge terms appears possible.

   d) $\gamma p \rightarrow p\pi^0$ and $\gamma p \rightarrow n\pi^+$ Backward.

Let us look at the backward cross-sections $\frac{d\sigma}{du}$ in an equally simple-minded way, trying to explain the data in terms of the exchange of the leading (lowest-mass) poles. We notice that in elastic πp scattering,
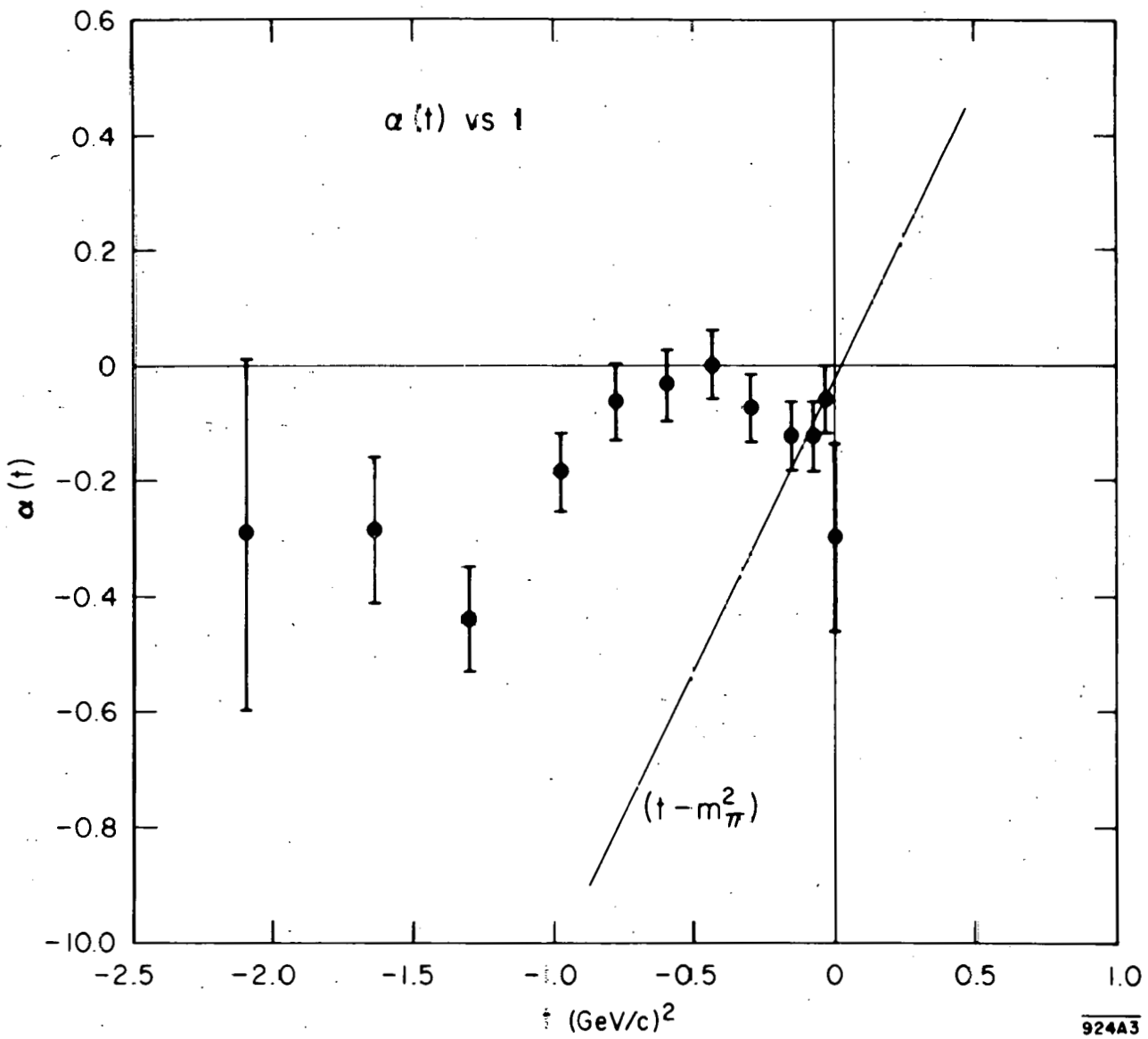
Fig. 3.3-4 Effective leading pole parameter α(t), from t dependence of K⁺ photoproduction. It is compatible with a fixed pole at 0. (From Ref. No. 84)

-116-

this approach appears successful. Fig. 3.3-5[77] illustrates our

point: For the case $\pi^+ p \rightarrow p\pi^+$

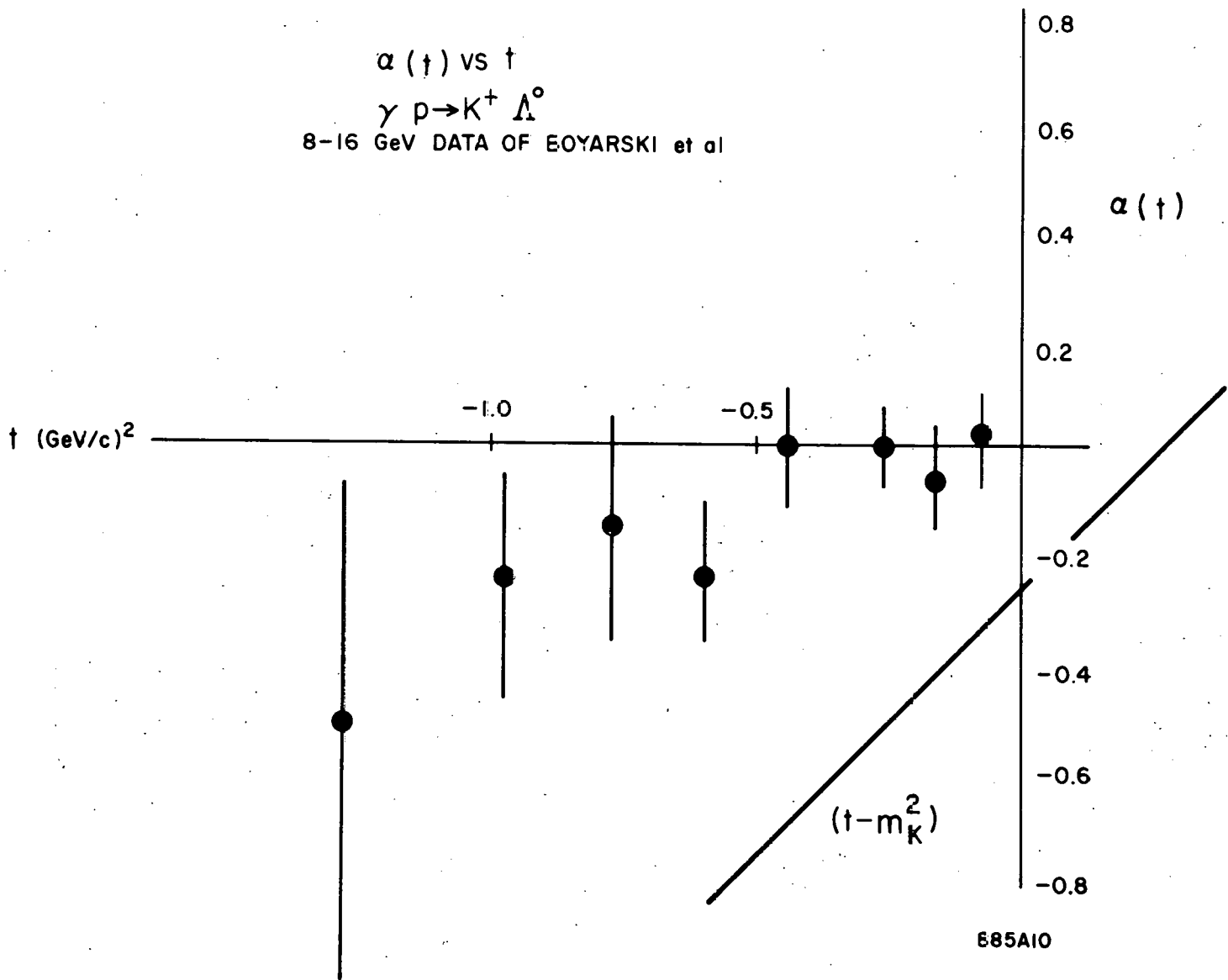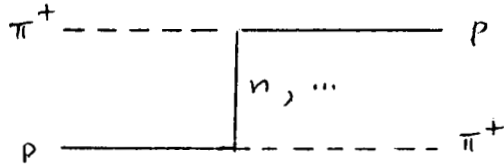the t channel quantum numbers determine the neutron pole as the lowest-

mass exchange; the nucleon trajectory, however, has a "nonsense zero"

at $\alpha_N(u) = 1/2$, corresponding to $-u \approx 0.15$ $(GeV/c)^2$. There is a

distinct dip visible. In the case of $\pi^- p$ backward scattering,
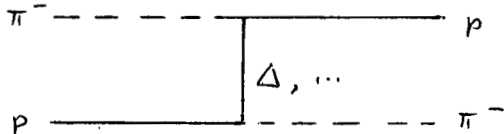
the I spin quantum number of the t channel does not allow for nucleon

exchange, but the Δ trajectory is expected to dominate. This is borne

out by the data (also in Fig. 3.3-5): The Δ trajectory has no nonsense

zero in the physical region u<0, at u values covered here; it may or

may not finally reach the nonsense point at $\alpha_\Delta = -3/2$, but no dip is

visible.

In the photoproduction of π^o and π^{-} in the backward direction,

we would expect the diagram
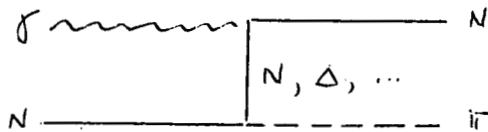
to be dominated by the nucleon pole in the u channel. However, the

data (Fig.s 3.2-2 and 3.2-3) make it quite clear that there is no

indication of a dip at $-u \approx 0.2$.

Fig. 3.3-5 Backward differential cross-sections for elastic scattering
$\pi^{\pm} p \to \pi^{\pm} p$. (From Ref. No. 77)

E. A. Paschos[78] at SLAC has recently given a careful evaluation of the backward cross-section for both πp elastic scattering and the photoproduction processes. Keeping track carefully of all the kinematical singularities involved, he fits the elastic scattering data with the nucleon ("N_α") and Δ trajectories, respe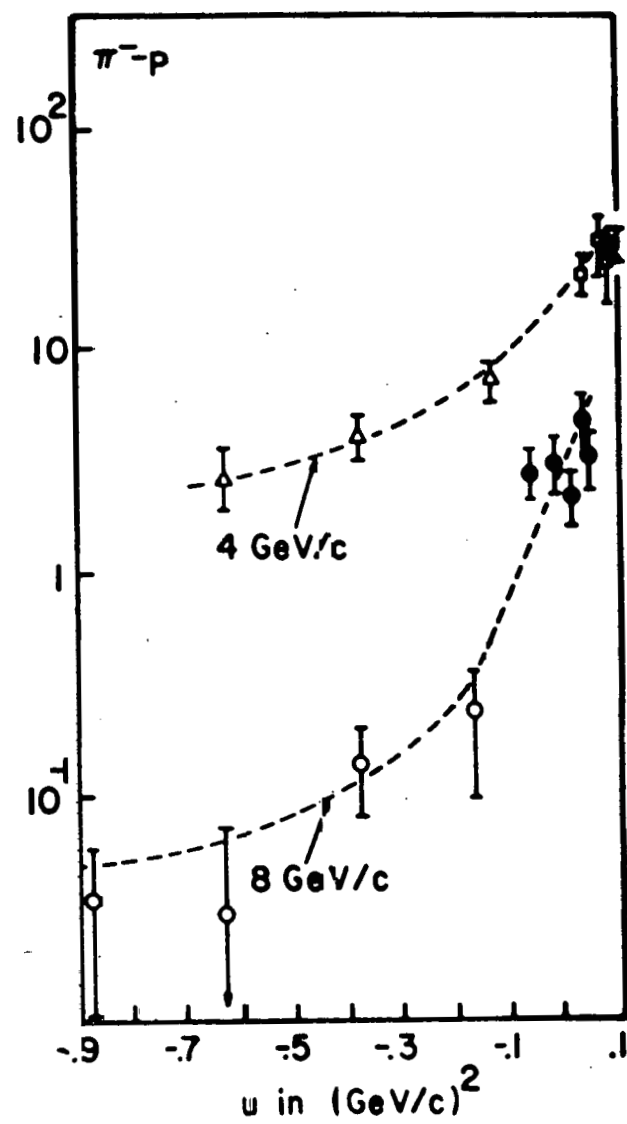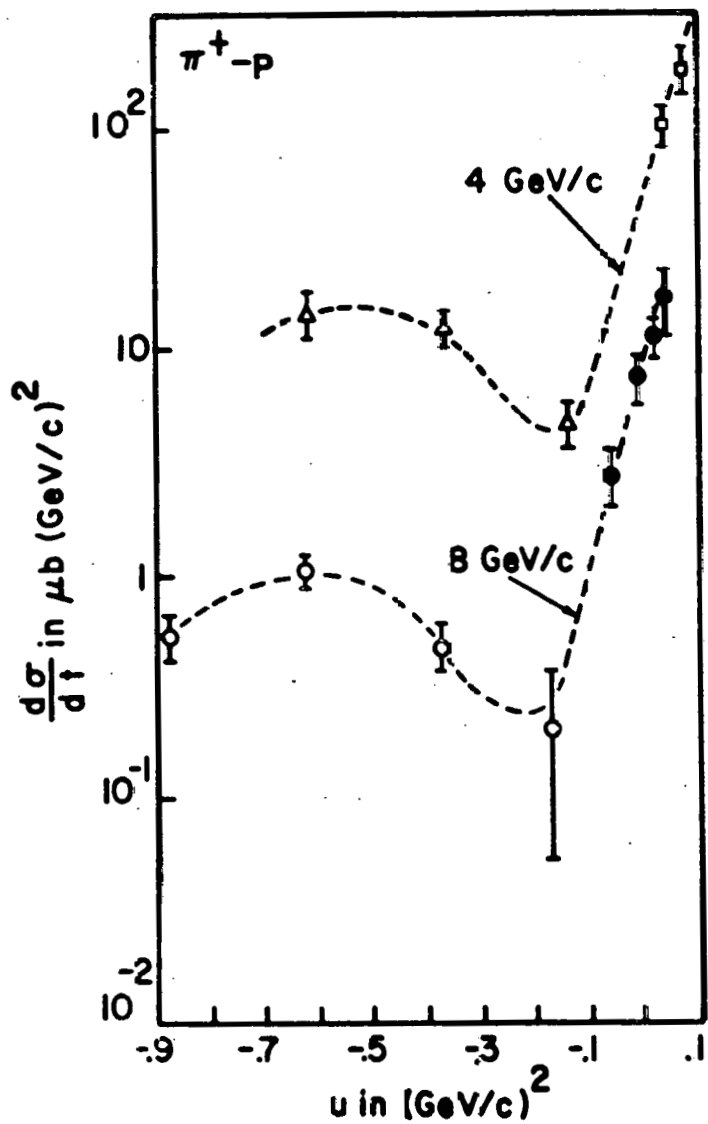ctively. Then, noting that the non-dip at the nucleon nonsense zero in photoproduction makes an interference effect likely, he excludes dominance of nucleon trajectory exchange. Similarly, however, Δ trajectory exchange is not the only process occurring. For pure Δ exchange, which has to be isovector, isospin invariance prescribes

$$\left. \frac{d\sigma}{du} \right)_{\pi^0} = 2 \left. \frac{d\sigma}{du} \right)_{\pi^+} \quad \text{if } \Delta \text{ exchange.} \quad (3.3\text{-}3)$$

However, the data make the two cross-sections of eq. (3.3-3) look about equal. Therefore, interference effects between the N_α and the Δ trajectories are likely to account for the observed structure.

It may not appear too surprising that the coupling of the Δ to N_γ is _not_ suppressed with respect to the coupling of the N_α trajectory: remember that, for the particular case of π^0 backward production (Fig. 3.2-1), the Δ states show up very strongly. Similarly, in the framework of the ρ dominance picture, we recall that the Δ's ($I = 3/2$) are favored in the coupling to the ρN system (cf. section 2.1).

3.4 The Not-so-simple Regge Picture: Cuts, Fixed Poles, Conspiracy.

In the above treatment, we have looked at the available π and K photoproduction data with the specific question in our minds: Can they

be reasonably described in terms of the exchange of one or a few

leading trajectories, associated with the lowest-mass particles whose

quantum numbers can be exchanged in the corresponding channel? The

answer appears to be: in the forward direction, certainly not.

Neither the sharp peak in π^+ production (and the corresponding dip

for K^+), nor the constancy of $"\alpha_\pi(t)"$ with t for larger $|t|$ values, nor

the general behavior of π^o photoproduction are explained in such

simple terms.

We cannot, in the context of these lectures, give an account of

the theoretical framework of the concepts which may be called to the

rescue when the simple picture fails. We'll just mention the main

ideas, without even there attempting to be complete.

For one thing, it has consistently been pointed out that the

singularity structure of the scattering amplitude in the complex

angular momentum plane will normally comprise cuts as well as poles,

in full analogy to normal polology in the complex momentum plane.

It would be a much-hoped-for accident, if we had only poles, and not

cuts, moving in the complex-l plane.

It is obvious that the presence of cuts would cloud the peak-

and- dip structure naively expected, and often found, due to domin-

ant poles. Physical concepts leading to such mathematical cuts can

be formulated in a number of different ways, one of which is the

idea of Ross et al.[76] to postulate rescatters in the ingoing and

outgoing channels, in addition to the dominant exchange. Absorption

corrections to single exchanges can lead to a similar picture.

Another way in which cuts can be introduced, but which need not lead to cuts, is through fixed poles in the ℓ plane (i.e., poles which do not move as a function of t). We mentioned the simple Regge analysis of π^+ forward production at moderate t values, which led to a picture consistent with the presence of a fixed pole at $J = 0$.

There is wide-spread controversy over whether such fixed poles exist in photoproduction[79,80,81]. In general, reactions involving spin have possible fixed poles at integer positions of ℓ, either positive or negative, $\ell_p \leq J_1 + J_2 - 1$ or $\leq J_3 + J_4 - 1$, whichever is larger[82]. This implies that, in spinless processes, fixed poles are located at negative integer values, so their influence is expected to be masked by the (higher-lying) trajectories of moving poles. L. Jones[83] has pointed out that a fixed pole at $J = 0$ will

a) contribute to the "negative signature" amplitude, from which we obtain the above-mentioned nonsense zeroes, such that there is a constant term as $\alpha \rightarrow 0$, filling in the dip; it will not affect the high-energy behavior;

b) will not affect the general structure of the "positive signature" amplitude in the vicinity of its nonsense point $\alpha = 0$, but rather add a term $\alpha \frac{1}{s}$ to the asymptotic value. This will then dominate the cross-section at $\alpha < 0$.

At present, there is no compelling evidence which points to the presence of this particular mechanism in photoproduction.

One concept which has recently attracted much attention is the

"conspiracy" of various trajectories - in its most general form the collusion of two or more trajectories to mask kinematical singularities normally occurring in scattering amplitudes. A "conspiracy relation" is then a constraint imposed on the four helicity amplitudes due to the conspiring trajectories at one particular kinematical point, such that the overall amplitude at that point is free from the singularity normally occurring there.

We will specifically mention one case, in which the conspiracy mechanism has been used to explain the absence of a dip in π^+ photoproduction at $t = 0$, in the next section.

3.5 Interpretation of Forward Dips or Peaks. Conspiracy or Not?

Consider, to start with, the simple one-particle exchange approach: the only s-channel helicity amplitude which will contribute to the 0° cross-section will be (cf. section 1.3) the so-called flip-flip amplitude $A_{\mu = 1/2, \lambda = 1/2}$ (or II_2 in our previous notation). In this amplitude, angular momentum conservation is effected through simultaneous flip of the nucleon helicity, and a change of helicity between the $\lambda_k = 1$ photon and the π. If this double-flip is brought about by the exchange of one particle, its contribution must be proportional to the momentum transfer t, because all helicity flip couplings involve the momentum of the exchanged object at least linearly.

In other words, <u>single-particle exchanges lead to</u> $\frac{d\sigma}{dt} \propto t$ for small t, and since $t = 0$ is very close to 0°, $\frac{d\sigma}{dt} (t = 0) = 0$ means

a dip in the forward cross-section.

Now recall the π^+ data shown in Fig. 3.1-5; there is a sharp forward peak rather than a dip. How can we explain this?

Richter[84] pointed out that the forward peak can be accounted for in terms of the Born terms alone. The diagrams (cf. section 1.2)
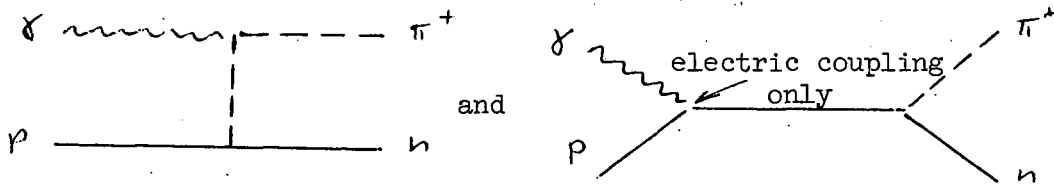
contribute to the forward amplitude like

$$A \sim \bar{u}(p) \left(\frac{\epsilon \cdot q}{k \cdot q} - \frac{\epsilon \cdot p}{k \cdot p} - \frac{i\sigma_{\mu\nu}}{2k \cdot p} \epsilon^{\mu}k^{\nu} \right) u(p) \qquad (3.5-1)$$

The first term, the π pole in the t channel, dips in the forward direction, as we mentioned. The minimal gauge- invariant form, $\propto \frac{\epsilon \cdot q}{k \cdot q} - \frac{\epsilon \cdot p}{k \cdot p}$, still dips at $t \to 0$, but the $\sigma_{\mu\nu}$ term has a 0° contribution (only in the low partial waves). Fig. 3.5-1 shows that in these terms alone, we can account for the forward behavior at all energies, whereas at larger momentum transfers, $|t| \gtrsim m_\pi^2$, the conventional Regge terms look more appropriate. One might object that at high energies there will certainly be some absorption of the low partial waves, which would eliminate the peak due to the $\sigma_{\mu\nu}$ term. However, absorption would simultaneously affect the first two terms, and they would then no longer dip around 0°, so that the overall picture remains consistent.
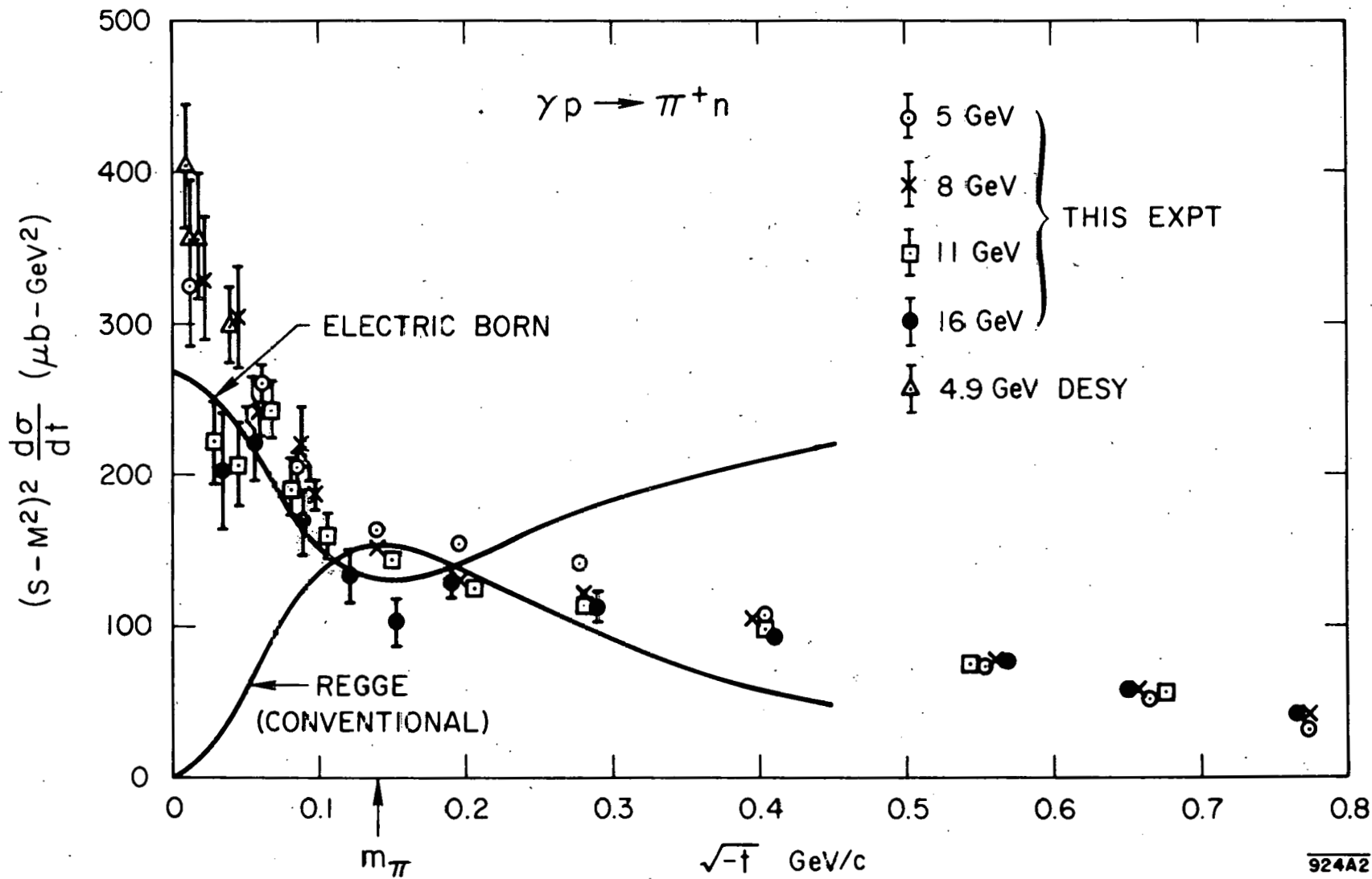
924A2

Fig. 3.5-1 Fit to forward peak in π^+ photoproduction, using Born terms (eq. 3.5-1) alone. Agreement is seen to be good for $|t| \leq m_\pi^2$. (From Ref. No. 84)

The forward peak can also be explained in terms of conspiring trajectories. Ball et al.[85] went through the details of π^+ and K^+ forward production. (For the general formalism, we refer to the literature cited in ref. 85.)

In section 1.3, we wrote down the helicity amplitudes for the s channel. Similarly, it is often convenient to define t-channel helicity amplitudes. We can write them in such a fashion that they are free from kinematical singularities, and find four independent parity-conserving amplitudes, corresponding to the exchange of natural (parity = $(-1)^\ell$) or unnatural ($P = (-1)^{\ell + 1}$) parity exchanges. Specifically, we can write

F_1, F_3 contain natural parity exchanges (0^+, 1^- ....)

F_2 contains unnatural parity exchange (0^-)-- e.g., π

F_4 contains unnatural parity exchange (1^+)--e.g., A_1

If we relate these amplitudes at the singular points $t = 0$, $4m_\pi^2$ such that the overall amplitude is regular (this is the meaning of the word <u>conspiracy</u>), we get relations among the various F's. In particular, the $t = 0$ condition links up F_2 and F_3. This means we obtain a condition between the π exchange and a normal parity exchange.

We can then postulate that in addition to the π trajectory, whose presence is expected, we also have a conspiring trajectory of opposite parity, the (in-) famous π_c (0^+) trajectory, making up a parity doublet. The specific conspiracy condition then relates the residues $\beta(t)$ and the $\alpha(t)$ values at $t = 0$ according to

$$\alpha_\pi(0) = \alpha_{\pi_C}(0) \, ,$$

$$\beta_\pi(0) = - \frac{m_\pi^2}{m_N} \beta_{\pi_C}(0) \, .$$

(3.5-2)

With these conditions among the opposite-parity trajectories, the dip at small $|t|$ disappears, and we can actually account for a peak structure. However, in order to have a somewhat palatable picture, we have to postulate also that the conspirator trajectory "choose nonsense" at $\alpha_{\pi_C} = 0$; otherwise we would have the embarrassing prediction of a 0^+ meson degenerate with the π, which has somehow eluded our observation.

After having given this example for a conspiracy-type explanation of the forward peak, we have to add that this approach does contain some uneasy features. In particular, we have to make the residue function $\beta_\pi(t)$ of the π trajectory vary strongly with t in order to get a consistent picture, whereas we leave the conspirator residue constant. Also, for a simultaneous explanation of the <u>dip</u> in forward K^+ production, the presence of a conspirator K_C will have to be suppressed in its influence on the 0^0 amplitude. This may be explained by the closeness in mass of K and K* (much closer than π and ρ), so that vector meson exchange may bring about the overall <u>dip</u> in the K^+ cross-section.

Amati et al.[86] shunned these features and showed that a slowly t-dependent background interferring with the π pole may also be used to explain the forward data. It may be interpreted as stemming from a fixed pole, or from absorptive corrections to the π pole.

3.6 The π^-/π^+ Ratio

A very important addition to our understanding of the π photo-production process can be expected from the study of the ratio R defined as

$$R \equiv \frac{\gamma d \to \pi^- p \; (p)}{\gamma d \to \pi^+ n \; (n)} \qquad\qquad (3.6\text{-}1)$$

where the (p), (n) are supposed to be "spectator" particles, not directly involved in the reactions. We have experimental results from CEA[87] and DESY[88], and expect more from SLAC at higher energies.

The analysis of such data is meaningful only if we make sure that the spectator model is solid in the momentum transfer range covered.

The earlier experiment[87] showed (Fig. 3.6-1) a ratio R which is strongly momentum-transfer dependent, and is considerably smaller than unity at the lowest t-value measured, $-t = 0.4$ $(GeV/c)^2$. This value for R may be taken as an indication for considerable interference between (in terms of the vector dominance model) the diagrams
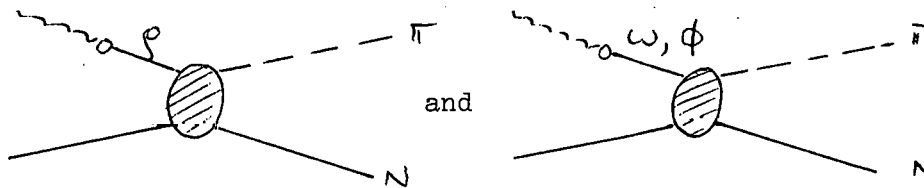
Although ω and Φ are more weakly coupled to the photon (cf. section 2.5) than the ρ, the fact that ω and ρ interfere with different signs in π^+ and π^- production may well account for this ratio (see eq. 2.6-4).

The more recent Hamburg experiment[88] investigated the ratio R down to much smaller $|t|$ values. Fig. (3.6-2) shows results of π^+ and π^- cross-sections from deuterium, and π^+ from hydrogen. It is seen

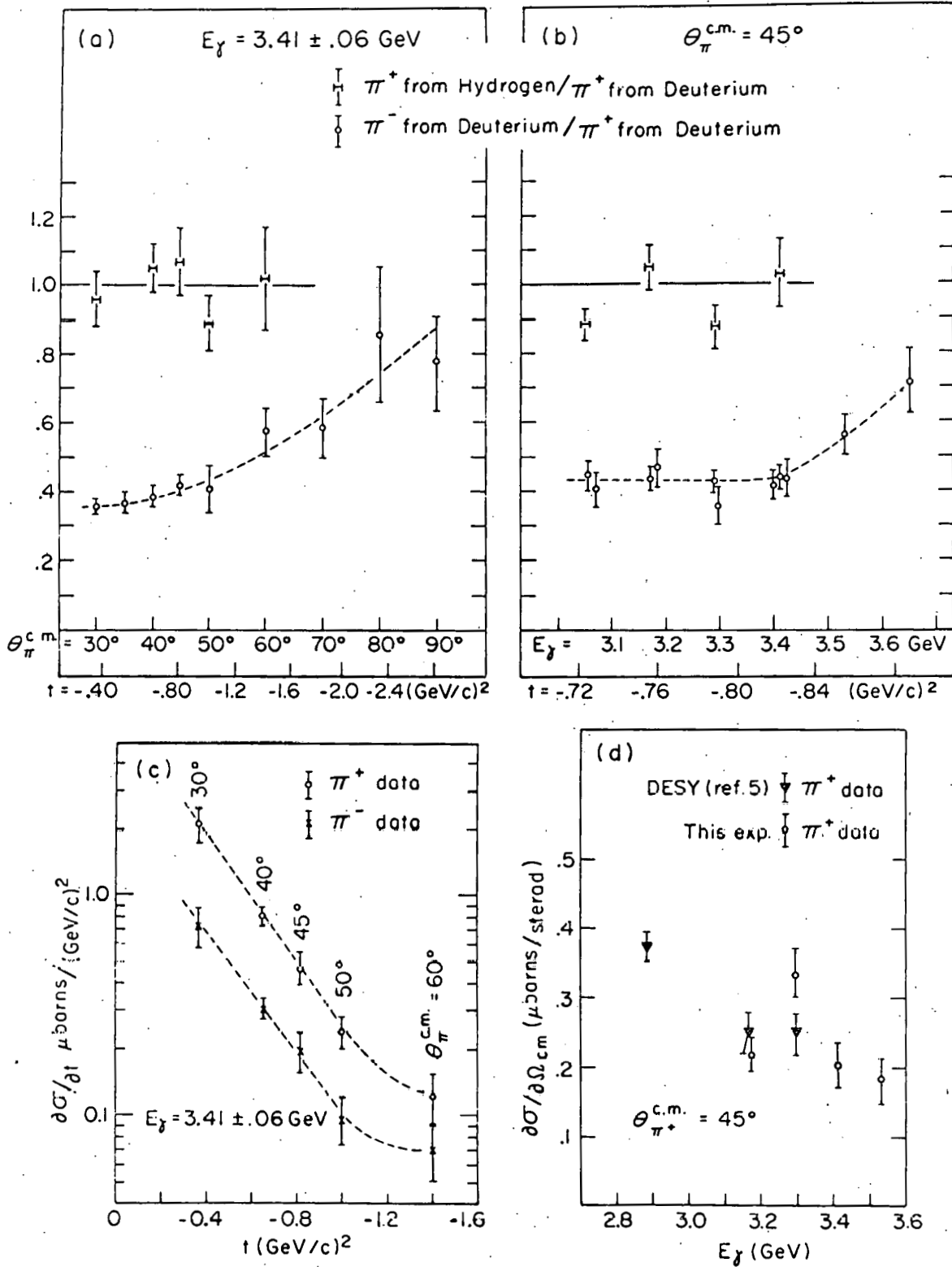Fig. 3.6-1 a,b: Ratios for π^+ production off hydrogen and deuterium, and for π^- and π^+ production off deuterium, for $|t| \geq 0.4$ $(\text{GeV/c})^2$; c,d: differential cross-sections for π^+ and π^- (From Ref. No. 87)
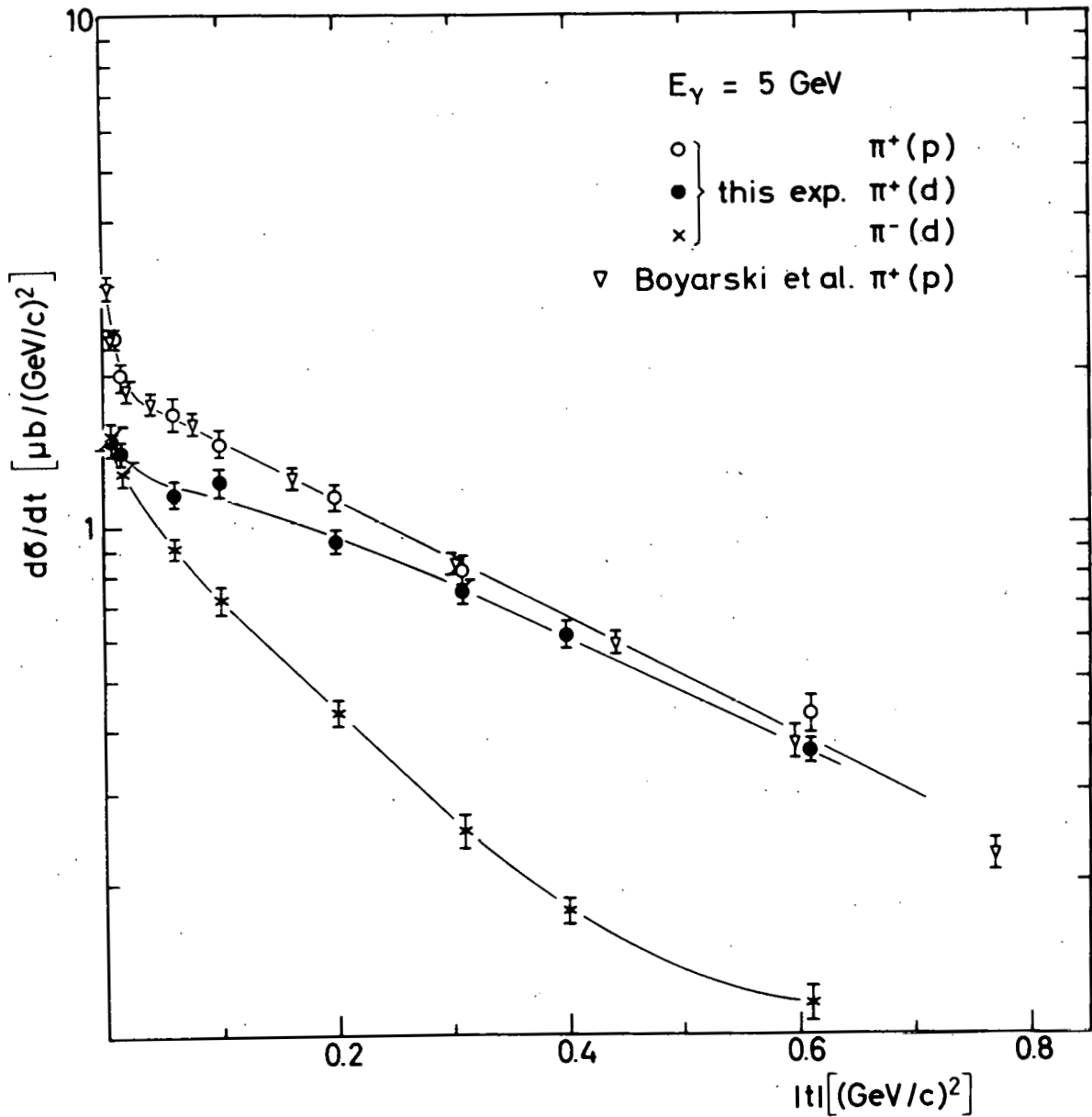
Fig. 3.6-2 Differential cross-sections for π^+ photoproduction off hydrogen and deuterium; and for π^- photoproduction off deuterium. (From Ref. No. 88)

that at small t, the π^+ rates off hydrogen are significantly larger than those off deuterium. This fact immediately points up one necessary correction to the spectator model; it is due to the Pauli principle which will not permit two final-state neutrons in the same spin and energy state. At larger $|t|$ values, this difference disappears.

There are more corrections we have to apply if we want to extract the free neutron (or free proton) cross-sections from experiments on deuterium. There are "Glauber corrections" for multiple nuclear processes, and the effects of Fermi motion of the nucleons within the deuterium nucleus. However, all of these corrections are expected to be closely similar for both reactions occurring in eq. 3.6-1, so that the ratio R is not affected. If we want to find the free neutron cross section $\frac{d\sigma}{dt}$ ($\gamma n \rightarrow p\pi^-$) from $\frac{d\sigma}{dt}$ ($\gamma d \rightarrow pp\pi^-$), we can take the corrections empirically from the corresponding π^+ cross-sections as shown in the two upper curves of Fig. 3.6-2.

The ratio R is plotted, in Fig. 3.6-3, for $0.005 \leq |t| \leq 0.8$ $(\text{GeV/c})^2$. While at -t = 0.4 the previous ratio is confirmed, the ratio appears to be unity in the very forward direction.

In the spirit of the previous two sections, the π^-/π^+ ratio in the region of the forward peak may provide a crucial test of some of the models proposed for the non-dip structure. In terms of an exchange model, either elementary or Regge-ized, $R \neq 1$ implies an interference between exchanged systems of different G-parity. $R(t = 0) \approx 1$, as experimentally found, is therefore compatible with the assumption of
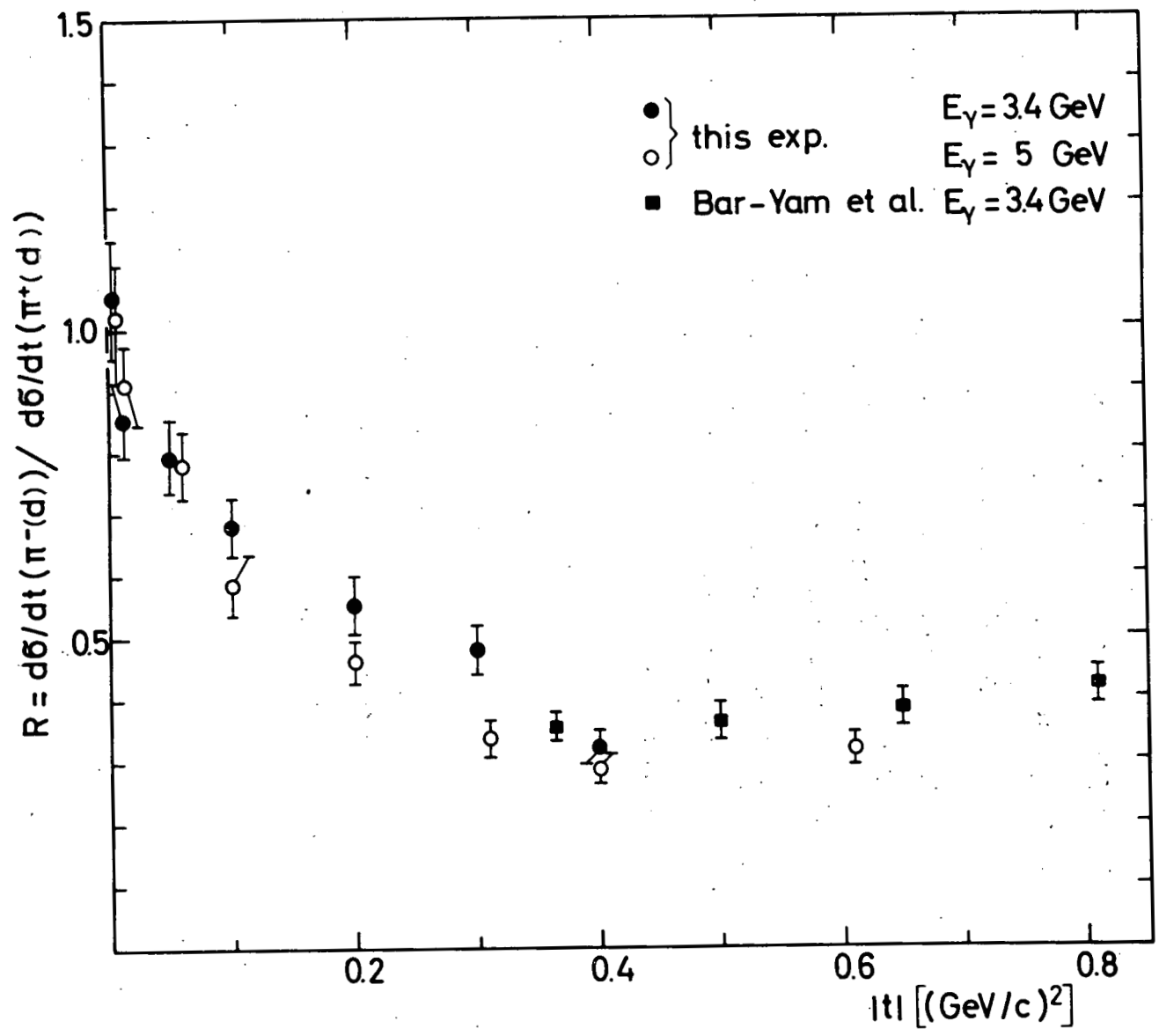
Fig. 3.6-3 Momentum-transfer dependence of the π^-/π^+ ratio R. (From Ref. No. 88)

conspiring π and π_C (0^+) trajectories, since they are of the same G-parity. It will be interesting to extend these measurements to higher energies.

For consistency, we show in <u>Fig. 3.6-4</u> the similarity of the energy dependence of the differential cross-section for π^+ and π^- production at $(t = -0.1$ $(GeV/c)^2$. However, we should point out that the momentum transfer dependence of the differential cross-sections $\frac{d\sigma}{dt}$ $(\gamma p \rightarrow n\pi^+)$ and $\frac{d\sigma}{dt}$ $(\gamma n \rightarrow p\pi^-)$ looks quite dissimilar; the two low curves in <u>Fig. 3.6-2</u> point up this difference for π^+ and π^- production off deuterium, as reflected in the t dependence of R. We can use our arguments about the similarity of the necessary corrections to find the free neutron cross-section through the relation

$$\frac{d\sigma}{dt} (\gamma n \rightarrow p\pi^-) = R \frac{d\sigma}{dt} (\gamma p \rightarrow n\pi^+). \qquad (3.6\text{-}2)$$

Its t-dependence is obviously very different from the π^+ production process; the forward spike is not affected, but the π^- cross-section continues to fall off more rapidly with increasing $|t|$. We can formulate this in terms of the amplitudes induced by isoscalar and isovector photons: the squared isovector and isoscalar amplitudes

$$|A_s|^2 + |A_v|^2 = \frac{(1 + R)}{2} \frac{d\sigma}{dt} (\gamma p \rightarrow n\pi^+) \qquad (3.6\text{-}3)$$

lead to the forward peaks, whereas the interference term

$$2A_s A_v = \frac{(1 - R)}{2} \frac{d\sigma}{dt} (\gamma p \rightarrow n\pi^+) \qquad (3.6\text{-}4)$$

is absent in the forward direction, since, for very small $|t|$, $R \approx 1$.
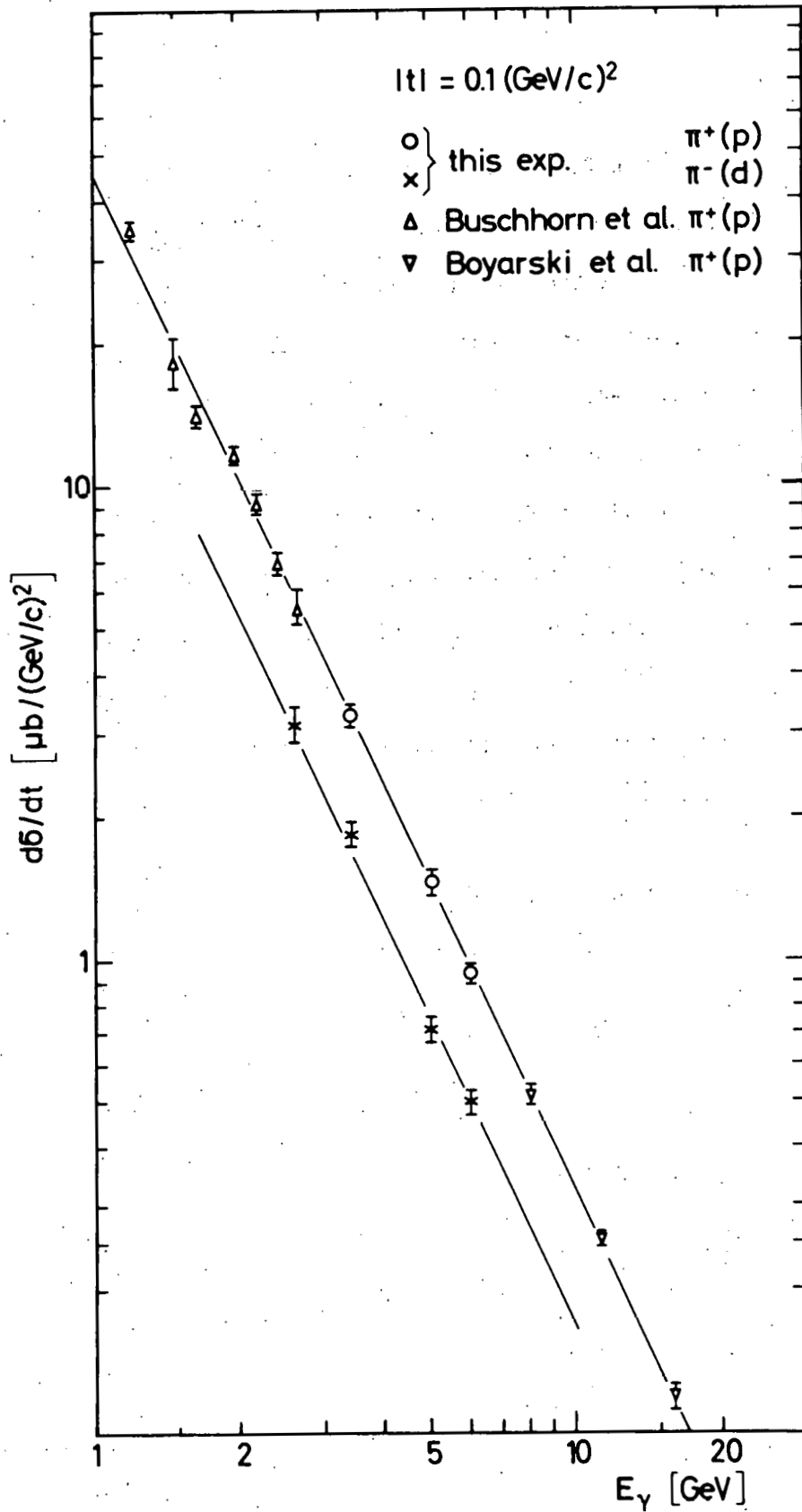
Fig. 3.6-4 Dependence of π^- and π^+ photoproduction cross-section for fixed $|t| = 0.1$ (GeV/c)^2, on photon energy. (From Ref. No. 88)

A successful model for single-charged-π photoproduction will have to reproduce this behavior as well as the differential cross-section, plus any data on polarization parameters that may show up. At the time of the writing of these notes, first results are being presented for the asymmetry parameter $\Sigma = \frac{\sigma_\perp - \sigma_{||}}{\sigma_\perp + \sigma_{||}}$, defined in section 1.3, at high energies from a π^+ production experiment[103]. They strongly indicate dominance of the exchange of a natural-parity object (0^+, 1^-, ...); since the π^-/π^+ ratio data postulate the interference of even and odd G-parity exchange at $|t|$ values not too close to zero, Frøyland and Gordon[104] chose a model incorporating π and ρ exchange; a ρP and a conspiring πP cut were additionally needed for a reasonable fit to the data for $\frac{d\sigma}{dt}$, Σ and R.

3.7 A Few Tests of SU(3) Symmetry.

The high-energy behavior of amplitudes which are governed by exchange diagrams should provide good tests for symmetry schemes, since we expect kinematical correction to become less important as s and t increase.

We mentioned in Section 1.1 that the conventional assignment of the photon as the $U = 0$ part of an octet is not entirely established. This assignment stems from the Gell-Mann Nishijima formula $Q = \frac{Y}{2} + I_3$, which is obeyed by all known hadrons.

There is no reason[89] why there should not be an additional additive quantum number D which may not transform like a member of an octet (remember that Y and I_3 can be identified with two of the

generators of the group SU(3), so that

$$Q = \frac{Y}{2} + I_3 + D \qquad (3.7\text{-}1)$$

may contain a non-octet part. However, since for all observed hadrons
$D = 0$, we will keep in mind that only the octet part of Q will have
non-vanishing matrix elements between known hadrons. Similarly, it
is possible that the relation between charge Q and electromagnetic
current j

$$Q = \int j_0 \, (\vec{x}, t) \, d^3\vec{x} \quad \left(+ \underbrace{\int \ldots d^3\vec{x}}_{=0} \right) \qquad (3.7\text{-}2)$$

contains an octet current j_0 whose space integral is equal to the
charge, plus a conjectured additional current which may transform
like a member of $\underset{\sim}{1}$ or $\underset{\sim}{27}$ but whose space integral happens to vanish.

Since the symmetry properties of the photon are those of the
electromagnetic current j_{em}, we will have to look for possible non-
octet parts of the photon in order to establish the initial assign-
ments. The difficulty in this search is that most predictions made
on the grounds of the U = 0, $(\underset{\sim}{8})$assignment can be obtained from the
U-scalar character of the photon alone. However, $\underset{\sim}{1}$, $\underset{\sim}{8}$ and $\underset{\sim}{27}$ all
contain a U spin singlet.

Among the many SU(3) tests proposed,[90] a few are sensitive to
the octet assignment. This holds particularly for the vector domin-
ance graph for the process $V^0 \to e^+ e^-$
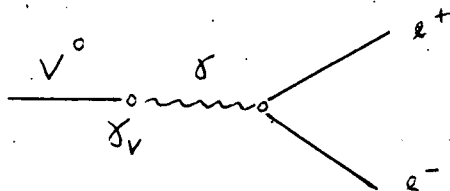
to lowest order in α. If we assume pure octet character for the photon, then we obtain (cf. section 2.5), with the usual $\Phi - \omega$ mixing,

$$\gamma_\rho^2 : \gamma_\omega^2 : \gamma_\Phi^2 = 9: 1: 2 \qquad (3.7\text{-}3)$$

and, by virtue of eq. 2.5-4 and ref. 50,

$$\Gamma(\rho \to e^+e^-): \Gamma(\omega \to e^+e^-): \Gamma(\Phi \to e^+e^-) \approx 9: 0.65: 1.30$$
$$(3.7\text{-}4)$$

where the neglected small terms in (2.5-4) may account for some discrepancy. The numerical check is, according to Table I,

$\Gamma_\rho = 6.4$ keV, $\Gamma_\omega = 0.5$ to 1.1 keV, $\Gamma_\Phi = 1.2$ keV. This check is not quantitatively tight enough to exclude some non-octet admixture for the photon, but the picture certainly looks consistent for the octet assignment.

Harari[90] has listed a large number of SU(3) tests in photoproduction, involving the U-scalarity of the photon. Predictions are usually for amplitudes, and high-energy experiments mostly yield cross-sections only. In the absence of phase information, we can then test inequalities rather than equalities. Assuming unbroken SU(3) symmetry, we can obtain two such inequalities for the photoproduction of pseudoscalar mesons off protons, $\sigma(PS,B)$:

$$\sqrt{2}\, \sigma^{1/2}(\pi^+ n) \leq \sqrt{3}\, \sigma^{1/2}(K^+\Lambda) + \sigma^{1/2}(K^+\Sigma) \qquad (3.7\text{-}4)$$

$$\sigma^{1/2}(\pi^0 p) \leq \sqrt{2}\, \sigma^{1/2}(K^0 \Sigma^+) + \sqrt{3}\, \sigma^{1/2}(\eta p) \qquad\qquad (3.7\text{-}5)$$

We can write eq. 3.7-4 in terms of the triangle inequality given in Fig. 3.7-1 where Φ is the unknown phase angle between the $K\Lambda$ and $K\Sigma$ amplitudes. Then SU(3) demands $|\cos \Phi| \leq 1$. Fig. 3.7-2 shows a check of the inequality 3.7-4 by Elings et al.[91], performed at energies $3.4 \leq k < 4$ GeV. Obviously $\sigma(\pi^+ n)$ is well contained within the allowed band.

More recently, the high-energy SLAC data[84] on forward K^+ production have permitted a check on the same relations. Fig. 3.7-3 gives the results at energies $5 \leq k \leq 18$ GeV, and at momentum transfers $|t|$ up to ~ 1.3 $(\text{GeV/c})^2$. Again, there is good agreement at $|t|$ values larger than 0.1 $(\text{GeV/c})^2$. At smaller $|t|$, there appears to be a strong violation of the condition $|\cos \Phi| \leq 1$. Although no precise account for this discrepancy can be given, the unequal masses involved in the processes will no doubt manifest themselves more strongly at small $|t|$ than at larger $|t|$ values.

The relation 3.7-5 cannot at present be checked since there are no good data available for $\gamma p \to K^0 \Sigma^+$. Predictions involving reactions with more than two particles in the final state are not well-enough studied experimentally to provide stringent tests.

3.8 High-Energy η Photoproduction.

In section 1.5, we mentioned the usefulness of η production in the isobar region as a probe for the $I = 1/2$ channel. In the framework of higher energy production t-channel exchange processes of
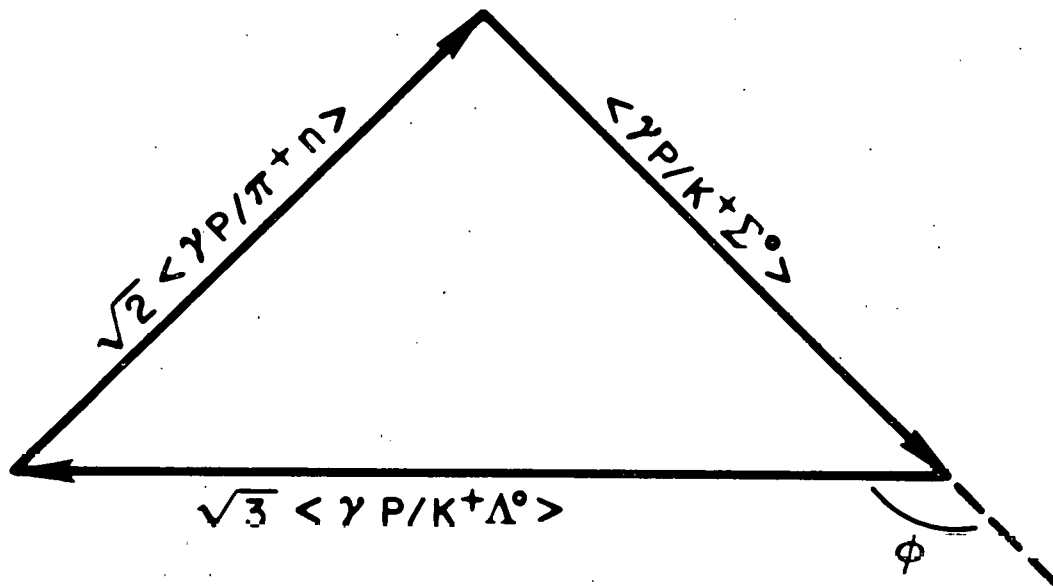
Fig. 3.7-1 SU(3) relation between photoproduction processes $(\pi^+ n), (K^+\Sigma^0)$ and $K^+\Lambda^\odot$. (From Ref. No. 91)
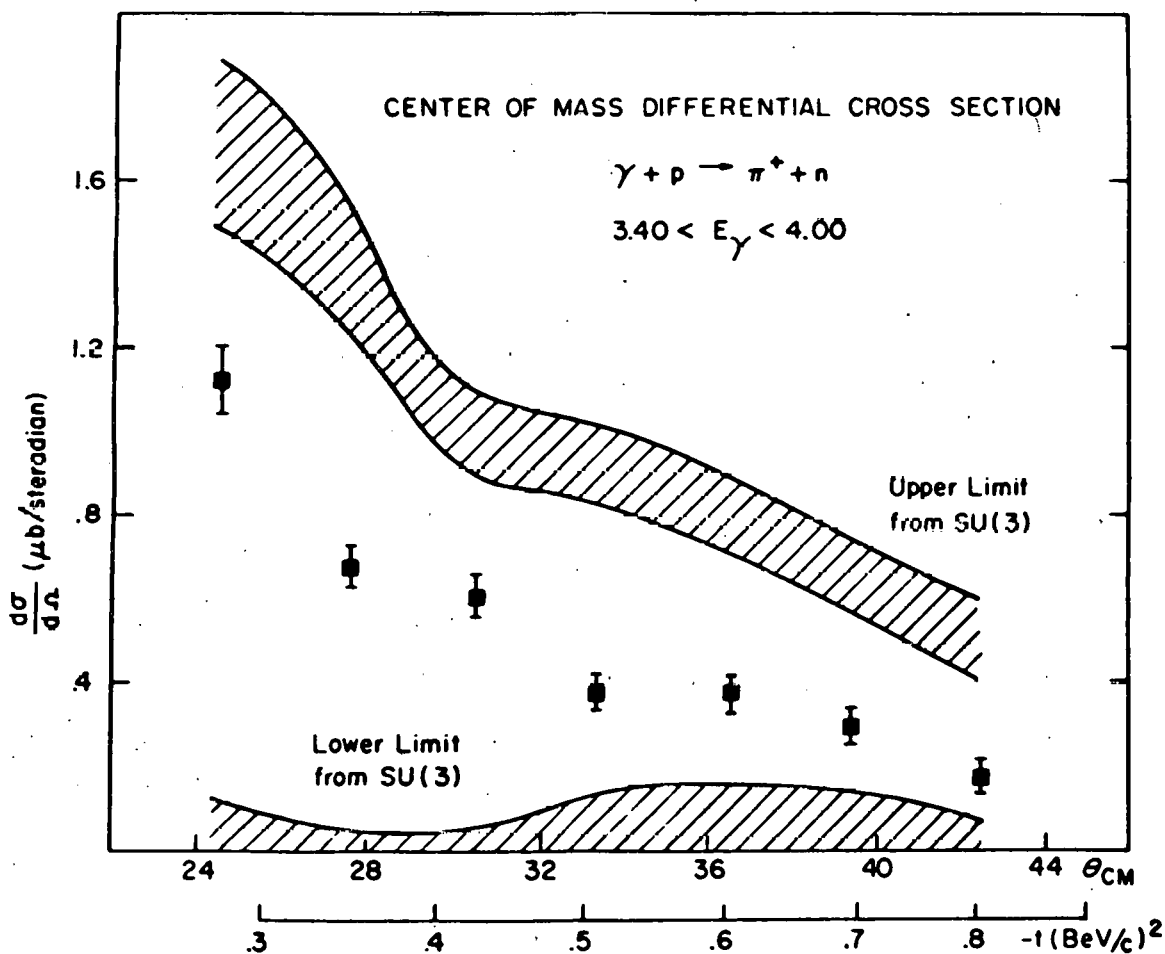

Fig. 3.7-2 Comparison of the experimental values for $\gamma p \to \pi^+ n$ with the SU(3) limits imposed by the inequality 3.7-4 and Fig. 3.7-1. (From Ref. No. 91)

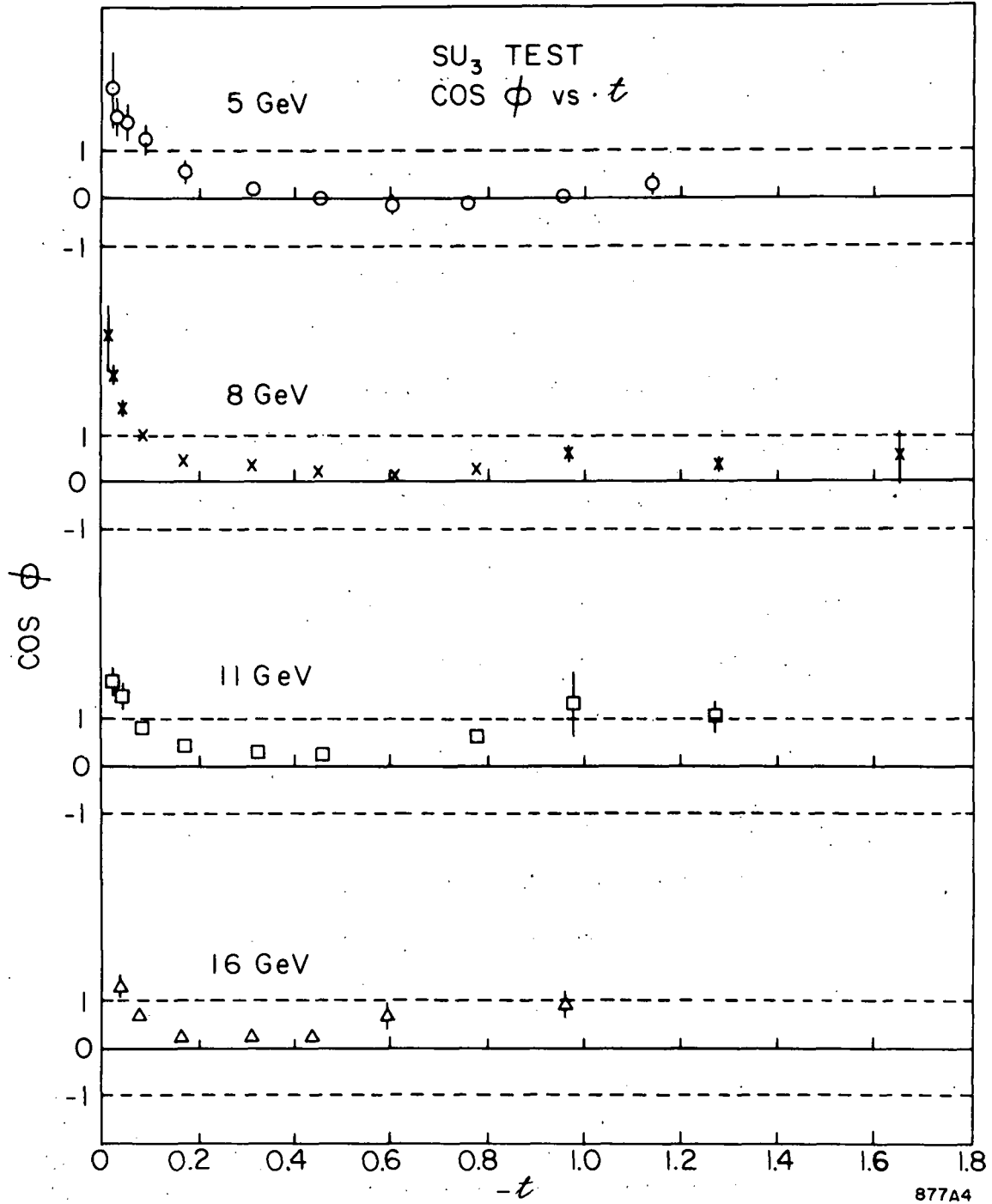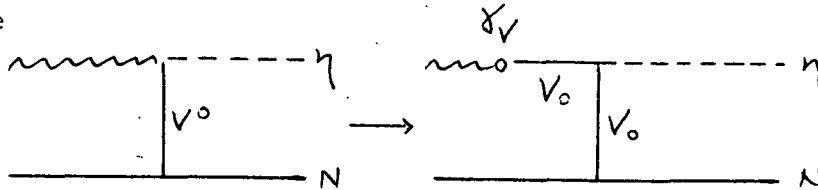Fig. 3.7-3 SU(3) check according to eq. 3.7-4, as a function of
momentum transfer |t|. The SU(3) condition |cosΦ|<|
is violated at small |t|. (From Ref. No. 84)

the type

are expected to play a dominant role in analogy to the π production

processes. If we invoke the vector dominance model, we have two

strong vertices to deal with, and can make statements stemming from

isospin and SU(3) invariance.

On such grounds, Dar and Weisskopf[92] made predictions for the

t dependence of the differential cross-section $\frac{d\sigma}{dt}$ $(\gamma p \rightarrow p\eta)$ at

higher energies. Note that, in this case, the prediction came <u>before</u>

the experiment!

One can safely assume[92] that, in the above diagram, ρ exchange

dominates the amplitude. Connecting the respective coupling constants

through SU(6) relations and isospin invariance, one can link up the

ρ exchange amplitudes in $\gamma p \rightarrow p\eta$ and $\gamma p \rightarrow \pi^+ n$. The vector dominance

model then relates the ρ exchange amplitude for $\gamma p \rightarrow \pi^+ n$ to the ρ

exchange amplitude for $\omega p \rightarrow \pi^+ n$. Note that for reasons of G-parity

conservation, we can have only the ω as the intermediate vector

meson in the graph
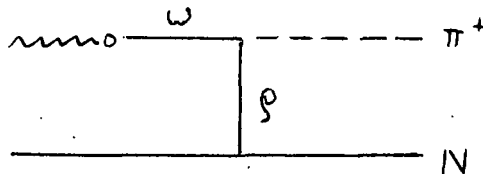
Finally, we invoke time-reversal invariance, and projecting out the transversely polarized ω's only, we arrive at the relation

$$\frac{d\sigma}{dt}(\gamma p \to p\eta) \approx \frac{3.3}{2}\frac{\pi\alpha}{\gamma_\omega{}^2}\ \rho_{11}\frac{d\sigma}{dt}(\pi^+ n \to \omega p) \quad (3.8\text{-}1)$$

where the numerical factor is due to the SU(6) coupling ratios, and to the assumption of an unpolarized photon beam; γ_ω denotes the strength for the direct coupling γ-ω, as introduced in section 2.5.

Since, by isospin invariance, we can replace $\pi^+ n \to \omega p$ by $\pi^- p \to \omega n$, we can draw on the data for both these reactions to predict the $\gamma p \to p\eta$ cross-section at given energies. This is done in Fig. 3.8-1, which gives the quantity $s^2\frac{d\sigma}{dt}$ vs. the momentum transfer t, for incident energies $\sim$ 3 and 10 GeV.

Note that this prediction does not show either a forward dip or a secondary dip around $-t \approx 0.5\ (\text{GeV}/c)^2$. Both these features are present in π^0 production (at least at intermediate energies), and would be expected here if we assumed simple ρ trajectory exchange (cf. section 3.3).

First data were recently taken at CEA[93] at $k = 4$ GeV and at SLAC[40] at $k = 6$ GeV. The 6 GeV data are shown in Fig. 3.8-2. The general trend appears to bear out the prediction; the dip structure observed in π^0 production is not seen here. The measurements were taken at $|t| > 0.2\ (\text{GeV}/c)^2$, so that no statement can be made about a forward dip. Quantitatively, there is agreement within a factor of 2. This ought to be regarded as reasonable agreement, considering the approximations made and the error bars on the cross-sections.
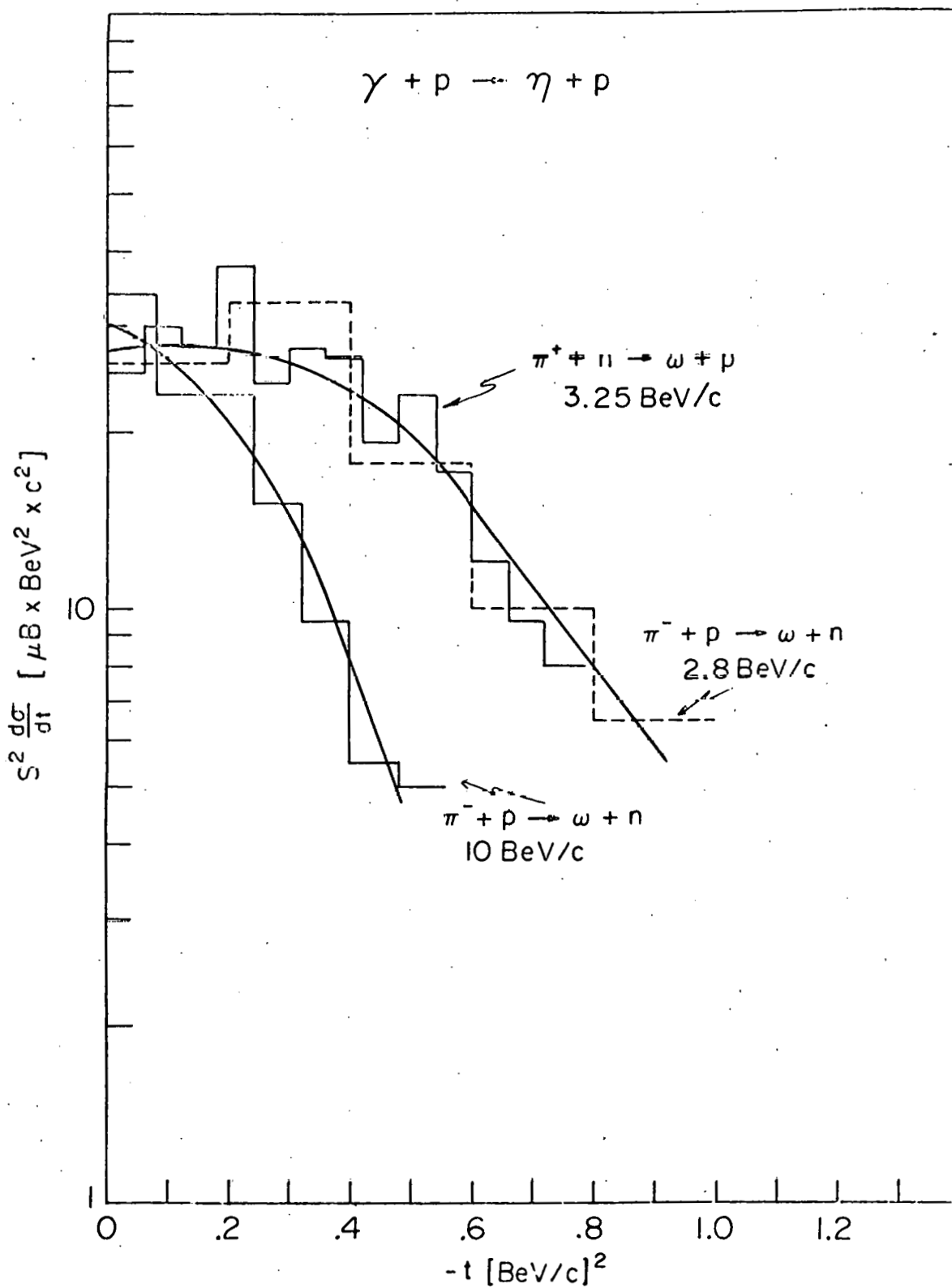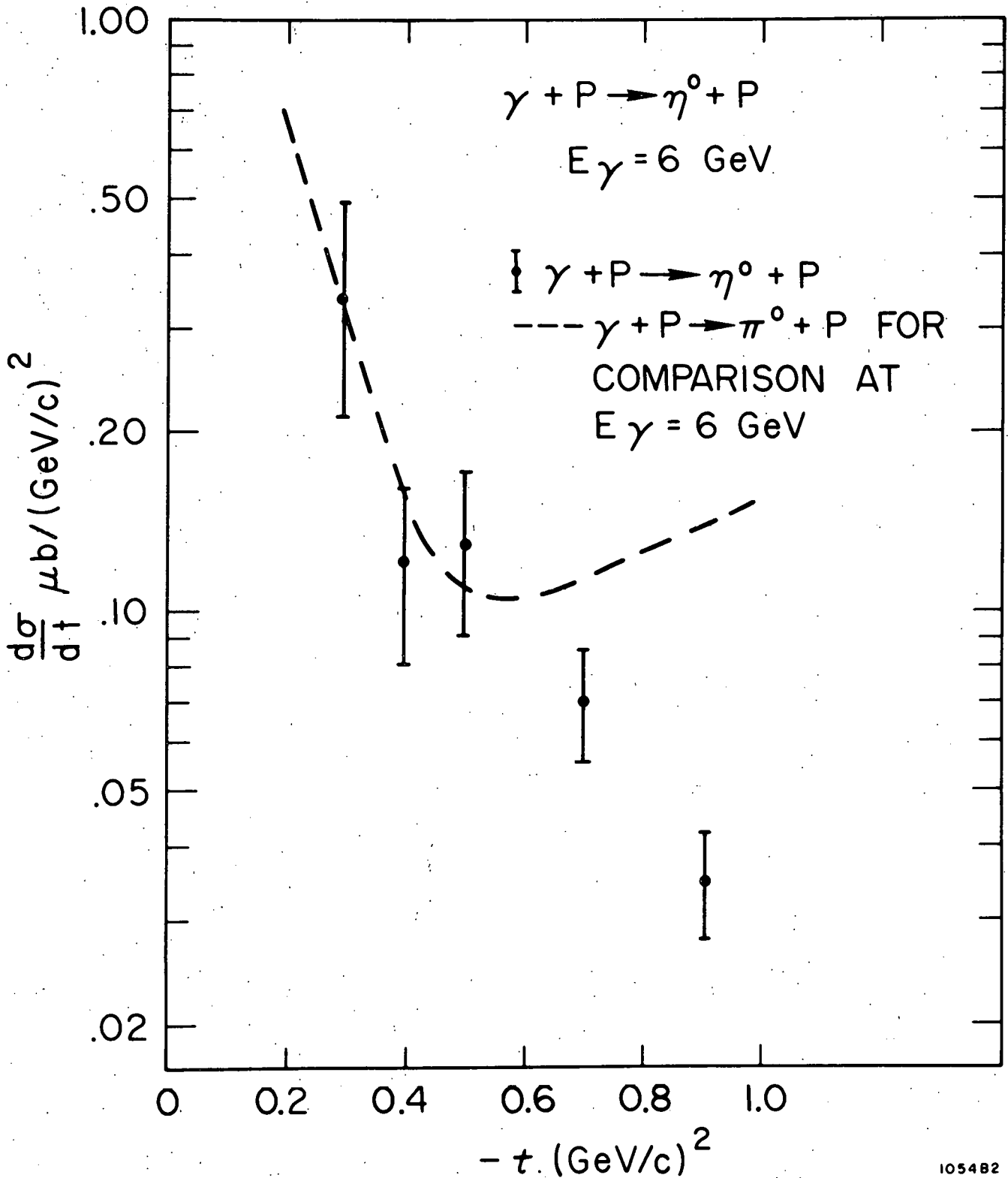
Fig. 3.8-1 Prediction for high-energy η photoproduction cross-section
according to eq. 3.8-1, using the vector dominance model
and πN → ωN data. (From Ref. No. 92)

Fig. 3.8-2 Differential cross-section for high-energy η photoproduction.
Dashed curve: general behavior of π⁰ photoproduction cross-
section in comparable region. (From Ref. No. 40)

The preliminary CEA data do go to smaller t, and may contain indications for a dip at $|t| < 0.5$ $(GeV/c)^2$. At larger values, they also agree qualitatively with the predictions[92]. Clearly, we will have to wait for more data before we can do a detailed analysis.

3.9 Concluding Remarks

In the preceding argumentation, we are left with a slightly uneasy feeling. We start with a simple ρ exchange picture which would make us expect a dip-and-peak angular structure somewhat like in the π^o case, Fig. 3.3-1. Invoking several reasonably well established invariance principles and models, we wind up with a predicted cross-section quite unlike the typical one-trajectory exchange picture of our "input". Maybe this points up a situation typical for the "state of the art". The theory is a curious blend of pragmatism, based on suggestive principles plus ad-hoc assumptions which may or may not appear compelling; they may carry little immediate intuitive appeal, and lack the solid basis to satisfy the more rigorous theorist.

Experiment is found, within reasonable error, to bear out some of the features we set out to describe - but the limited range of parameters measured,and the need for more precise data leave agreement in a doubtful state.

On this open-ended note we will conclude these lectures. They may, altogether, indicate that photon-induced hadronic reactions are particularly suited to study distinctive features of the strong interactions; that photon experimentation, which carries its own

difficulties, has come a long way in recent years; that theoretical understanding is in no better and no worse shape here than in the general field of <u>hadron</u>-induced hadronic interactions; and that physicists in this field will not be on the unemployed roll for some time to come.

A final remark appears in order on what important experimental development can be anticipated in the field of photon-hadron physics in the near future. In the course of these lectures, we have stressed time and again that the need for the fixing of photon momentum and polarization parameters, and the need to check truly asymptotic behavior, leave present interpretation of the data open to doubt.

The production of polarized photon beams is just now becoming practically feasible, along several lines. At DESY and CEA, coherent bremsstrahlung production off crystals[95] is yielding photon beams of good intensity ($\lesssim 10^{11}$ equivalent quanta/min) with a high degree of plane polarization ($\lesssim 80\%$), at energies up to about one-half of the final machine energy (i.e. $\lesssim 3.6$ GeV at DESY). The cross-sections for two-body reactions can be broken up into parts with only natural or unnatural parity exchanges[95], so that these beams will help greatly in the understanding of exchange processes. One simply has to study the distribution

$$\frac{d\sigma(\Phi)}{d\Phi} = A + B \cos^2\Phi + C \sin^2\Phi$$

where Φ is the angle between the photon polarization and the reaction

plane, and the successive terms on the RHS indicate the contributions from unpolarized photons, from natural (0^+, 1^-, ...), and from unnatural (0^-, 1^+, ...) parity exchanges. In the concluding remarks of section 3.6, we saw that first results from such data in π^+ photoproduction put an important constraint on the models used to describe the process.

Monochromatic beams from positron annihilation[96] and from backscattered laser photons[97] are in initial use at SLAC with intensities useful for bubble chamber experimentation. The laser photons can carry circular as well as plane polarization, and the attractive feature of this scheme is that 180° scatters preserve this polarization fully.

Lastly, it should be mentioned that even in the absence of plans to build higher-energy electron machines, photon experimentation at energies more closely satisfying asymptotic conditions will become one of the standard features at the 200-500 GeV proton accelerators now being projected at Weston and Saint-Tropez*. Fig.s 3.9-1 and 3.9-2 give rough estimates[98] of the photon yield per interacting proton, per BeV energy interval, from pp collisions at 200 BeV. Intensities are lower but still respectable even for purified beams[98], and together with the good duty-cycle characteristics of the proton machines, and large-solid-angle detection devices, make us look forward to the solution of some presently unanswerable questions.

---

* The error bars on this last statement presently reach from the Escorial to somewhere in Northern Sweden.
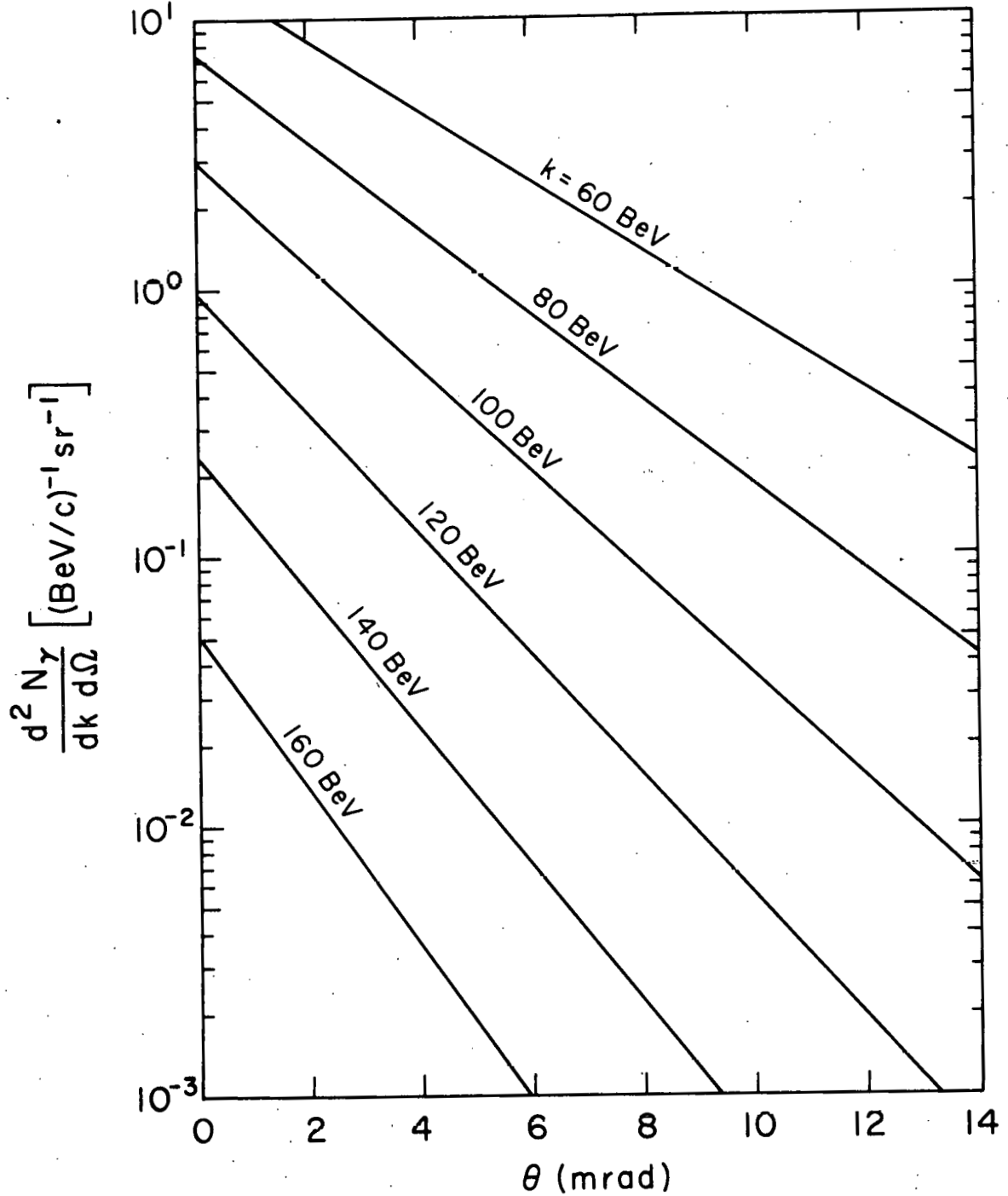
XBL672-844

Fig. 3.9-1 Angular dependence of photon yield per unit energy interval, per 200 GeV proton interacting with a proton target at rest. (From Ref. No. 98)
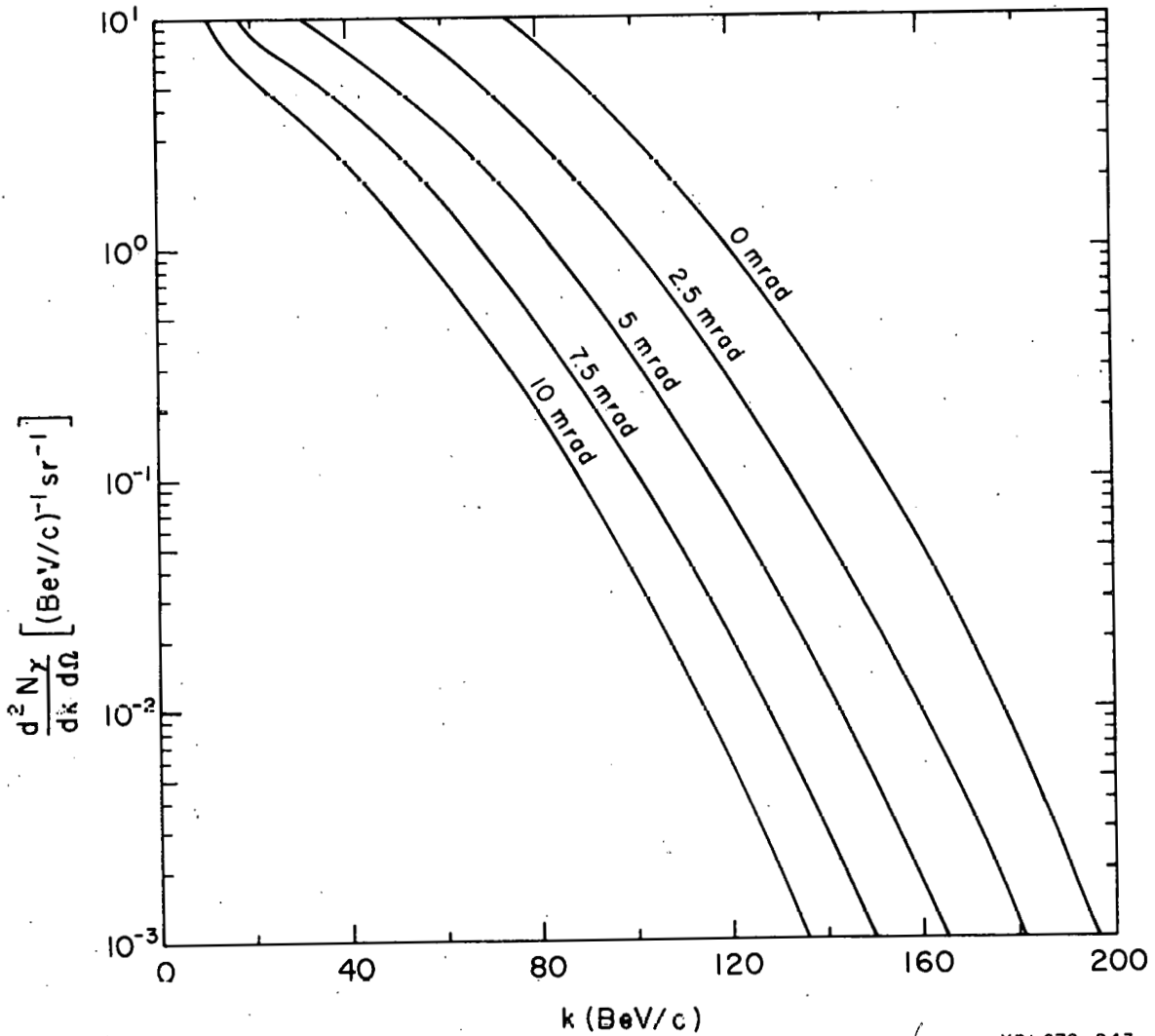
Fig. 3.9-2 Estimate of photon yield per unit energy, per interacting 200 GeV proton, as a function of photon energy, for various angles. (From Ref. No. 98)

Acknowledgments

I would like to thank many colleagues for informative discussions. In particular, I am grateful to experimenters at SLAC, DESY, and CEA who made their results available to me prior to publication. I appreciate the hospitality of the Aspen Center for Physics, where these notes were written up. Drs. Stephen Adler, Leon Rochester, and Karl Strauch gave them a critical reading, for which I am grateful.

References

1) M. J. Moravcsik, P.R. 104, 1451 (1956).

2) M. Gourdin, P. Salin, N.C. 27, 193 (1963).

3) P. Salin, N.C. 28, 1294 (1963).

4) D. Beder, N.C. 33, 94 (1964).

5) R. L. Walker, submitted to P.R. (1968).

6) M. Jacob and G.C. Wick, Ann. Phys. 7, 404 (1959).

7) See the data compilation of J. T. Beale, S. D. Ecklund,
   R. L. Walker, Caltech Report CTSL-42 (1967).

8) M. Borghini, CERN preprint; Contribution to Dubna Conf. (1967).

9) G. F. Chew, M. L. Goldberger, F. E. Low, and Y. Nambu,
   P. R. 106, 1345 (1967).

10) S. D. Ecklund and R. L. Walker, P. R. 159, 1195 (1967).

11) E. D. Bloom, C. A. Heusch, C. Y. Prescott, L. S. Rochester,
    P.R.L. 19, 671 (1967).

12) H. Harari, Summary talk, Proc. SLAC Symposium (1967).

13) N. Cabibbo, L. Radicati, P.L. 19, 697 (1966).

14) F. J. Gilman, H. J. Schnitzer, P.R. 150, 1362 (1966).

15) S. D. Drell, A. G. Hearn, P.R.L. 16, 908 (1966).

16) Y. C. Chau, R. C. Moorhouse, N. Dombey, P.R. 163, 1632 (1967), and
    contribution to SLAC Symposium(1967).

17) C. A. Heusch, Lecture at the 1966 Erice Summer School.

18) E. D. Bloom, C. A. Heusch, C. Y. Prescott, L. S. Rochester,
    P.R.L. (to be published).

19) German Bubble Chamber Collaboration, DESY 68/8 (1968).

20) S. D. Deans, W. G. Holladay, P.R. 161, 1466 (1967).

21) C. A. Heusch, C. Y. Prescott, E.D. Bloom, L. S. Rochester,
    P.R.L. 17, 573 (1966).

22) C. A. Heusch, C. Y. Prescott, R. F. Dashen, P.R.L. 17, 1019 (1966).

23) J. Tyson, et al., quoted by K. Strauch, Proc. SLAC Symposium (1967).

24) H. Rollnik, Proc. Heidelberg International Conference on Elementary Particles, (1967); Lectures at Int. School of Physics, Herceg-Novi (1967).

25) J. S. Ball, P. R. 114, 2014 (1961).

26) R. Taylor, private communication.

27) R. Dalitz, Lectures at Grenoble Summer School, 1965.

28) R. Moorhouse, P.R.L. 16, 772 (1966).

29) S. D. Drell, Proc. SLAC Symposium (1967), p.

30) M. Ross, L. Stodolsky, P.R.L. 149, 1172 (1966); see also S. D. Drell and J. Trefil, P.R.L. 16, 552 (1966).

31) P. Söding, P.L. 19, 702 (1965).

32) V. Auslander et al., Novosibirsk preprint (1967).

33) J. Pisut, M. Roos, Nuc. Phys. B6, 325 (1968).

34) Y. Eisenberg et al., P.L. 22, 223 (1966).

35) G. Kramer, DESY 67/32 (1967).

36) M. Davier, et al., SLAC preprint (1968).

37) H. Blechschmidt, et al., DESY 67-30 (1967).

38) J. G. Asbury, et al., P.R.L. 19, 865 (1967).

39) J. Fleischer, DESY 68/15 (1968).

40) W. G. Jones, et al., SLAC preprint (1968); and R. Anderson, et al., SLAC-PUB-431 (1968).

41) K. Schilling and F. Storim, DESY 68/23 (1968).

42) D.R.O. Morrison, P.L. 22, 528 (1966)

43) Preliminary results, quoted by S.C.C. Ting (1968).

44) Y.S. Tsai et al., P.R.L. 19, 915 (1967).

45) A. Boyarski et al., P.R.L. 20, 877 (1968).

46) S. Meshkov and R. Ponzini, National Bureau of Standards preprint (1968).

47) For a list of references, see H. Joos, Proc. Heidelberg Conference (1967).

48) S. C.C. Ting, private communication (based on $\sim$ 50 $\Phi \to e^+e^-$ events (1967).

49) A. Zichichi, private communication (based on $\sim$ 10 events for both ω and Φ), (1968).

50) R. J. Oakes and J. J. Sakurai, P.R.L. 19, 1266 (1967).

51) K. Kajantje and J.S. Trefil, CERN Th. 736 (1966).

52) A. Dar et al., P.R.L. 20, 1261 (1968).

53) H. Fraas, D. Schildknecht, DESY 60/4 (1960).

54) R. Diebold and J. A. Poirier, P.R.L. (SLAC-PUB-412 (1968)).

55) M. Krammer, DESY 68/6 (1968).

56) J. S. Asbury et al., P.R.L. 20, 227 (1968).

57) H. Joos, D. Schildknecht, DESY preprint (1968).

58) L. Stodolsky, P. R.L. 18, 135 (1967).

59) H. G. Hilpert et al., DESY preprint (1968).

60) L. N. Hand, P.R. 129, 1834 (1963).

61) L. W. Mo, Y. S. Tsai, SLAC-PUB-380 (1968).

62) M. Braunschweig, et al., Bonn preprint 1-038 (1968).

63) G. C. Bolon et al., P.R.L. <u>18</u>, 926 (1967).

64) G. Buschhorn et al., P.L. 25B, 622, (1967).

65) G. Buschhorn et al., P.R.L. <u>18</u>, 571 (1967).

66) P. M. Joseph, et al., Contribution to the SLAC Symposium (1967);
P.R.L. <u>19</u>, 1206 (1967).

67) A. M. Boyarski, et al., P.R.L. <u>20</u>, 300, (1968).

68) A. M. Boyarski, et al., quoted by B. Richter,
Proc. SLAC Symposium (1967).

69) G. Buschhorn et al., P.R.L. <u>20</u>, 230 (1968).

70) B. Gittelman, private communication (1968).

71) R. Anderson et al., SLAC-PUB-428 (1968).

72) M. P. Locher, H. Rollnik, P.L. <u>22</u>, 696 (1966).

73) J. P. Ader, M. Capdeville, P. Salin, CERN Th. 803 (1967).

74) P. Stichel, Lectures on Photoproduction, DESY 66/2 (1966).

75) L. S. Osborne, private communication (1968).

76) M. Ross, private communication (1968).

77) J. Orear, et al., P. R. <u>152</u>, 1162 (1966); also J. Orear,
Proc. of the Topical Conference on Hadrons, CERN, Geneva (1968).

78) E. A. Paschos, SLAC preprint (1968).

79) H. Abarbanel et al., P. R. <u>160</u>, 1329 (1967).

80) R. F. Dashen, S. C. Frautschi, P. R. <u>143</u>, 1171 (1966).

81) H. R. Rubenstein et al., P. R. <u>167</u>, 1441 (1967).

82) S. Mandelstam, Wang, P. R. <u>160</u>, 1490 (1967).

83) Lorella Jones, Caltech internal note (1968).

84) B. Richter, Proc. SLAC Symposium (1967); SLAC-PUB- 353 (1967).

85) J. S. Ball et al., P.R.L. 20, 518 (1968), see also

   A. Bietti et al., P. L. 26B, 457 (1968).

86) D. Amati et al., P. L. 26B, 510 (1968).

87) Z. Bar-Yam et al., P.R.L. 19, 40 (1967).

88) P. Heide et al., DESY 68/22 (1968).

89) M. Nauenberg, P.R. 135, B. 1047 (1964).

90) H. Harari, P.R. 155, 1565 (1967); cf. also H. Harari,

   SLAC-PUB-349 (1967).

91) V. Elings et al., P.R.L. 16, 474 (1966).

92) A. Dar, V. F. Weisskopf, P.R.L. 20, 762 (1968).

93) D. Belenger et al., M.I.T. preprint (1968).

94) L. Criegee et al., P.R.L. 16, 1031 (1966), and references there.

95) J. P. Ader et al., CERN Th. 886 (1968).

96) G. Chadwick, Note in SLAC Handbook (1967).

97) J. J. Murray, P. R. Klein, SLAC-TN-67-19 (1967), and

   references there.

98) C. A. Heusch, 200 BeV Accelerator, Studies on Experimental

   Use, p. 156 UCRL 16830 (1967).

99) C. Bacci et al., P.R.L. 20, 571 (1968)

100) A. Donnachie, P.L. 24B, 420 (1967).

101) Orsay Contribution to the Vienna Conference (1968).

102) I. Derado, Z.G.T. Guiragossian, SLAC-PUB-460 (1968).

103) C. Geweniger et al., Contribution to the Vienna Conference (1968).

104) J. Frøyland, D. Gordon, M.I.T. preprint CTP38 (1968).

LEGAL NOTICE

This report was prepared as an account of Government sponsored work. Neither the United States, nor the Commission, nor any person acting on behalf of the Commission:

A. Makes any warranty or representation, expressed or implied, with respect to the accuracy, completeness, or usefulness of the information contained in this report, or that the use of any information, apparatus, method, or process disclosed in this report may not infringe privately owned rights; or

B. Assumes any liabilities with respect to the use of, or for damages resulting from the use of any information, apparatus, method, or process disclosed in this report.

As used in the above, "person acting on behalf of the Commission" includes any employee or contractor of the Commission, or employee of such contractor, to the extent that such employee or contractor of the Commission, or employee of such contractor prepares, disseminates, or provides access to, any information pursuant to his employment or contract with the Commission, or his employment with such contractor.